1. Introduction

An international and multidisciplinary group of scientists have recently joined efforts to organize the challenging endeavor of drilling through the thick Messinian evaporites found in deep Mediterranean basins (IODP pre-Proposal P857B DREAM; Camerlenghi et al., 2014; Lofi and Camerlenghi, 2014). The targeted deep basin evaporites reach up to 3 km in thickness (Hsü, 1973) and are thought to have resulted from restricted connectivity of the Mediterranean Basin to the Atlantic Ocean that le~~a~~d to the Messinian Salinity Crisis (MSC). It has been suggested that deposition of the MSC salt giant has greatly affected the global oceans by sequestering 5% (Ryan, 1973; 2008)~~)~~ to 10% (Garcia-Castellanos and Villaseñor, 2011) of their salt content into the Mediterranean. Also, by contributing warm, saline water to northern latitudes, the MSC influenced Atlantic Meridional Overturning Circulation and, consequently, global climatic shifts (Hernández-Molina et al., 2014). Among the major stratigraphically-driven findings of modern geoscience, the MSC stands alone as being supported by an 'outrageously under-sampled stratigraphic record' (CIESM, 2008). For several decades, focused investigation of the MSC within various interdisciplinary studies was aimed at understanding the mechanisms governing its timing, paleogeography, and the inter-relationship between external forcing and physical systems response. However, while the deep-basin halite was penetrated in its uppermost part (Fig. 1), the prohibitive risk and high drilling cost of ~~drilling~~ recovering cores through the entire deep-basin MSC unit has resulted in a critical lack of data. Scientific drilling of the deep Mediterranean basins has been repeatedly called for in order to test and validate different hypotheses regarding the MSC in the deep Mediterranean basins (CIESM, 2008; Dela Pierre et al., 2014; Gvirtzman et al., 2017; Manzi et al., 2015, 2018; Meilijson et al., 2018), but has yet to be achieved.

The MSC came into awareness and was documented as early as the 1950's, when massive evaporite outcrops in the peri-Mediterranean were identified as co-occurring around the end of the Miocene (Selli, 1954; Ogniben, 1957). However, the MSC magnitude and extent became clear only when seismic imaging penetrated the massive diapiric and stratified salt bodies of the Mediterranean Sea, reaching more than 2 km in thickness and stretching across vast parts of the basin (e.g., Bourcart et al., 1958; Alinat and Cousteau, 1962; Cornet, 1968; Ryan et al., 1971; Bellaiche et al. 1974; Ryan, 1976). One of the oldest controversies related to the MSC concerns the magnitude and timing of sea-level lowering and desiccation, where several models for evaporite formation have been suggested. Some have proposed that salt was precipitated in deep basins under a deep-water environment (Schmalz, 1969; Debenedetti, 1982; Sonnenfeld and Finetti, 2011), while other scenarios promoted a desiccated shallow-water environment (Hsu, 1973). A hybrid model was proposed, with early brine formation in the deep Mediterranean, preceding substantial drawdown, followed by massive salt precipitation during gateway closure (Ryan, 2008; Garcia-Castellanos and Villaseñor, 2011; Lofi et al., 2011). Clauzon et al. (1996) recognized the occurrence of shallow-water first cycle gypsum beds of the same age in many localities in the western and eastern Mediterranean. Based on this observation they presented a 2-step model, in which the surface of the Mediterranean Sea remained close to the global oceans level during the early part of the crisis, and deep-basin evaporites formed following sea-level drop of the subsequent step. Based on this model, Ryan (2011) described the geodynamic response of the basin to each of these steps: 1) Significant deepening of the basins by isostatic load due to an increase in weight of the brine layer. 2) As the basins dried out, the loss of weight of the water led to regional isostatic uplift that permanently closed the prior inlets.

Van Couvering et al. (1976) were the first to propose a similar 2-step model, which also portrays an early deposition of halite in the deep basins: (1) An initial deep-water phase marked by refluxive concentration of brines and controlled by a tectonically elevated sill, during which evaporites and associated sediments accumulated simultaneously near the surface in marginal areas (gypsum) and within great saline water bodies in the depths of the basin (halite). (2) A terminal phase of total isolation, caused by an eustatic sea--level drop, during which erosion and desiccation features were developed that fit the "deep-basin, shallow-water" model. However, this model was later abandoned in favor of what developed into the CIESM (2008) workshop consensus stratigraphic model, which was elaborated in the extensive review of the MSC by Roveri et al. (2014a) and widely cited.

The CIESM (2008) stratigraphic model of the MSC is based on correlation of Mediterranean evaporite sequences deposited in marginal to intermediate basins, and their isotopic signatures (Keogh and Butler, 1999; Müller and Mueller, 1991; Flecker and Ellam, 2006). While the division of MSC units differs slightly in terminology between the CIESM (2008) model and the widely used review of the MSC presented by Roveri et al. (2014a), they both stem from the same stratigraphic concepts, and are jointly referred to here as the ‘consensus model’ for MSC chronology. These studies demonstrate that partial connectivity with the Atlantic Ocean persisted throughout the first phase of gypsum deposition, lasting for ~370 kyr and known as MSC phase 1: Primary Lower Gypsum [PLG], 5.97–5.6 Ma.

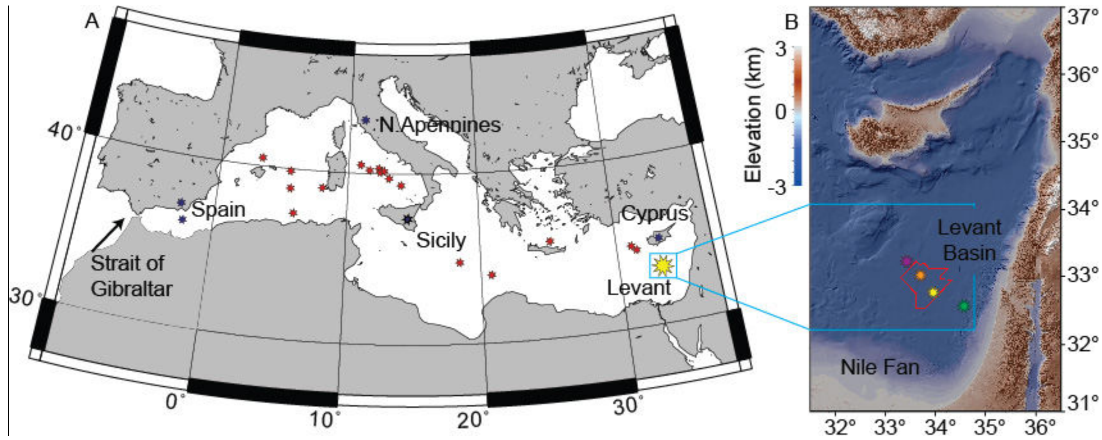

Figure 1. Map of the Mediterranean Sea marking the study area and referenced sections. **A.** Map of Mediterranean Sea marking study area (yellow star); main referenced sections (blue stars); and Deep Sea Drilling Project and Ocean Drilling Program wells (red stars), which penetrated MSC halite deposits only at their uppermost part. **B.** ~~Bathymetry~~ A shaded relief map of the Levant Basin and surrounding area (Hall et al., 1994, 2015). Red polygon outlines the three-dimensional seismic cube referred to in this study. Well locations marked by stars: Aphrodite-1 (purple star), Leviathan-1 (orange), Dolphin (yellow), and Sara (Green).

During the PLG, euxinic shales and dolostones were thought to have been deposited in the deep basins in parallel to gypsum deposition in the proximal settings (Lange and Krijgsman, 2010). However, using sonic and resistivity logs and samples from cuttings of the 497-Muchamiel oil-industry well, Ochoa et al. (2015) ~~found~~ observed all 14 of the known first-stage gypsum beds present in the Sorbas Basin, offshore southeast Spain, deep (875 -965 m) below the present-day sea level. This ~~finding~~ observation was ~~interpreted to contradict~~regarded opposite to previous assumptions that only shales would be present in this interval of the deep basins (CIESM, 2008; Roveri et al., 2014a).

The thick salt unit was interpreted as being accumulated during the succeeding MSC acme, a short period of ~50 kyr known as MSC phase 2: Resedimented Lower Gypsum [RLG], 5.6–5.55 Ma (although its top is often marked at 5.53 Ma in different cyclostratigraphic schemes (e.g., Roveri et al., 2014a; Manzi et al., 2015) due to the ‘Messinian gap’, during which Messinian erosion and/or deposition of resedimented gypsum and halite occurred). A model depicting the desiccation of the Mediterranean during stage 2 was proposed to explain its formation over such a short period of time. This model entails a massive sea~~-~~-level drawdown and consequent removal and re-deposition of the PLG gypsum, and a seasonal or long-term deposition of halite in intermediate to deep-water basins. Lastly, the third phase of the MSC was defined within the Upper Evaporites or Gypsum sequences (UG), which include clastic or brackish sediments culminating in the Lago-Mare deposits (5.55-5.33 Ma). The latter consist~~s~~ of several units with 7-10 sedimentary cycles identified in the Upper Gypsum of Italy overlying erosional surfaces and angular unconformities, and underlying Pliocene sediments (Hilgen et al., 2007; Krijgsman et al., 2010; Roveri et al., 2014a). A recent review of different Lago-Mare deposits depicts that three main pulses of seaward-transport occurred within the time-interval 5.~~70~~64-5.~~30~~ 33 Ma, and suggests abandonment of previous concepts dealing with a unique chronostratigraphic unit, favoring several episodes of flooding (Couto et al., 2014). Nonetheless, the first influx of Paratethyan organisms, identified through the dinoflagellate cyst record near Malaga within a fan delta, was found overlying the intra-Messinian truncation surface (IMTS) (Couto et al., 2014).

Recent industrial activities targeting hydrocarbon reservoirs in the Eastern Mediterranean ~~basin~~ Basin provide the scientific community with unparalleled seismics, well logs, and cuttings across the salt interval. The current work takes advantage of these industrial data to address two critical issues regarding Messinian stratigraphy in the deep Eastern Mediterranean Basin, which impact our basic understanding of this event: (1) To evaluate the composition, age and duration of evaporite deposition in the Eastern Mediterranean. (2) To characterize, interpret, and stratigraphically position the sediments overlying the IMTS (as in Gvirtzman et al., 2017), termed here the Interbedded and Argillaceous Evaporites. Here, we report previously unknown features and lithology of the deep basin MSC~~,~~ and, by using a multi-disciplinary approach, we provide further interpretation of their stratigraph~~ic significance~~y.

2. MSC deposits in the Levant

Feng et al. (2016) analyzed jointly well-log measurements and a pervasive seismic dataset, and demonstrated that the seismically transparent layers composing the majority of the Messinian evaporite~~s sequence~~ deposits across the deep Levant Basin ~~is~~ are composed of pure halite. The reflective layers appearing within the halite (Figs~~.~~ 2, 3) were interpreted as bundles of thin clay layers interbedded in the halite background, having a cumulative thickness of 25~~–~~-40 m. Feng et al. (2016) also reported high-~~-~~amplitude fan structures on the deepest internal reflectors, which may suggest transport mechanisms. Later, Gvirtzman et al. (2017) argued against a complete desiccation of the Eastern Mediterranean, following the seismic identification of the IMTS at ~100 m below the Messinian-Zanclean boundary in the Levant Basin. Based ~~solely~~ on interpretion of well logs and correlation to shallower-water wells, Gvirtzman et al. (2017) suggested that the post-truncation Messinian unit is different from the underlying salt deposits and mostly consists of shale, sand and anhydrite. Lastly, two separate studies (Manzi et al., 2018; Meilijson et al., 2018) have investigated the sediments underlying the evaporites, based on data from different wells within the Levant Basin. Both studies address the stratigraphy of the Pre-Evaporites and are aimed at providing an indication for the age of the base of the halite in the deep Eastern Mediterranean, represented on seismic data in the region as the 'N' reflection (Ryan, 1978; Bertoni and Cartwright, 2007)~~)~~. Establishing the age and duration of the deep-basin halite is perhaps the most enigmatic aspect of MSC research. Both recent studies test the CIESM stratigraphic model of the MSC (CIESM, 2008; Dela Pierre et al., 2014; Roveri et al., 2014a).

Manzi et al. (2018) and Meilijson et al. (2018) report several similar findings, such as the seismic interpretations regarding the conformity of the base of the evaporites, and thus refuting the occurrence of a long hiatus at the base of the evaporites. In addition, both studies indicate little deformation of the Levant ~~pre~~Pre-~~e~~Evaporite interval and a continuous record of the ~~upper~~ Tortonian to ~~Lower~~ Messinian ~~interval~~sediments. Still, different observations reported in these studies have led to continued uncertainty concerning the age and duration of salt deposition.

Meilijson et al. (2018) considered two alternatives for the age of the base evaporites in the deep basins: (1) during stage 1 (PLG) of the MSC at around 5.9 Ma, or (2) at around 5.6 Ma during stage 2 (RLG) of the MSC, as is described in the CIESM stratigraphic model (CIESM, 2008; Roveri et al., 2014a). The latter would imply a major hiatus of ~370 kyr (missing the PLG equivalent unit) at the base of the salt, or alternatively that the PLG is expressed as a very thin interval in the uppermost Pre-Evaporites unit. A hiatus in the deep basin has not been identified, but rather a visible lateral continuity of seismic reflectors below and at the boundary itself (Meilijson et al., 2018). This finding is consistent with published regional seismic sections (Feng et al., 2016; Manzi et al., 2018; Roberts and Peace, 2007) and elsewhere in the deep domain of the Mediterranean (Lofi et al., 2011). Thus, Meilijson et al. (2018) concluded that the studied section is in fact conformal and halite began to precipitate around the onset of the PLG in the marginal basins, predating the CIESM consensus for halite deposition by ~300 kyr.

Manzi et al. (2018) reported that in the Aphrodite-2 well (Fig. 1), which is the deepest location along their four-well cross-section, a complete absence of foraminifera occurs from 3959 m upwards, 28 m below the first occurrence of anhydrite, and 33 m from the base of halite deposition. They interpret this foraminifera barren interval (FBI~~I~~) as corresponding to the Non-Distinctive Zone (NDZ) marking the onset of the MSC (5.971 Ma) in marginal settings (Gennari et al., 2013; Manzi et al., 2013). Manzi et al. (2018) proposed that this interval represents the deep basin expression of the PLG, followed by halite deposition during stage 2 of the MSC at around 5.6 Ma. This FBI is argued by them to be further substantiated by a prominent peak of *Sphenolitus abies* at 3961 m, closely followed by a decrease in the number of species of calcareous nannofossils. The FBI was also identified by Manzi et al. (2018) in the Myra well, which is situated in a more proximal position, 90 km SW to the Aphrodite well. ~~Further~~ Farther landward to the west, the FBI is no longer recognized in the Sara well, where the Aphrodite well equivalence of about 60 m underlying the base of the evaporites is missing. This observation indicates that the Dolphin well should also include an equivalent FBI, as it is positioned between the Myra well, and closer to the latter (Fig. 1). However, such an FBI is not present in the Dolphin well, in which the samples include a relatively open-marine foraminiferal assemblage up to the uppermost sample available for analysis, representing the interval 0-9 m below the base of the evaporites (Meilijson et al., 2018). Thus, the MSC timing and events are still debated after more than 50 years of research and over 10,000 publications.

In recent years, different studies have been leaning towards new and very different ideas regarding MSC chronology, and thus the mechanisms controlling the deposition of salt giants in deep sea basins. Ochoa et al. (2015) demonstrated synchronous deposition of evaporites in marginal and intermediate basins. Simon and Meijer (2017) modeled stratification in the Mediterranean during the MSC and raised the possibility of a much earlier onset of halite in the deep basins. Finally, García-Veigas et al. (2018) even went so far as to draw a model for an early onset of halite, yet added a question mark next to this assumption due to lack of proof for this claim (their ~~Fig~~fig. 12). Here, we address this debate on the chronology of MSC events in the Mediterranean by examining the recovery of deep-~~-~~basin evaporites from the Levant Basin for stratigraphic indicators that can promote a better understanding of MSC chronology.

The MSC (CIESM, 2008; Roveri et al., 2014a) is expressed in the southeastern Levant Basin margins as a thick evaporitic sequence (locally named the Mavqiim Formation), as well as clastic evaporite deposits along local topographical lows (Buchbinder and Zilberman, 1997; Druckman et al., 1995; Lugli et al., 2013). The MSC deposits in the deep Levant Basin have been identified through seismic data, and interpreted as mainly consisting of halite, reaching a thickness~~es~~ of ~2 km in the central part of the basin and pinching out upslope towards its southeastern margin (Bertoni and Cartwright, 2007, 2006; Feng et al., 2016; Gardosh et al., 2008; Netzeband et al., 2006; Steinberg et al., 2011). The halite sequence base and top are generally imaged as pronounced high-amplitude seismic reflections, known as the N and M reflectors, respectively (Ryan, 1978). Up-dip, the evaporitic sequence thins below ~~the~~ seismic resolution and is entirely represented by the M ~~reflection~~ reflector (e.g., Steinberg et al., 2010). The nomenclature of the MSC section in the Levant Basin is currently based on the regional identification of a number of key markers within seismic sections across the basin, with several divisions presented by different studies: division of the section into 6 or 7 units (Gvirtzman et al., 2013b, 2017; Lugli et al., 2013), or into ME 1-4 (Messinian evaporites)~~,~~ and MC 1 and 2 (Messinian clastics; Feng et al., 2016). In this manuscript we refer to the unit numbers (Gvirtzman et al., 2017, 2013b) and ME/MC units (Feng et al., 2016), corresponding seismically to the lithostratigraphic descriptions and division of the Dolphin well sediments.

Several studies have shown that the seismic records of the MSC greatly differ between the Western and Eastern Mediterranean basins, and argued that it is impossible to properly correlate individual sub-units (Lofi et al., 2011). Some authors have also questioned the possible diachronism between both basins (Blanc, 2000; Ryan, 2008). However, the Levant has been for many years at the center of debate regarding the evolution of the MSC across the entire

Mediterranean ~~basin~~Basin. An example for such a long-term debate includes the formation of the vast drainage systems at the Mediterranean margins and the deposition, or re-deposition, of gypsum within them. An important type location for this debate is the Afiq canyon along the continental margin of Israel. The presence of evaporite layers at different levels along the Afiq canyon~~s~~ was brought as one of the first evidence for a substantial Messinian sea~~-~~-level drawdown (800 m sea~~-~~-level drop; Druckman et al., 1995). However, these deposits were recently argued to result ~~of~~ from evaporite~~s~~ recycling through slope mass-wasting, a phenomena suggested to characterize the upper parts of the MSC throughout the Mediterranean (Lugli et al., 2013). The wells investigated in this study were drilled in the Levant Basin, and may ~~be argued to~~ represent local conditions rather than account for the entire Mediterranean Basin. However, by recovering one of the most extensive evaporite deposits of the MSC, the analysis of these wells bears key implications for unraveling the MSC across the entire Mediterranean.

3. Methodology

This study is based on the combined analyses of well cuttings, 3D pre-stack depth-migrated reflection seismic~~s reflection~~, and well~~-~~-log data of two~~,~~ deep-water industry wells recently drilled in the Levant Basin (Fig. 1). We have also used a time-migrated 2-D seismic survey acquired by TGS-Nopec Geophysical Company in 2000, and the 3-D depth-migrated Pelagic seismic survey acquired by CGG-Veritas in 2009. Lithological and biostratigraphic data presented in this study are from the Dolphin well (N 3628144.05 m, E 575444.97 m), drilled by the Leviathan partnership at a water depth of 1~~,~~500 m and penetrating the 1~~,~~590 m thick Messinian evaporite section at depths of 2~~,~~026-3~~,~~616 m below sea level. The second studied well is the Leviathan-1 ~~well~~ (N 3653455.35 m, E 553663.40 m), also drilled by the Leviathan partnership at a water depth of 1~~,~~644 m and penetrating the 1~~,~~694 m thick Messinian evaporite section at depths of 2~~,~~090-3~~,~~784 m below sea level. The record presented in this study supplements the 350 m section immediately below the base of the halite shown in Meilijson et al. (2018). Samples were curated and archived in both the Organic Geochemistry Laboratory at the University of Colorado (organic extracts) and the Department of Marine ~~Geosciences~~ ~~,~~Geosciences, Leon Charney School of Marine Sciences, University of Haifa.

Drilled cutting~~s~~ returns are available starting down from a depth of 2~~,~~535 m and 2~~,~~497 m in the Dolphin and Leviathan-1 wells, respectively. The Pre-Evaporites interval of the Dolphin (Meilijson et al., 2018) and Leviathan wells was sampled every 3 m. The evaporite interval was sampled every ~9 m, with a total of 123 samples from the Dolphin well. Due to standard drilling activities, many fallouts of ~~the~~ clastic deposits occur downhole from the lower part of the ~~interbedded~~ Interbedded ~~evaporite~~ Evaporite unit to the upper part of the Main Halite unit, appearing as an interval of clastic deposits in the XRD log of the Dolphin well from 2~~,~~560 to 2~~,~~675 m. Well-log data does not respond to this high-clastic content (i.e., high RE log values and low GR log values), and so does not show a shift from halite deposition. This observation confirms that the clastic material arrive~~s~~ from the ~~Interbedded Evaporites~~ unit above, as drilling fallouts into the halite interval. While not in-situ, these fallouts, together with the well logs, allow us to interpret ~~at~~ the distinct lithological transition ~~occurring~~ that occurs at the boundary between the Main Halite and Interbedded Evaporites unit. However, these fallouts might also originate from the Argillaceous Evaporites unit above.

Individual cutting bits were separated by their lithology under a microscope, cleaned with deionized water and 10% hydrochloric acid, dried, and then crushed in an agate pestle and mortar. Fine powders were pressed and used for bulk mineralogical X-ray diffractogram (XRD) analysis using a Rigaku 600 MiniFlex X-Ray Diffractometer with a CuKα source at 30kV / 15-

mA from 3° to 70°. Mineralogical compositions of assemblages were determined using the ICDD PDF2 mineral database references. Next, fine powders were pressed in ~~telephone~~ Teflon crucibles with X-Ray transparent mylar (which was replaced between samples). Each sample was then analyzed using a Nitton X-Ray XL3 GOLDD+ Fluorescence apparatus for elemental composition.

Samples found to be bearing microfossils were investigated for their faunal assemblages, which included washing and picking foraminifera from the Pre-Evaporites (detailed in Meilijson et al., 2018) and the preparation of smear slides for the study of the diatomites interbedded within the halite. For the latter, samples were weighed, treated several times with 10% HCl for carbonate removal, and 30% hydrogen peroxide for organic matter removal, and then loaded onto glass slides. A total of 50 diatom valves were counted and identified from 10 samples. Diatoms were characterized by their habitat preferences: planktonic vs. benthic, and marine vs. freshwater.

We also studied the distribution of selected biomarkers (i.e., *n*-alkanes, algal steranes, and bacterial hopanes) from different intervals to gain insight into variations in organic matter sources and thermal alteration. Rock cuttings were cleaned and handled with solvent-rinsed metal tweezers, a Dremmel 8220 wire-brush tip, spatulas, and combusted aluminum foil, and then powdered with a solvent-rinsed agate mortar and pestle. Approximately 5-10 grams of sample were extracted using a Dionex Accelerated Solvent Extractor (ASE 200; 100 ºC; 2,000 psi) and a mixture of dichloromethylene:methanol 9:1 (v:v) until no more color was observed (typically 3-6 extractions). Each extraction cycle included heating of the cell for 5 minutes, static mode for 5 minutes, and flushing for 2 minutes time. A cocktail of internal standards containing 500 ng of D4 C_{29} ααα (20R)-Ethylcholestane, and 1,000 ng of each 3methyl heneicosane, D14 pTerphynyl, 1-nonadecanol, behenic acid methylester (Docosanoic acid), and 2methyl octadecaonoic acid, was added to samples before extraction for quantitation purposes. Total lipid extracts (TLEs) were combined and evaporated under a gentle nitrogen flow using a Turbovap. Elemental sulfur was removed using HCl-activated copper shots. TLEs were then filtered through small Pasteur pipettes filled with combusted glass wool and sand to remove impurities and any copper-sulfide residues. Asphaltenes were separated from maltenes by precipitation in hexanes at 4^0C for 3 hours, followed by centrifugation at 2000 rpm (3x). Maltenes were later separated into five different lipid classes by liquid chromatography on small Pasteur pipettes filled with silica gel. Aliphatic (F1) and aromatic (F2) hydrocarbons were recovered with hexane (3/4 dead volumes) and hexane:dichloromethylene 8:2 (v:v; 4 dead volumes), respectively. The more polar fractions (F3, F4, F5) were eluted using dichloromethylene, dichloromethylene:EtOAc 1:1, and EtOAc (v:v, 4 dead volumes), respectively. Aliphatic hydrocarbons were analyzed on full scan and selected reaction monitoring (SRM) modes via gas chromatography – triple quadrupole-mass spectrometry (GC-QQQ-MS) using a Thermo Trace 1310 Gas Chromatograph interphase to a TSQ Evo 8000 triple quadrupole mass spectrometer (GC-QQQ-MS) equipped with a split-less PTV injector and electron impact ion source. Helium was used as a carrier gas with a flow rate of 1.2 ml min^{-1}. Chromeleon 7 was used for data integration. Aliphatic hydrocarbons were separated using a 60-meter DB-1MS GC column (60 m, 0.25 mm I.D., 0.25 μm film thickness; Agilent Technologies). For FS analysis, sampled were injected at 60°C and then the PTV was heated to 300°C at 14.5°C/second. The GC oven temperature program was: 60°C (2 min) to 150°C at 15°C min^{-1}, to 315 (held 24 min) at 3°C min^{-1}. The total GC program was 90 minutes. MS conditions were: 300°C ion source at 70eV electron energy, 50uA emission current, and 15V electron lens voltage. The mass range was 50-

600 m/z with a dwell time of 0.2 seconds per scan. For SRM analysis, the GC oven temperature program was: 60°C (0 min) to 220°C at 15°C min^{-1}, to 315°C (held 25 min) at 3°C min^{-1}. The total GC program was 68 minutes. Samples were injected at 65°C and then the PTV temperature was heated to 400°C at 3 °C min^{-1}. MS conditions were: ion source temperature of 250°C; transfer line temperature of 320°C, electron energy of 70eV, electron lens voltage of 35V, and emission current of 35uA. Peak scanning windows ranged from 0.6 to 1 minute for 147 timed transitions for regular and methylated steranes and hopanes, and their stereoisomers.

4. Evidence from the Levant Basin for an early onset of halite deposition in a deep-water environment

4.1 Lithologic composition of the Levant deep-sea salt-giant

4.1.1 Pre-Evaporites

This interval is detailed in Meilijson et al. (2018). Here we provide a generalized summary, followed by a more elaborate account of the overlying evaporites of the deep Levant Basin. The ~~pre~~Pre-~~evaporite~~ Evaporite interval in the Dolphin well (3850–3616 m; Fig. 2) is seismically characterized by sub-horizontal and sub-parallel continuous high-amplitude reflections, implying a stratified and relatively un-deformed marine succession (Meilijson et al., 2018). It is composed of fine-grained clastic-micritic and carbonate bathypelagic sediments, primarily gray to dark gray or greenish calcareous soft to hard shale, with several thin layers of white to light gray hard limestone, and light gray very fine to fine-grained unconsolidated sandstone. Diverse assemblages of nannofossils, benthic and planktic foraminifera are recognized within this interval.

Figure 2. The MSC succession of the Dolphin well in the deep Levant ~~basin~~Basin.

A juxtaposed simplified display of the primary proxies used to characterize the Dolphin well section (five central columns), and our depositional (left) and lithological (right) interpretations. The attributes are (left to right): the faunal composition; the seismic response, with transparent intervals representing predominantly evaporites and high-~~-~~amplitude reflections representing clastic beds (a seismic trace (center) emphasizes relative intensity of the seismic phases); XRD mineralogy, showing the relative abundance of halite (bright) vs. non-halite (dark; 'marine clastics'), where the uppermost clastic interval (<2~~,~~650 m) represents fallouts from the ~~interbedded~~ Interbedded ~~evaporites~~Evaporites; the gamma ray (GR ~~—~~- API units) and resistivity (RE ~~—~~- log ohm-m units) logs, color coded based on the characteristic responses to halite and clastics. The lithological interpretation is color coded as in the attribute columns. Planktonic foraminiferal (PF) bio-events in blue circles correspond to the following ages: 1- 7.72, 2- 7.24, 3- 6.72, 4- 6.36, and 5- 6.13 Ma (Meilijson et al., 2018).

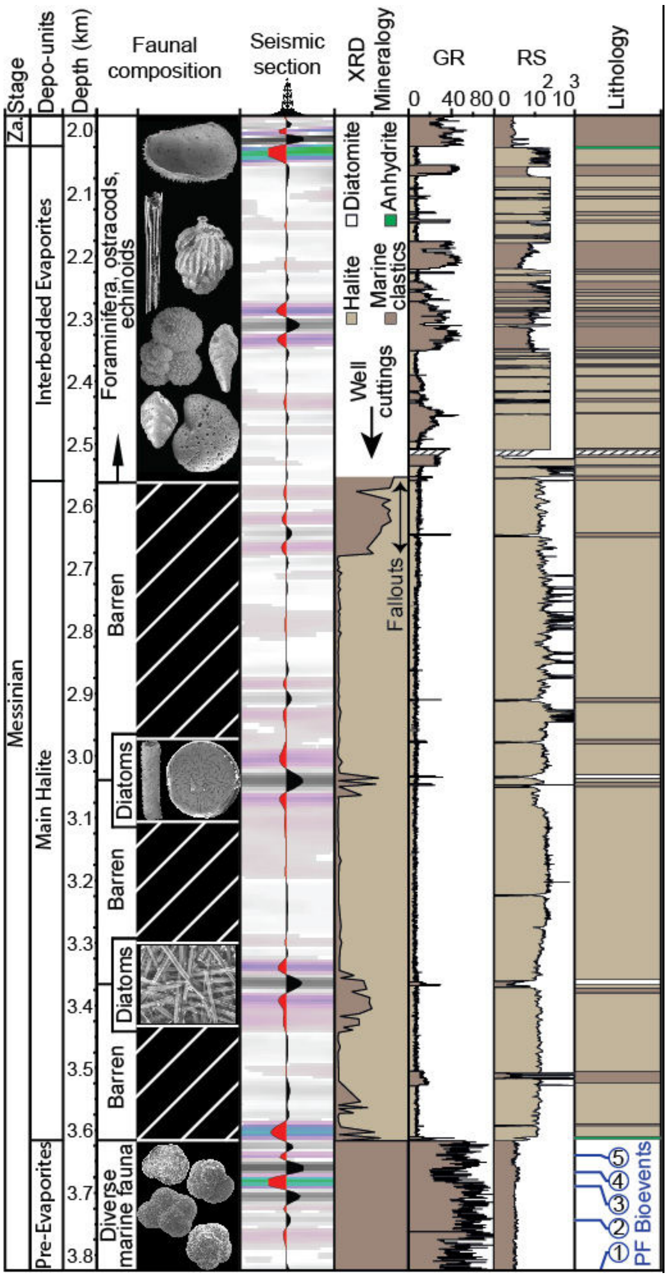

Stage
Depo-units
Depth (km)
Faunal composition
Seismic section
XRD Mineralogy
GR
0 40 80
RS
0 10^2 10^3
Lithology
Za.
Messinian
Interbedded Evaporites
Main Halite
Pre-Evaporites
2.0
2.1
2.2
2.3
2.4
2.5
2.6
2.7
2.8
2.9
3.0
3.1
3.2
3.3
3.4
3.5
3.6
3.7
3.8
Foraminifera, ostracods, echinoids
Barren
Diatoms
Barren
Diatoms
Barren
Diverse marine fauna
Diatomite
Anhydrite
Halite
Marine clastics
Well cuttings
Fallouts
PF Bioevents
1
2
3
4
5

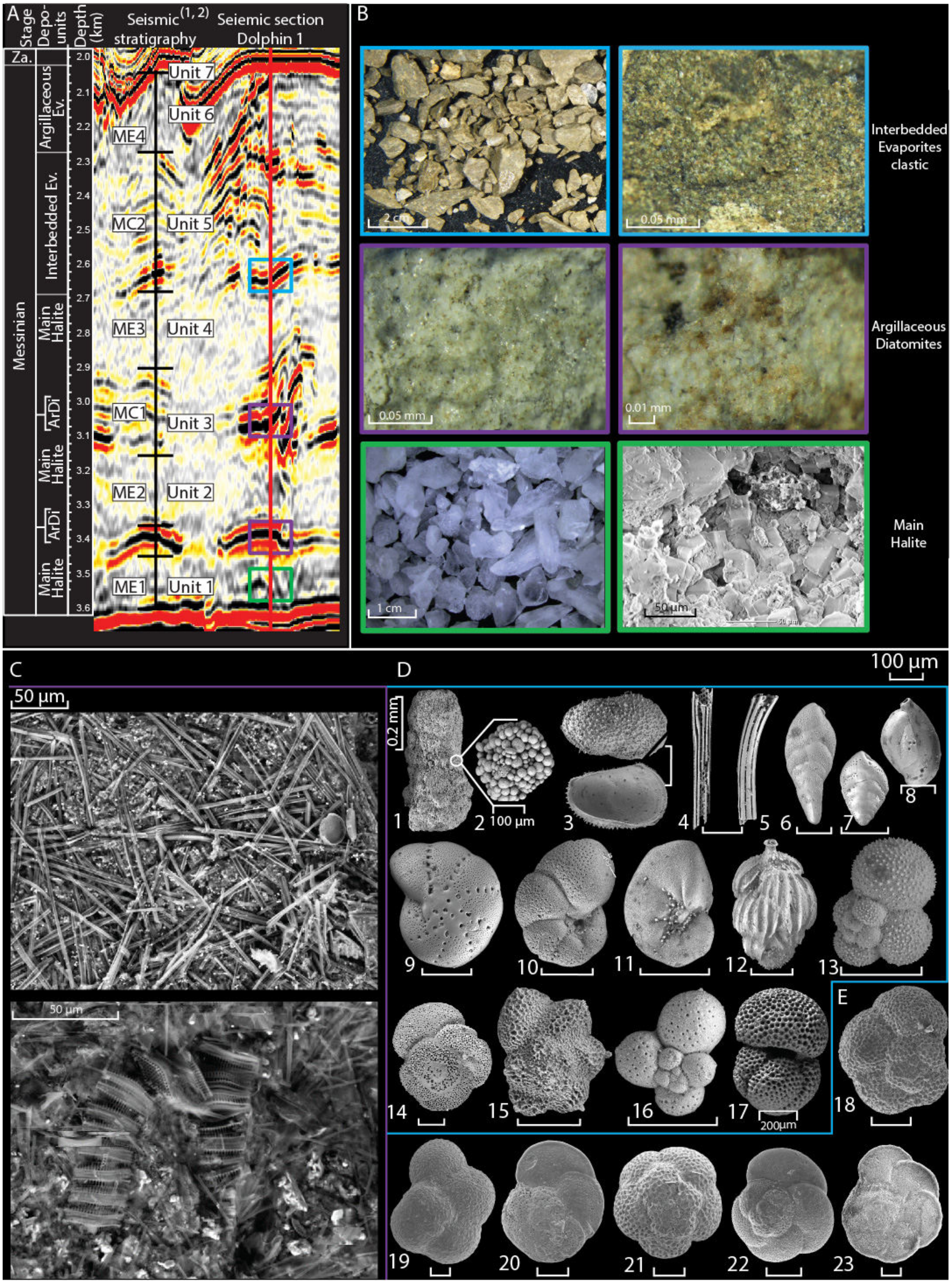
A
Stage
Depo-units
Depth (km)
Seismic(1, 2) stratigraphy
Seiemic section Dolphin 1
Za.
Messinian
Argillaceous Ev.
Interbedded Ev.
Main Halite
ArDi
Main Halite
ArDi
Main Halite
2.0
2.1
2.2
2.3
2.4
2.5
2.6
2.7
2.8
2.9
3.0
3.1
3.2
3.3
3.4
3.5
3.6
Unit 7
Unit 6
ME4
MC2
Unit 5
ME3
Unit 4
MC1
Unit 3
ME2
Unit 2
ME1
Unit 1
B
2 cm
0.05 mm
Interbedded Evaporites clastic
0.05 mm
0.01 mm
Argillaceous Diatomites
1 cm
50 µm
Main Halite
C
50 µm
50 µm
D
100 µm
0.2 mm
100 µm
200µm
E
1
2
3
4
5
6
7
8
9
10
11
12
13
14
15
16
17
18
19
20
21
22
23

Figure 3. Seismic stratigraphy, common lithologies, and SEM imaging of the studied section. **A.** The seismic profile crossing the sampled Dolphin well position and its division into the MSC depositional units, compared to previously published seismic stratigraphy of the deep Levant MSC ((1) Feng et al., 2016; (2) Gvirtzman et al., 2017). ArDi ~~—~~- Argillaceous Diatomites; Ev. - Evaporites. Color coded rectangles corresponding to lithologies described in (B). **B.** images of the three main facies recognized in the Levant evaporite section: the homogeneous ~~main~~ Main ~~halite~~ Halite (green rectangle) made of pure halite as seen in hand specimen (left) and SEM imagery of cubic cleavage (right), corresponding with subdued internal seismic reflectivity in (A); Argillaceous Diatomite beds (purple rectangle), represented by high amplitude reflections in (A); and Interbedded Evaporites (blue rectangle) identified as brown marine clastics, characterized by interchanging low and high amplitude reflections in (A). **C.** Selected SEM images from the densely packed and very well preserved diatoms from the diatomite facies. **D.** Selected SEM images of the >63 µm size fraction of the washed residue from the Interbedded Evaporites unit clastic sediments (P.1-17) showing: large grains of framboidal pyrite (P.1-2), well-~~-~~preserved ostracod valves (P.3), sea urchin spines (P.4-5), benthic foraminifera (P.6-12), and planktic foraminifera (P.13-17). **E.** SEM images of the planktic foraminifera used for the biostratigraphic age -model (Meilijson et al., 2018) of the ~~pre~~Pre-E~~e~~vaporites (P.18-23): *Neogloboquadrina* sp. (P.18), *Sphaeroidinellopsis seminulina* (P.19), *Globorotalia miotumida* (P.20), *Globoquadrina altispira* (P.21), *Globorotalia scitula* (P.22); *Globorotalia menardii*-4 (P.23). All scales are 100 µm unless indicated otherwise.

Shale samples are organic-~~-~~rich (>1 wt.% TOC) and reach peak values of 4 wt.% TOC immediately underlying the base of evaporite deposition (Meilijson et al., 2018). Lower values of gamma ray (GR) are associated with silt/carbonate-rich sediments, while higher GR corresponds to shale/organic-rich sediments (Fig. 2).

4.1.2 Main Halite

Here we reference our lithologic interpretation to the recently defined seismic stratigraphy of the Levant MSC (~~units~~ Units 1-6; Gvirtzman et al., 2013), and ME1-4 for the transparent and

MC1-2 for the high reflectivity intervals (Feng et al., 2016) (Fig. 3). Different velocity models reported high seismic velocities of 4200-4400 m/s (Gvirtzman et al., 2013a), 3850-4240 m/s (Reiche et al., 2014), and 4400-4600 m/s (Feng et al., 2016) for the seismic transparent layers, interpreted as representing the halite facies. Here we advocate this interpretation by providing the first semi-quantitative XRD analysis (Fig. 4) of well cuttings spanning the transparent high velocity layers.

The Main Halite unit in the vicinity of the Dolphin (3616- 2755 m) and Leviathan-1 (3759-2800 m) wells is characterized by low seismic reflectivity, which is internally interrupted by several main high reflectivity bands (Figs. 5, 6). These instances are clearly recognized in the well -logs (Fig. 2, 5), and represent a different facies within the hyper-saline deposits, described aheadbelow. Using XRD analysis coupled with SEM (Fig. 4), we conclude that the transparent intervals are indeed composed of nearly pure (~ (>90%) halite (Fig. 4), with minor quantities of anhydrite, magnesite and barite. Anhydrite appears is also present as a relatively thin bed (<-3 m) at the base of the Main Halite section, where it represents the transition to the Main Halite. Anhydrite also further appears in the upper, more clastic Interbedded Evaporites part of the section (2560-2025 m; Fig. 2), as is also reported from the same stratigraphic level interval by Gvirtzman et al. (2017). The halite is clear to milky white with a firm to very hard macrocrystalline structure (Fig. 3), while the anhydrite minerals are white, soft to firm, nodular and amorphous to massive. A sharp transition from the Pre-Evaporites to halite is marked by a decrease in GR well log counts from 53 API to 12 API as well as a sharp increase in the formation resistivity (RE) well log reaching 10,000 ohm (Fig. 2; see also Feng et al., 2016).

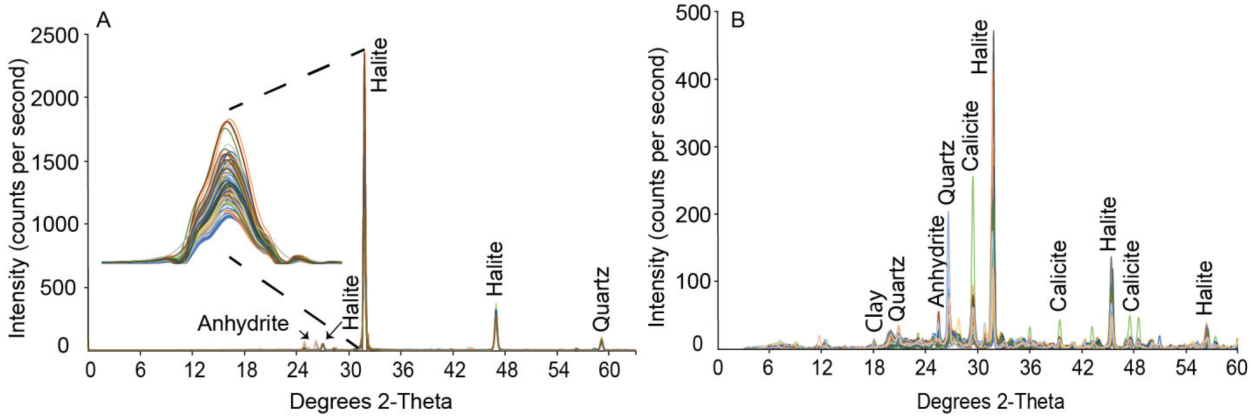

Figure 4. X-ray diffraction results

A. Overlaid (color coded) XRD analysis of 89 halite samples from the Dolphin well produced diffractograms, which are practically identical. The main halite peak is zoomed for emphasis. **B.** Higher variability is recorded both in peaks location and intensity when analyzing samples from the non-evaporitic marine sediments, sampled along the section between the depth of 3,616 m to 2560 m.

These values remain relatively constant within the halite deposits, although inter-halite variations are observed, mainly on the RE log. The pronounced high-amplitude reflection at ca. 3520 m (Dolphin well; Figs. 2, 3), also recognized as an increase in the GR well -logs, represents a short-term return to the clastic Pre-Evaporites facies although with low abundance and poorly preserved foraminiferal content. This interval is not part of the Argillaceous Diatomites facies.

4.1.3 Argillaceous Diatomites

Distinct reflective layers appear within the seismic transparent halite expressions, correlating with relatively lower velocity zones in the seismic velocity models developed for the deep Levant Basin MSC strata (e.g., 3800-4000 m/s in Gvirtzman et al. (2013); 3650-4030 m/s in Reiche et al. (2014)). These reflective layers are easily identified across the study area (Figs. 5, 6).

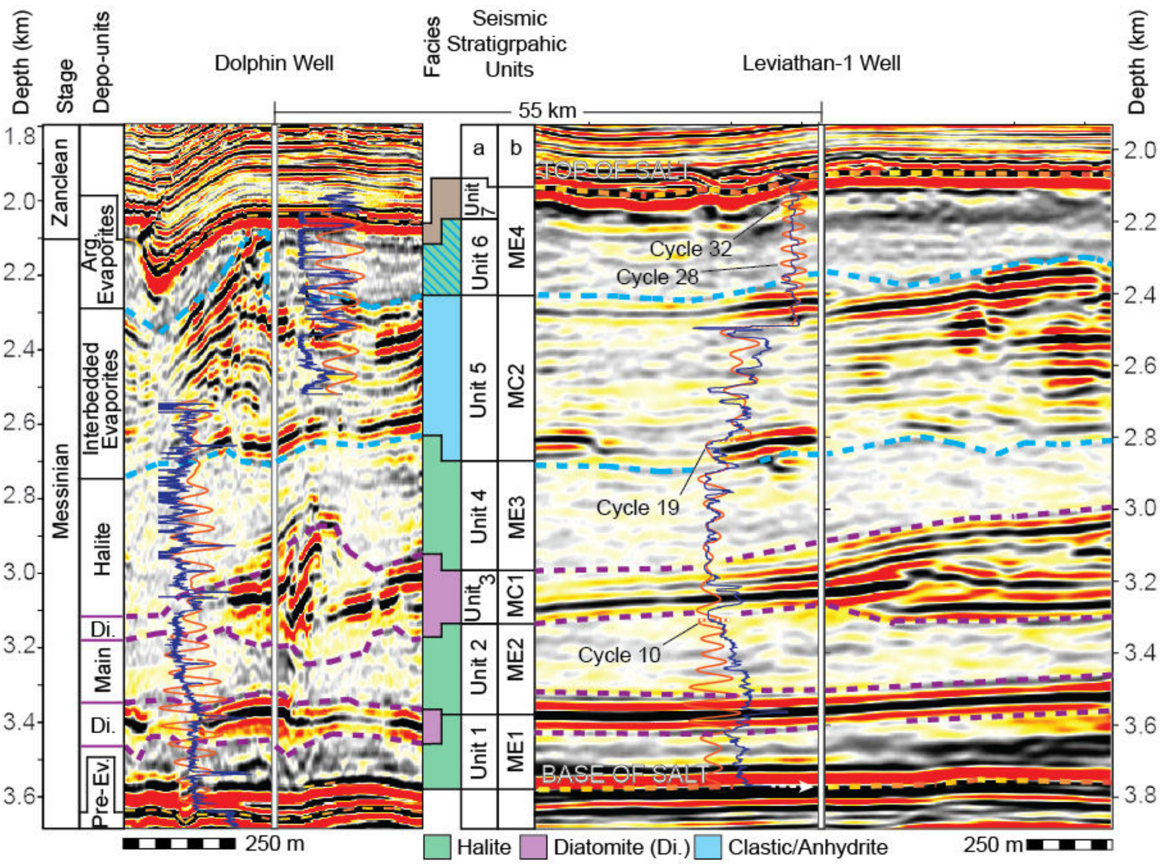

Figure 5. Geophysical data and seismic stratigraphy of the Dolphin and Leviathan-1 wells. Depth-migrated sections crossing the Dolphin (left) and Leviathan-1 (right) wells (marked by a vertical white line). Overlaid on the sections are the well logs (blue curve left to the well), and the filtered well-log cycles superimposed on the target curves (orange). The depth and lithostratigraphic units (this work) related with the sampled Dolphin well are displayed on the left, and the depth related with the Leviathn-1 well is displayed on the right. Data columns in the middle are seismic-stratigraphic units from (a) Gvirtzman et al. (2013, 2017), and (b) Feng et al. (2016). Note the relatively deformed area of the Dolphin well relative to the more conformal vicinity of the Leviathan-1 well.

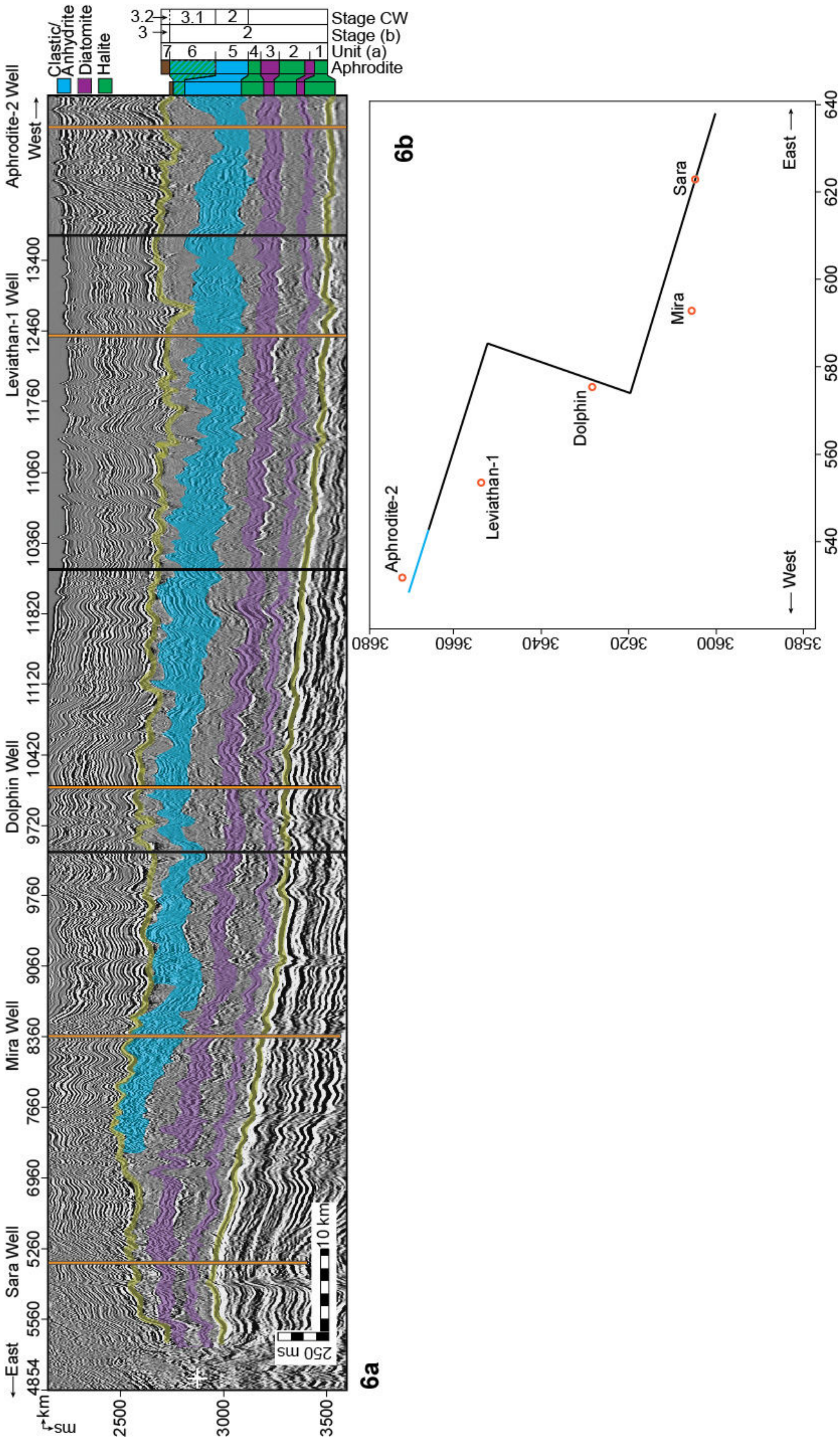

6a
6b
Stage CW
Stage (b)
Unit (a)
Aphrodite
Clastic/Anhydrite
Diatomite
Halite
Aphrodite-2 Well
Leviathan-1 Well
Dolphin Well
Mira Well
Sara Well
West
East
10 km
250 ms
Aphrodite-2
Leviathan-1
Dolphin
Mira
Sara

Figure 6. A composite seismic section linking the commercial wells across the Levant Basin. A composite time-migrated seismic section (a), and location map (b), combining three 2D traverses of the TGS survey (dark line) with a transect through the Pelagic 3D volume (blue line) across the Levant Basin, all plotted at a common scale with a vertical exaggeration of ca. x10. Orange vertical lines note the positions of the wells discussed in the text, while black lines note the section stiches, primarily at turning points. The wells are projected laterally onto the seismic profiles by up to 10 km (in the case of the Leviathan-1 well). Note the similar relative spatial thickness of the diatomite beds (purple) in comparison with the largely varying thickness of the Interbedded Evaporites (blue). Stage CW (current work); Stage (b) (Manzi et al., 2018); Unit (a) (Gvirtzman et al., 2013; 2017).

In the Dolphin well, this seismic facies includes five seismic high-reflectivity bands, corresponding to peaks in the GR and troughs in the RE well-logs, appearing within the Main Halite interval between 3375 and 2560 m (Fig. 2). Using a GR value of 20 API as an upper cutoff value for determining the location and thickness of these intervals, results in estimated bed thicknesses of 0.9-2.4 m (Fig. 2). Of the 1,056 m Main Halite interval in the Dolphin well, the non-halite sediments form a regional cumulative thickness of 25-40 m (see also Feng et al., 2016; Gvirtzman et al., 2013). At the macro-scale, the content of these layers appears as light gray to white, soft to firm, porous, and occasionally fibrous. SEM imaging and smear-slide analyses indicate that the rock-mass is made of densely packed, very well-preserved, and intact diatoms (Fig. 3), and fine-grained terrigeneous sediments (Fig. 4). No other transported or local faunal remains were recognized. Identified diatoms include abundant marine planktonic genera, such as *Coscinodiscus*, *Asteromphalus*, and *Actinoptychus* (*sensu* Tomas, 1996).

XRD analysis from available samples of these high-amplitude intervals confirms the log data response and shows an increase in terrigeneous grains, mainly composed of quartz, calcite, some clay minerals, and low amounts of anhydrite, dolomite and magnesite (Fig. 4). Halite appears within these samples in a high relative abundance, reaching 45% (Figs 2, 4).

Due to the nature of well cuttings, samples from these intervals were only retrieved from the two thickest beds, at 3367.7 m of the Dolphin well with a thickness of 2.4 m, and the two adjacent beds at 3047 and 3034 m with a cumulative thickness of 2.1 m. These intervals are also represented by bands of much higher seismic reflectivity than the thin (1.2-1.4 m), overlying intervals at 2910 and 2646.5 m. Consequently, the two upper intervals might be the same diatomite facies, or only represent marine clastic sediments.

4.1.4 Interbedded Evaporites

This facies is represented in the seismic sections by high-amplitude reflections interbedded with nearly transparent intervals with weak internal reflections (Fig. 3), interpreted in previous studies to represent an alternation of clastic sediments and evaporites (Gvirtzman et al., 2013a; Feng et al., 2016). More recently, Gvirtzman et al. (2017) and Manzi et al. (2018) presented further evidence based on well logs from deep-basin wells in the region (Aphrodite), or by correlation to more proximal well sections (Hannah-1), showing that this interval mostly consists of shale, sand, anhydrite, and halite. The Interbedded Evaporites unit correlates to Unit 5 in Gvirtzman et al. (2013). It covers 2560-2025 m in the Dolphin well, and 2548-2276 m in the Leviathan-1 well. The GR well log in the Leviathan-1 well indicates 3 to 20 m thick clastic beds, interbedded with evaporites varying in thickness from 6 to 30 m. A relatively large diameter wellbore used while drilling this interval might have reduced the GR signal and thinner clastic beds might not have been detected.

Due to drilling limitations, the material made available from this interval is partial, and the only sampled sequence consists of the lowermost part above 2560 m in the Dolphin well. We consider grains from this interval as fallouts from the Interbedded Evaporites unit, confirmed by the absence of any indications for a clastic interval in the well-log and seismic data from the top of the Main Halite interval, were these grains appear. The samples are made of hard, light to dark brown sandy shales (Fig. 3). The grain composition of the >63 µm washed residue is very different compared to the underlying Main Halite or Argillaceous Diatomite facies. It contains a higher amount of sub-rounded larger sand grains compared to the diatomite facies, different types of pyrite including large agglutination of pyritohedrons reaching several mm in size, and a diverse faunal composition (Fig. 3). The latter includes few mollusk fragments, ostracods, echinoid~~sea urchin~~ spines and a relatively rich assemblage of benthic and planktic foraminifera (Fig. 3). The most common foraminifera are different *Globigerinoides* species, *Orbulina universa* and *Sphaeroidinellopsis seminulina* (younger than 15 Ma; Berggren et al., 2006). Older Cretaceous to Eocene foraminifera species are also present, indicating reworking processes, most likely from exposed basin margins. These include *Parasubbotina pseudobulloides* (Daninan-Selandian; Fig. 3.D.13), *Plummerita hantkeninoides* (Maastrichtian; Fig. 3.D.15), and *Subbotina triloculinoides* (Paleocene; Fig. 3.D.17). While no overlying samples exist, this interval was logged and a reliable lithological interpretation is presented by extrapolating the coupling between sample analysis (XRD and micropaleontology) and the log data from the lower to the upper part of the section (Fig. 2). The clastic input is estimated from the geophysical data as ~40% of the 535 m thick unit in the Dolphin well. However, due to local deformations in the Dolphin well area, the Interbedded Evaporites are displaced and ~~reach at~~ their top is reached at the top of the MSC section.

~~Comparing~~ Comparison with~~to~~ Manzi et al. (2018) suggests that~~,~~ Unit 6 is not represented in the Dolphin well but ~~rather~~ that Unit 5 ~~reaches~~ marks the top of the section (Fig. 5). However, seismic and well~~-~~-log interpretation indicates that in the Leviathan-1 well another ~200 m of evaporites appear above the Interbedded Evaporites, ~~correlating~~ which corresponds to Unit 6 in Manzi et al. (2018). There, the Interbedded Evaporites (Unit 5) are 260 m thinner than in the Dolphin well (Fig. 5). This discrepancy is presumably the result of post-depositional halokinetic deformation and imbrication of ~~unit~~ Unit 5 in the Dolphin well, as imaged in the seismic data (Fig. 5).

4.1.~~4~~ 5 Argillaceous Evaporites

This interval was not sampled in any of the Levant Basin studies and ~~any~~ its interpretation ~~of it in the present~~ is only based on the interpretation of seismic and well~~-~~-log data. In the Leviathan-1 well this interval covers the ~~top~~ uppermost part of the evaporites ~~at~~ between 2~~,~~090 ~~m~~ and~~to~~ 2~~,~~320 m (Fig. 5). The transparent reflective character of this interval in the seismic section includes cyclic darker bands. The unit appears to be composed of clastic sediments, probably clays, silts and sands, which are characterized by GR values of 7~~api~~ to 15 ~~api~~API. Intervals of ca. zero GR are interpreted as argillaceous anhydrite. Gvirtzman et al. (2013; 2017), Feng et al. (2017), and Manzi et al. (2018) refer to this interval as Unit 6, ~~and it~~which is generally lumped with the underlying halite as part of the evaporite unit. Regionally, the presence of Unit 6 is limited to the westernmost and deeper areas of the basin, while it is truncated to completely removed landward to the east (Fig. 6). The amount of truncation on Unit 6 gradually increases eastwards, eroding also Units 5-2 at the eastern parts (Gvirtzman et al., 2013, Feng et al., 2017; the current study). Both the Dolphin and the Leviathan wells are within the deeper areas in which Unit 6 is present, but due to local deformations it might be underrepresented in the Dolphin well.

A 5 m clastic and ~~anhydrate~~ anhydrite ~~interval~~ bed defines the top of~~tops~~ ~~the MSC~~this unit, marked by a nearly transparent seismic interval in the Leviathan-1 well, as indicated by a sharp drop in GR and drilling penetration rate relative to the overlying Pliocene sediments. This anhydrite interval ~~might be~~is most likely part of Unit 7 in Gvirtzman et al. (2018), or the Nahal Menashe in Madof et al. (2019).

4.2 Chronology of halite deposition and well log frequency analysis

In order to attain a direct age control on the duration of halite deposition, the halite samples were washed and inspected for microfossils, prepared as smear slides, and examined under SEM in search for the preservation of eukaryotic life in the evaporites, which failed.

We also measured the Sr-~~-~~isotopic composition of evaporite samples in order to compare them with the well-established Sr isotope stratigraphy constructed from elsewhere in the Mediterranean (e.g., Topper et al., 2011; Roveri et al., 2014; Flecker et al., 2015). This published dataset shows that Sr-~~-~~isotope data from stage 1 lie~~s~~ mainly within error of the ocean-~~-~~water curve (McArthur et al., 2012), suggesting that the Mediterranean was connected to the global ocean during the initial phases of the MSC (e.g., Roveri et al., 2014; Flecker et al., 2015). During stages 2 and 3 the Mediterranean's Sr record diverges from ocean-~~-~~water values towards much lower ratios that reflect a substantially smaller connection to the global ocean and dominance of fresh-~~-~~water sources such as the Nile, Rhone, and input from the Paratethys, particularly during the Lago Mare phase (e.g., Roveri et al., 2014; Flecker et al., 2015). Sr-~~-~~isotope data from the lowest Pliocene are again within error of ocean-~~-~~water values, indicating an abrupt transition back to full connectivity after the MSC (e.g., Roveri et al., 2014; Flecker et al., 2015). Despite the wide geographical distribution of the Mediterranean samples from which this published Sr-isotope stratigraphy has been constructed, the pattern appears to be consistent, indicating that the controlling factor was Mediterranean-Atlantic exchange and that the Mediterranean behaved as a single basin throughout the MSC (Flecker et al., 2015). However, the dataset does not include samples from these deep-water Eastern Mediterranean sites as they were previously not available; ~~and~~ it therefore makes sense to compare new analyses from these locations with the existing Sr-~~-~~chemostratigraphic scheme.

Halite is highly soluble and it is therefore challenging to clean samples prior to analysis. We used the basic method described in Gvirtzman et al. (2017) and Manzi et al. (2018), with additional eleven different techniques (Fig. S1, Table S1) for attempting to isolate the halite ~~grains~~ crystals from any contaminant phases coating the samples such as clay or industrial drilling additives. The data generated for each of the nine different samples analyzed is highly variable, ranging from a few values within error of Late Miocene ocean water (McArthur et al., 2012), to substantially higher values (Fig. S1, Table S1). There is no consistency between the data generated and the technique used for dissolving the halite (Fig. S1, Table S1), suggesting that we have not been able to reliably isolate the halite from contaminant phases coating the crystals by any of the methods used. We therefore conclude that none of this data should be considered as representing a primary record of Eastern Mediterranean water at this time.

Similar high values have been reported for halite from other industrial wells in the Levant Basin (Gvirtzman et al., 2017; Manzi et al., 2018). Manzi et al.~~,~~ (2018) attributed the anomalously high values to “local, diverse, short-term Sr input”, but did not specify what this input might be. One possibility is that these published halite values from industrial cuttings may, like our data, ~~also~~ be contaminated. We conclude that a robust Sr-~~-~~isotope record for the deep-basin halite deposits will only be achieved either by establishing a reliable method for removing contaminant phases or by recovering halite samples without the use of industrial drilling fluids, e.g., through scientific drilling (Camerlenghi et al., 2014).

Next, we attempted to construct a chronostratigraphic framework for the Levant MSC deposits based on astrochronological tuning. We carried out spectral analysis of GR and RE well-logs to correlate the Levant MSC section to astronomical target curves, and the more proximal to onshore Mediterranean MSC deposits. REDFIT spectral analyses (Schulz and Mudelsee, 2002) of the Dolphin and Leviathan-1 well-log data from the base to the top of the evaporite unit (3616-2025 m in the Dolphin well, divided into three intervals for spectral analysis; Fig. S2) indicates statistically significant, periodical signals in the RE and GR logs. However, the GR produces a weaker signal than the RE log within the massive halite intervals. This is expected, as pure halite does not contain the elements U, Th, and K and their decay series responsible for natural GR radiation emitted by rocks. However, several examples indicate how different log responses occur within halite sequences. For example, inner-halite variations such as thin clay ~~laminas~~ laminae caused by microstratification within the brines might occur (Sonnenfeld, 1983). Alternatively, thin sulphate layers (Biehl et al., 2014) have also been shown to produce log-responses.

Each of the analyzed log segments is characterized by several frequency peaks exceeding the chi 95% confidence interval (Fig. S2). Each segment was bandpass filtered according to these frequencies, and the fit of the filtered version to the original well-log was examined, ultimately selecting the best-fit result for subsequent analysis. Both logs are composed of significant and approximately overlapping periodical frequencies, with an average cycle thickness of ~50 m (Fig. S2). While the RE log appears to be more attuned to inner-halite variations in the Main Halite interval, the GR log is more consistent and provides a more reliable fit to the well log target curve in the ~~Interbedded Evaporites~~ units above 2833 m. Consequently, the Dolphin well cyclostratigraphy is constructed from information derived from the GR and RE logs that cover the lower and upper parts of the section (Fig. S2). The lower part of the Main Halite interval (cycles 1-11; Fig. S2) is not very well represented by the Gaussian filter, with some five cycles that fit well with the target curve. The upper part of the Main Halite interval is best filtered by using the RE log with a bandwidth of 49 m (cycles 12-24; Fig. S2). The cycles within the upper part of the section in the ~~interbedded~~ Interbedded ~~evaporite~~ Evaporite interval are picked up relatively clearly by the GR log (cycles 25-32; Fig. S2). However, as the Dolphin well section from the Interbedded Evaporites and above experienced significant deformation (Figs~~.~~ 5, 6), the well~~-~~log cyclostratigraphy of the upper part of the studied section is not reliable in this well.

Several frequency peaks exceeding the chi 95% confidence interval were also identified in the Leviathan-1 well~~-~~log analysis, where deformation ~~was minimal~~is reduced and Unit 6 is represented (Figs~~.~~ 5, 6). The RE log was cleaned from ~~clear~~ outlier spikes and used for bandpass filtering. The original log includes several short intervals in which values ~~go~~ range from 10's or 100's of ohm*m to extremely high 18,000+ ohm*m values, masking cyclic trends in the data. Fig~~.~~ure 5 ~~includes~~ shows the cleaned RE log overlain on the seismic data. There is a much-improved fit between the log and filtered cycles, relative to the Dolphin well ~~filtering~~, with only a few examples of a misfit between the two. A good fit is also generally apparent between the seismic signal and the well~~-~~log response. The Main Halite interval includes 19 cycles, in which cycles 4 and 5 are within the first Argillaceous Diatomite beds, and cycles 11-13 are within the second. The cycles within the Interbedded Evaporite interval are picked up relatively clearly by the RE log (cycles 19-27; Fig. 5). ~~The~~ In the Argillaceous Evaporites ~~toping~~ in the uppermost part of the studied section in the Leviathan-1 well, the RE log response fits with banding in the seismic data, which is also picked by bandpass filtering (cycles 27-33; Fig. 5).

Consequently, bandpass filtering of the well ~~-~~logs results in ~33 cycles from the base to the top of the evaporite~~s~~ sequence in the Levant Basin. In the next two sections, we present different findings supporting the occurrence of lithological cycles along the studied section, followed by the astrochronologic interpretation of these cycles in the discussion section.

4.3 Cyclicity of seismic reflective phases

Modern high-quality 3D seismic imagery represents a new frontier for astronomical calibration, potentially adding a chronological time-frame for seismic stratigraphy. However, in most marine settings, precession-scaled cycles are registered ~~as~~ at a thicknesses-to-cycles ratio which has a much higher resolution than the seismic data. Yet, several studies show a good match between the number of precession-induced astronomic cycles and the number of positive vs. negative seismic phases within MSC deposits (Driussi et al., 2015; Geletti et al., 2014). This is explained by the considerably higher sedimentation rates that characterize evaporite deposits, relative to the much lower rates typical of normal-marine clastic or carbonate deposition. The higher sedimentation rates result in an improved alignment between the spacing, or resolution, of lithologic variations and the resolution of the seismic imagery. As orbital forcing was repeatedly identified as determining lithological variations during the MSC (e.g., Krijgsman et al., 1999; Ochoa et al., 2015; Roveri et al., 2014a; Sierro et al., 2001; van den Berg et al., 2015), seismic data recording these variations can be used with caution for strengthening the well-log astronomical tuning-~~-~~based age models. This is not the case for the Pre-Evaporites in this area, which deposited at an average sedimentation rate of 11.4 cm/kyr and a cycle thickness of around 2-3 m, as shown by Meilijson et al. (2018). This thickness is below the resolution of the seismic data. Here, we use the seismic 3D data for additional validation of our results from well-log curves based on REDFIT spectral analysis and bandpass-filtering within the Main ~~h~~Halite and overlying ~~Interbedded Evaporites~~ intervals.

In practice, the seismic tuning analysis was performed by counting the number of reflectivity phases on three different sections where wells were drilled within the 3D geophysical dataset of the study area (Figs~~.~~ 1, ~~and~~ 7). Yet, as halokinetic deformation affected the Levant deep-basin evaporites, and particularly their upper units (Gvirtzman et al., 2013a), spatial variations are expected even considering a scenario of regionally uniform deposition. Such variations in the number and thickness of cycles are indeed observed when comparing different seismic sections, reflecting the local variabilities (Fig. 7). In total, a consistent number of ~30 reflectivity cycles is identified in different locations ~~(Fig. 7)~~, which is in agreement with the cyclicity identified through well-log spectral analysis.

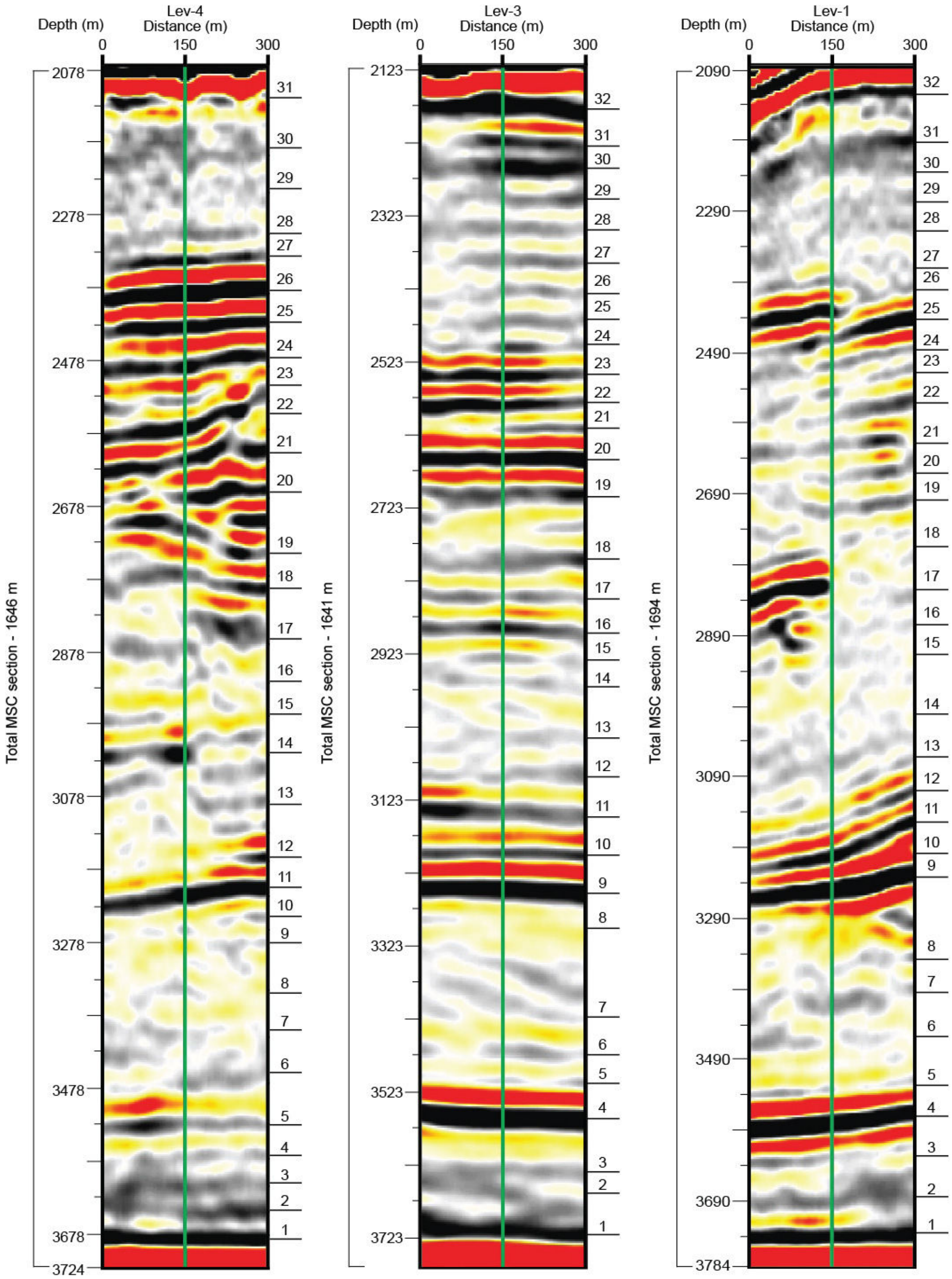

Figure 7. Seismo-cyclostratigraphy of three seismic profiles around wells in the study area.

Three depth--migrated profiles that are aligned with wells in the central Levant. Black lines with numbers on the right hand side of each seismic profile represents a reflectivity phase (black) cycle count along the section. Left bar shows actual depth for each section and the total depth from base to top of the MSC section in each well.

4.4 Elemental variations within evaporite samples

The wellbore cuttings do not allow recognition of macro-scale sedimentological features, which may reflect the cyclicity identified in the well logs and seismic data within the halite sequence. Tuning of marginal MSC sections has been done based on lithological transitions, such as branching selenite to massive selenite, or chaotic deposits to clastic evaporites in stages 1-3 (e.g., Roveri et al., 2014a), or diatomite-shale-carbonate transitions in the Pre-Evaporites (Ochoa et al., 2015; Sierro et al., 2001). Here, we explore whether minor inner-halite chemical variability down-~~-~~section can account for the filtered cycles and variable log response within apparently massive and homogenous halite. Other Miocene intervals of homogeneous lithology have also been shown to contain cyclic changes in the chemical composition of the sediments (van den Berg et al., 2015), which are assumed to represent shifts in the depositional environment~~ shifts~~. We hypothesize that these variations, if present in deep Mediterranean basins, could correspond to: 1) ~~disparities~~ variations in riverine runoff and associated influx of clastic material into the basin, and/or 2) shifts in the degree of evaporation determining the type of deposited evaporites. Both of these drivers can be related to orbital forcing (Marzocchi et al., 2015; Simon et al., 2017).

We observe a relatively low correlation (R^2=0.46; Fig. 8A) between Fe and K in the Levant halite samples, which is not in agreement with the occurrence of continentally-derived material transported to the Eastern Mediterranean. In contrast, a high elemental correlation (R^2=0.91; Fig. 8B1) is observed between S and Ca, which confirms that low and variable amounts of minerals rich in $CaSO_4$ (i.e., gypsum and anhydrite) represent an integral part of evaporite deposition in the Main Halite of the deep Levant Basin.

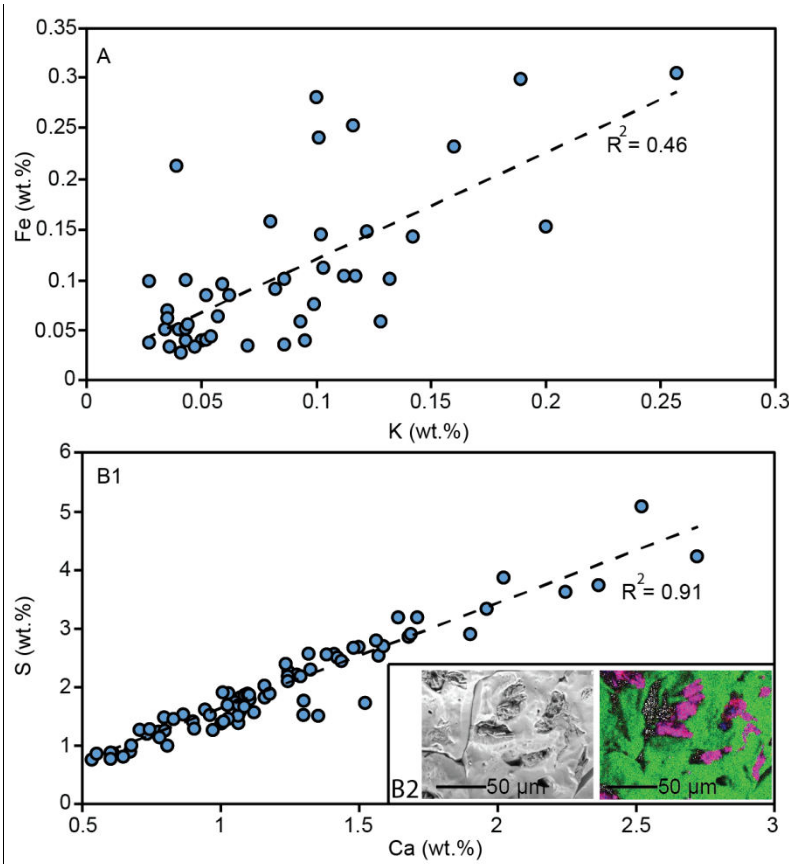

Figure 8. X-ray fluorescence elemental analysis of the Levant evaporites

Results of XRF elemental analysis are shown for 77 halite samples for specific elemental composition. (A) Note the low correlation between iron and potassium, while (B1) shows a high sulfur to calcium correlation. The high correlation between sulfur and calcium is corroborated by SEM-EDS imagery and element maps (halite sample from 3058 m; (B2)) showing the distribution of Na (green), Ca (blue) and S (red),~~.~~ ~~Note that the~~indicating the occurrence of gypsum microcrystals (purple; B2) within cavities of the larger and much more common halite crystals.~~has a distinct swallowtail twinned microcrystals pattern.~~

This notion is further confirmed by the recognition of ~~anhydrite~~ calcium sulfate microcrystals minerals ~~and small-scale but distinct swallowtail twinned microcrystals fabrics~~ within the halite cuttings (Fig. 8B-2). Note that not all halite grains crystals included a similar deposition precipitation of calcium sulfates in small pores. We suggest that shifts in the amount of gypsum or anhydrite deposition~~al~~ along the section might correspond with the cycles obtained by well-log spectral analysis.

4.5 Organic geochemistry as a stratigraphic marker

Biomarker data allow~~s~~ us to identify sources of sedimentary organic matter preserved in the cuttings as well as to gain insights into its thermal history. We observed distinct differences in the biomarker distribution found in the Pre-Evaporites, the Argillaceous Diatomites within the Main Halite deposits, and the overlying Interbedded Evaporites interval. The *n*-alkanes range~~d~~ from *n*-C_{16} to *n*-C_{38} (Table 1, Fig. 9), and their distribution ~~varied~~ varies between samples. For example, while short- and long-chain alkanes ~~were~~ are more predominant in the Pre-Evaporites and the Argillaceous Diatomites, mid-chain alkanes ~~were~~ are more prominent in the Interbedded Evaporites. Additionally, the carbon preference index (CPI) of long-chain *n*-alkanes, which portrays the degree of oddity in the distribution of the different *n*-alkanes, varie~~d~~s around 5-7 in the Pre-Evaporites, 4-12.3 in the Main Halite (Argillaceous Diatomites) interval, and around 1.9-2.9 in the Interbedded Evaporites (Table 1; Fig. 10). ~~The CPI reports on the degree of oddity between the distribution of the different *n*-alkanes.~~ The Argillaceous Diatomites also contain the lowest Pr/Ph ratios (Table 1, Fig. 10) compared to other samples. The relative abundance of long-chain *n*-alkanes (C_{25}–C_{35}) ~~was~~ is more elevated within the Argillaceous Diatomites and ~~pre~~Pre-~~evaporite~~Evaporite. This ~~was~~ is reflected in the ratio of long chain (C_{25}-C_{37}) to short chain (C_{16}-C_{21}) *n*-alkanes, which maximize~~d~~ in the Argillaceous Diatomites (1.9), followed by the Interbedded Evaporites (1.6) and the Pre-Evaporites (1.2). The C_{31} *n*-alkane ~~was~~ commonly is the most dominant homologue.

Selected hopane- and sterane-based thermal maturity indices (Table 2; Fig. 11; Peters and Moldowan, 1993; Rullkötter and Marzi,1988; Peters et al., 2005) also indicate major differences between samples from the Pre-Evaporites and Argillaceous Diatomites, relative to those from the lower part of the Interbedded Evaporites~~ interval~~. As summarized in Table 2, the diatomite facies exhibit the lowest thermal maturity values, to be followed by the Pre-Evaporites~~,~~ ~~and~~ while much more mature ~~indicative~~ indices are reached in the overlying Interbedded Evaporites. This is clearly indicated by the presence of hopanes with the biological ββ configuration, in addition to low values of the C_{31} S/R hopanes ratio and the C_{28} ααα 20S/20R steranes ratio, and more elevated values of the C_{30} βα/αβ hopanes ratio in immature samples (Fig. 11). Additionally, the Argillaceous Diatomites samples exhibit~~s~~ a lack of re-arranged steranes compared to the overlying and underlying intervals (Fig. 11; Table 2).

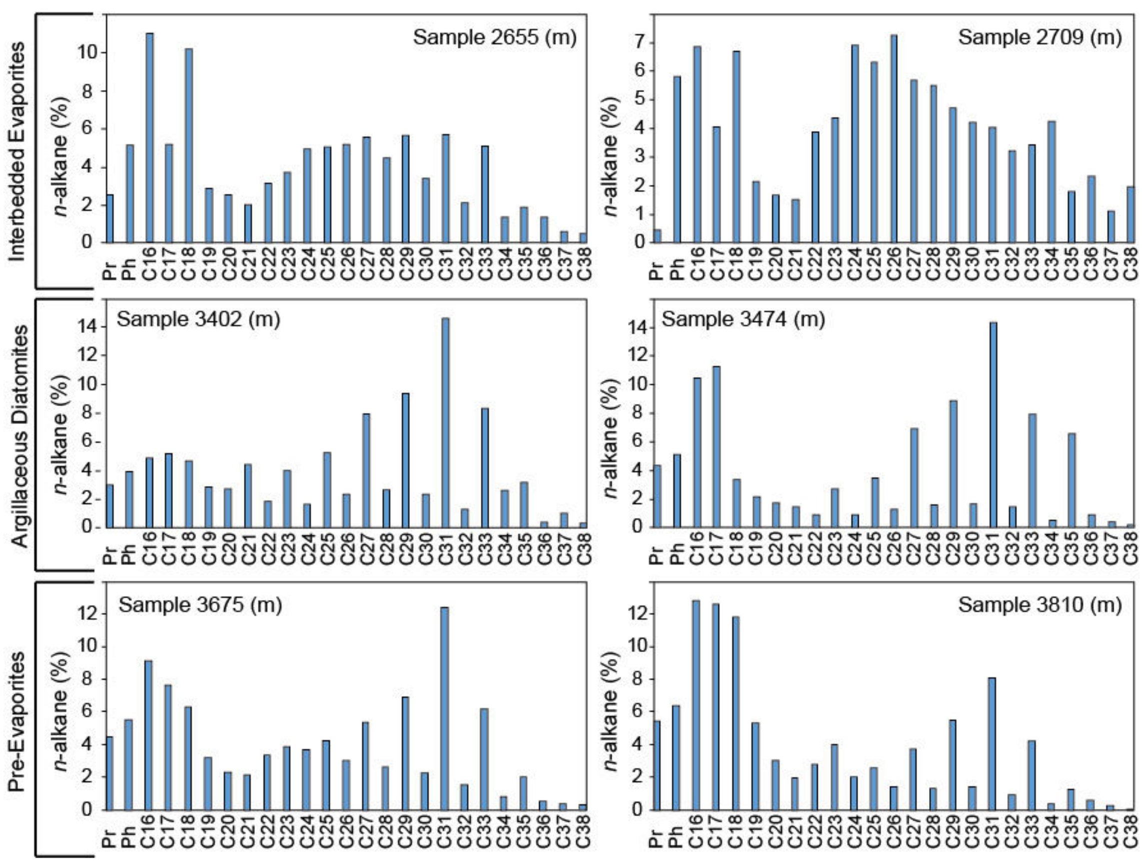

Figure 9. n-alkane distribution in non-halite intervals.

Two samples from each depositional unit (left and right columns) show the relative abundance of pristane (Pr), phytane (Ph), and C_{16}-C_{38} *n*-alkanes. Note the odd-over-even carbon-number predominance of long-chain *n*-alkanes in the Argillaceous Diatomites (center) and ~~pre~~Pre-~~evaporites~~ Evaporites (lower) relative to the overlying Interbedded Evaporites. Also observe the higher CPI, i.e., ~~the distribution~~the distribution of *n*-alkanes, in the Pre-Evaporites and Argillaceous Diatomites relative to the Interbedded Evaporites, and higher relative abundance of medium-long chained compounds.

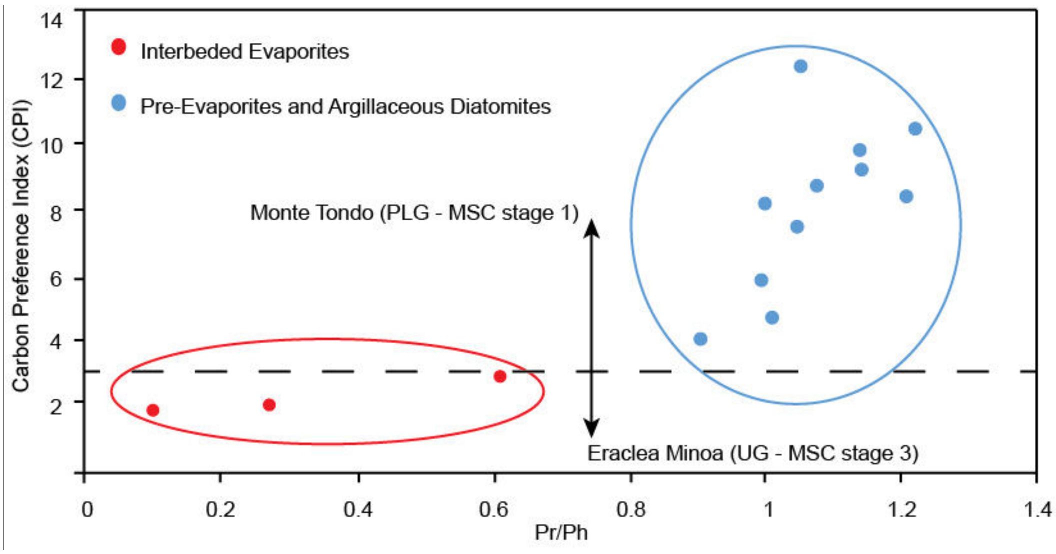

Figure 10. Pristane/phytane ratio to carbon preference index (CPI) plot.

Legend indicates the strata of plotted samples. Horizontal dashed line indicates the separation of CPI values of marginal section across the MSC reported by Vasiliev et al. (2017). Note that the samples from the Interbedded Evaporites plot in the area of values measured in stage 3 of the MSC (Vasiliev et al., 2017), while the lower samples from the Levant plot in the area of MSC stage 1. Also note the separation in Pr/Ph values between the Interbedded Evaporites relative to the Pre-Evaporites and Argillaceous Diatomites.

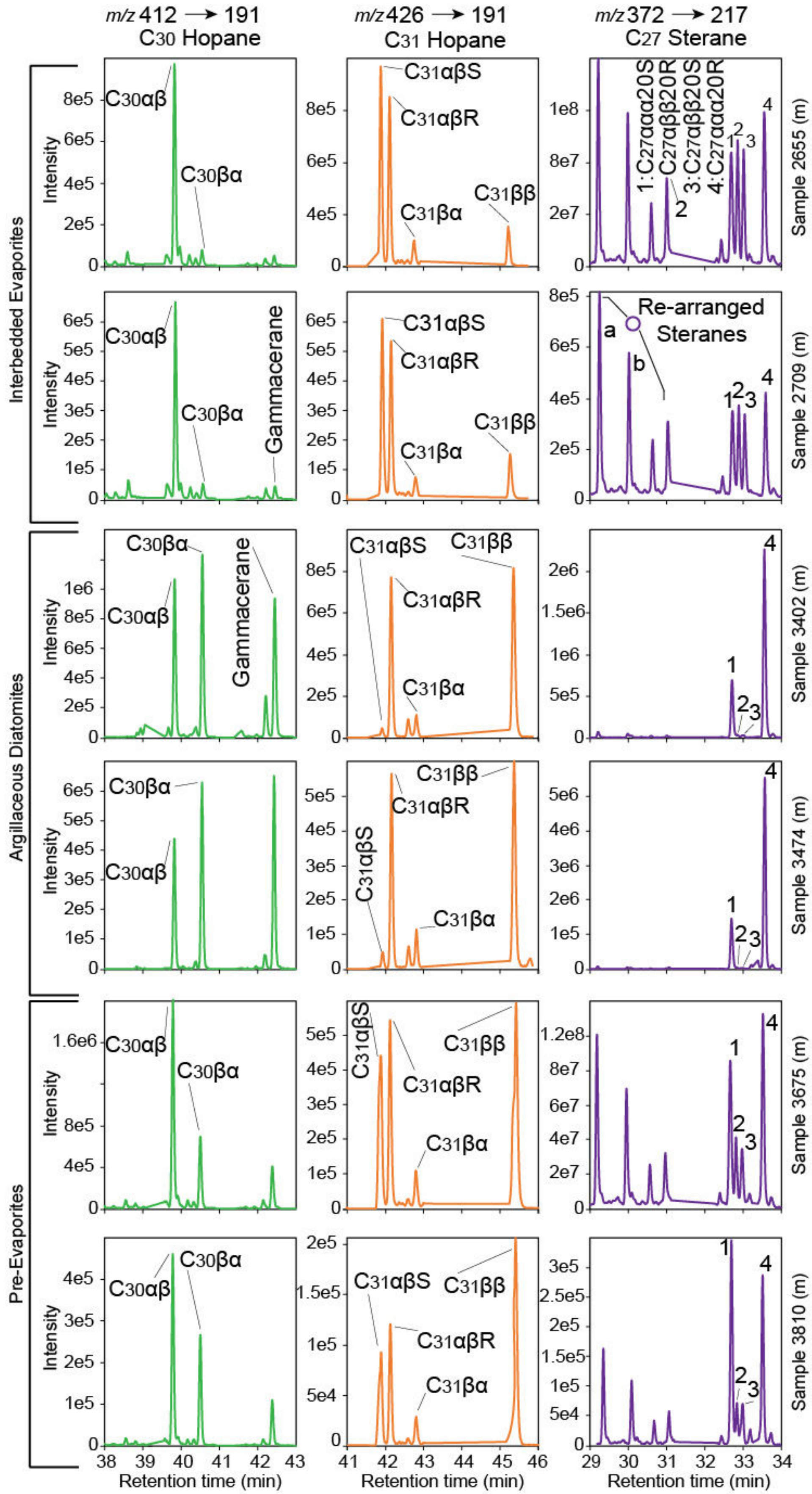

m/z 412 → 191
C30 Hopane
m/z 426 → 191
C31 Hopane
m/z 372 → 217
C27 Sterane
Interbedded Evaporites
Argillaceous Diatomites
Pre-Evaporites
Intensity
C30αβ
C30βα
Gammacerane
C31αβS
C31αβR
C31βα
C31ββ
1:C27ααα20S
2:C27αββ20R
3:C27αββ20S
4:C27ααα20R
Re-arranged Steranes
a
b
1
2
3
4
Sample 2655 (m)
Sample 2709 (m)
Sample 3402 (m)
Sample 3474 (m)
Sample 3675 (m)
Sample 3810 (m)
Retention time (min)

Figure 11. Distribution of selected bacterial hopanes and algal steranes-.

Two samples from each depositional unit (left and right columns) were investigated for the distribution of aliphatic hydrocarbons using selective reaction monitoring (SRM) analysis. Each sample (numbered on the right) includes a chromatogram for three given SRM transitions: 412 → 191 (C_{30} Hopane); 426 → 191 (C_{31} Hopane); 372 → 217 (C_{27} Sterane). The C_{27} rearranged steranes are marked as (a) $C_{27}\beta\alpha$ 20S and (b) $C_{27}\beta\alpha$ 20R. High ratios of $C_{31}\alpha\beta$S/R hopanes and $C_{27}\alpha\alpha\alpha$S/R steranes, along with low values of $C_{31}\beta\beta/\alpha\beta$ and $C_{30}\beta\beta/\alpha\beta$ hopane ratios, indicate a higher, yet mixed, maturity of the organic matter preserved in the Interbedded Evaporite shale samples compared to samples from the Pre-Evaporites and Argillaceous Diatomites. The underlying diatomite facies sediments are immature in nature, while the ~~pre~~Pre-~~evaporite~~ Evaporite shale samples exhibit mixed signatures (e.g., high $C_{31}\beta\beta/\alpha\beta$ hopanes and C_{27} $\alpha\alpha\alpha$S/R steranes).

5. Discussion

5.1 Deep-~~-~~sea halite depositional environment

The halite in the Dolphin well appears to be a pure, homogeneous layer, indicating a monotonous deposition of halite in the deep Levant Basin. Transmitted-~~-~~light microscopy and SEM analysis of halite ~~grains~~ crystals (<0.5 cm) throughout the section reveals no distinct sedimentological variations. XRD analysis also confirms a uniform, halite-dominated mineralogical composition (Fig. 4). ~~Swallowtail twinned~~Gypsum microcrystal~~s~~ ~~structures made out of calcium sulfates~~ were observed ~~on~~ within several halite ~~grains~~ crystals as seen in SEM-EDS (Fig. 8B-2), and elemental variations s~~. S~~upporting shifts in the relative amounts of calcium sulfates deposited along the halite part of the section were apparent in XRF analysis (Fig. 8). However, we found no features similar to the lithological variations reported from the Realmonte salt mine (Lugli et al., 1999) or the intermediate depth halite of the Balearic Basin (~~site~~ Site 134; Lugli et al., 2015), such as cumulates of halite plates settled out from a stratified water column, plate cumulates in a shallowing-upward sequence containing kainite layers, ~~n~~or cumulates of skeletal hoppers with chevron overgrowths. The above conclusion might be biased due to the usage of well cutting, possibly not allowing to recognize these features. However, the mm-scale variations in the salt deposits shown by Lugli et al. (2015) should have been recognizable ~~on~~ in the halite well cuttings. The lack of comparative features between the marginal halite and the Levan deep-basin halite is also evident when comparing the halite samples in the Dolphin well and halite deposits penetrated by DSDP drilling. There is a clear distinction between the featureless Dolphin halite and the halite interbedded with detrital sand and small anhydrite nodules recovered at DSDP ~~site~~ Site 134 offshore Sardinia in the margins of the western Mediterranean (Hsü et al., 1973). The halite sampled in ~~site~~ Site 134 is banded similarly to the

Sicily halite reported by Lugli et al. (1999), with alternative cloudy and translucent beds. Similarly, the banded halite and polyhalite at DSDP Sites 374, 375 and 376 in the Eastern Mediterranean (Garrison et al., 1978) does not resemble the homogenous halite recovered in the Dolphin well. The homogeneous nature of the halite observed in the Dolphin well suggests continuous deep-sea deposition, in comparison to halite deposition in the shallower marginal basins.

Modern analogs for ancient deep-water halite depositional environments are scarce. An exception is the hypersaline Dead Sea, in which active precipitation of halite occurs within the deepest parts of the basin (Arnon et al., 2016; Sirota et al., 2016, 2017; Steinhorn, 1983; Stiller et al., 1997). The Dead Sea floor is divided into two principal environments: a deep, hypolimnetic lake floor, and a shallow, epilimnetic lake floor (Sirota et al., 2016, 2017). Halite continuously precipitates with seasonal variations influencing the type of halite formation on the deeper hypolimnetic lake floor. However, the shallow epilimnetic lake floor is also subject to seasonal variations, which produce annual unconformities related to halite deposition and dissolution. The epilimnion part of the lake is under-saturated during the summer and halite is dissolved, while winter is characterized by a heavily supersaturated water column and halite is crystallized (Sirota et al., 2016). Summer is associated with higher loss of water by evaporation from the lake compared to the winter. Sirota et al. (2016) argue that the seasonal halite deposition cycle in the Dead Sea epilimnion is controlled by the decrease in the saturation with increasing temperature, which overcomes the effect of enhanceds summer evaporation. The hypolimnion is supersaturated and halite is crystallized throughout the year, with higher super-saturation and higher crystallization rates during winter. During summer, the undersaturated epilimnion dissolves halite, forming highly saturated dense solutions. These solutions flow to the hypolimnion, which becomes supersaturated and crystallizes halite. This process results in focusing of halite deposits in the deep hypolimnetic parts of the evaporitic sea, and thinning of the shallow epilimnetic deposits occurs (Sirota et al., 2016, 2017). The Dead Sea modern analogue provides a mechanism for explaining the great thickness of the deep Mediterranean MSC halite deposit. A similar model might have applied during the MSC, with halite dissolution in the marginal and intermediate basin evaporites, and focusing and thickening of halite deposition in the deeper parts of the basin, as also partly proposed by Roveri et al. (2014c).

5.2 Stratigraphic markers in deep basin MSC deposits

5.2.1 Deep--basin diatomites as environmental and lithostratigraphic markers

As no chronostratigraphic indicators were found in the studied section, we aim to use the litho-chemical analysis performed on the Dolphin well samples to identify lithostratigraphic and chemostratigraphic markers, that could may serve as tie-points for establishing an age model for the deep basin MSC deposits (Fig. 12). In this context, the occurrence of diatomites within the Main Halite unit provides a primary observation. Diatomites are known to occur within Pre-Evaporite and PLG intervals in some of the marginal sections (Dela Pierre et al., 2014; Hilgen et al., 2007; Hilgen and Krijgsman, 1999; Krijgsman et al., 2001; Manzi et al., 2011; Roveri et al., 2014a), and more rarely within stage 3 Upper Gypsum deposits (e.g., Eraclea Monia section; Manzi et al., 2009). Diatom-rich aggregates within laminated layers, appearing as mudstone intervals interbedded within the PLG deposits of the Piedmont basin, were used by Dela Pierre et al. (2014) to establish the existence of normal--marine (not brackish or hypersaline) waters during deposition of non-evaporitic intervals during stage 1 of the MSC. Here we show that open -marine planktonic diatom taxa abundant in the Piedmont during the PLG (e.g., *Coscinodiscus* sp. and *Thalassionema longissimi*), are also abundant or closely related to abundant species within the Dolphin assemblage.

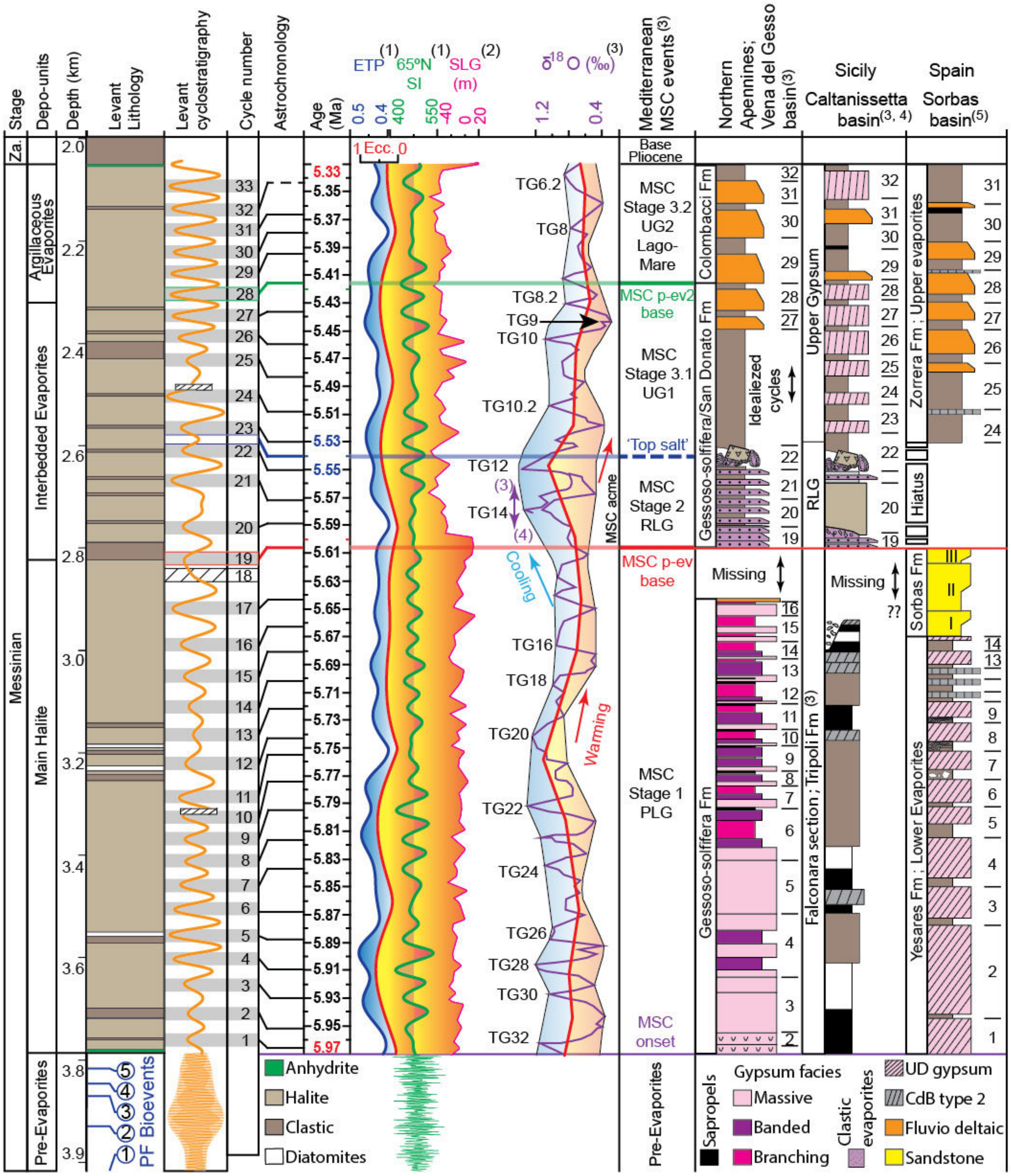

Figure 12. Astronomical age model and regional correlation of the Levant MSC

The Levant interpreted lithology (left, from Fig. 2), biostratigraphic reference levels (PF – planktic foraminifera, below) and filtered well-~~-~~log model (Fig~~s~~. 5) determine a cyclostratigraphic model, resulting with 33 cycles for the Levant MSC (shaded cycles). Note the significantly lower cycle frequency in the ~~pre~~Pre-~~evaporites~~ Evaporites (2.3 m compared to 51 m per-cycle), due to the much higher sedimentation rates in the evaporites interval. This cyclostratigraphic model is tuned to astronomic target curves (center) of ETP (blue; calculated as eccentricity (Ecc; red) + obliquity - precession ((1) Laskar et al., 2004~~)~~), 65°N summer insolation (65°N SI; green) (Laskar et al., 2004), and marginal MSC deposits (right columns) based on astronomical calibrated ages and cycles identified across the Mediterranean ((1) Laskar et al., 2004; (3) Roveri et al., 2014a, CIESM (2008); (4) Manzi et al., 2011; (5) Krijgsman et al., 2001). The drop in sea level (SLG; sea level Gibraltar; (2) Ohneiser et al. 2015) corresponding to glacial peaks TG12-14 ($\delta^{18}O$; as summariezed in Roveri et al. (2014)) marks the top of the ~~main~~ Main ~~halite~~ Halite unit. The shift to post-evaporitic and clastic deposits of MSC stage 3 (Hilgen et al., 2007; Krijgsman et al., 2001; Laskar et al., 2004; Roveri et al., 2014), through a stepwise deglaciation associated with sea-~~-~~level rise (TG12-9), is here astronomically tuned to enhanced clastic deposition in the Interbedded Evaporites and Argillaceous Evaporites units of the Levant.

To date, there are no reports of diatomites, or a diatom-rich assemblage in stage~~s~~ 2 of the MSC across the Mediterranean. Based on the taxonomic similarities between the deep and marginal planktonic marine diatom assemblages, we propose that the Levant diatomites constitute a temporal lithostratigraphic marker. If we follow the interpretation for the occurrence of planktic marine diatoms as indicators of partial connectivity with the Atlantic Ocean (Dela Pierre et al., 2014; Hüsing et al., 2009; Krijgsman et al., 2000), then their appearance interbedded within the halite in the Levant suggests that deposition of the halite layer occurred at a time of at least partial, periodic Atlantic connectivity, most likely during deposition of the PLG on the margins (5.97-5.6 Ma).

5.2.2 Allochthonous grains in the Interbedded Evaporites-Argillaceous Evaporites and stages 2-3 of the MSC

The abrupt change that marks the onset of enhanced clastic input in the Interbedded Evaporites in the Levant Basin, together with endemic and reworked Eocene and Cretaceous foraminifera into the basin, matches other similar episodes reported from the MSC in the Mediterranean. Primarily, these are the clastic-rich deposits that result in the deposition of the Reworked Lower Gypsum (stage 2) and the Upper Gypsum and Lago-Mare deposits (stage 3) on the margins. These clastic deposits, including a similar abundance of minerals and reworked fauna, are not only reported from marginal sections (e.g., Lofi et al., 2011; Roveri et al., 2014), but also from cores of deeper parts of the basin (e.g., Site~~s~~ 124 in the Western Med (Ryan et al., 2007), Site 654 ~~from~~ in the Tyrrhenian Sea (Borsetti et al., 1990), and from Sites 374 and 376 in the Eastern Mediterranean (Cita et al., 2006; Hsü et al., 1978a, 1978b)).

DSDP ~~sites~~ Sites 375 and 376 ~~on~~ at the Florence Rise in the Eastern Mediterranean recovered nannofossil marlstones and dolomitic marlstones of latest Miocene age, overlying a gypsum with marlstone ~~evaporite~~ sequence~~,~~ (Hsü, et al., 1978b). The gypsum with marlstone ~~evaporites~~, which are interpreted as deposits of a shallow subaqueous environment, are followed downwards by anhydrite and halite at Site 376 and are collectively recognized as the upper part of the Mediterranean evaporites. The interbedded gypsum contains reworked Cretaceous, Paleogene and lower/middle Miocene foraminifera and nannofossils, similar to the fauna identified in the clastic interval of the Interbedded Evaporites in the Dolphin well. The reworked fauna from ~~the~~ Florence Rise are common to abundant in the bedded evaporites and rare to absent in the overlying Pliocene and underlying Tortonian and Serravallian (Hsü, et al., 1978b), indicating a distinctive phase of reworked sediments deposited within the Mediterranean basins. The sedimentary response of the Interbedded Evaporites and Argillaceous Evaporites (Units~~e~~ 5 and 6, respectively; Gvirtzman et al., 2013; 2017; Manzi et al., 20018) in the Levant Dolphin and Leviathan-1 wells (from ~2270 m in the Dolphin well, Figs~~.~~ 5, 12) resembles similar observations reported from shallower deposits in the Levant. For example, the Afiq Formation overlies the anhydrite-siliciclastic stage 2-RLG equivalent Mavqiim Formation (Druckman et al., 1995; Lugli et al., 2013) and was penetrated by the Or-South 1 well. It consists of Eocene-aged lithoclasts made of limestone, dolomite, and chert- and quartz-~~-~~rich sand, overlying a conglomerate unit with brackish ostracods indicating a plausible correlation to the Lago-Mare stage (Derin, 2000). A fluvial or sabkha environment is attributed to this interval with subaerial exposure, supporting the idea of a considerable desiccation phase and subaerial exposure near the end of the MSC (Cita et al., 1978; Lofi et al., 2011; Madof et al., 2019; Ryan, 1978). Similar lithologies, including clasts of Eocene and Cretaceous age, were described from the marginal Nir-1 well in the Levant Basin above an erosion surface and beneath earliest Pliocene marls (Frey-Martınez et al., 2007). Similar clastic-conglomeratic and sandy lithologies are also reported from the Messinian Qawasim and Rosetta formations offshore Egypt (Leila et al., 2016); the latter correlates with the Afiq Formation in the Levant (Derin, 2000). Unfortunately, no samples are available from above the base of the Interbedded Evaporites in the deep Levant Basin to further confirm the lithological correlation between these sections and the deep Levant Basin. Correlation to more proximal sections and well-log interpretations indicate ~~(see also Gvirtzman et al., 2013; 2017; Manzi et al., 2018)~~ that the overlying Argillaceous Evaporites mark a shift to more clastic and gypsum/anhydrite deposition (see also Gvirtzman et al., 2013; 2017; Manzi et al., 2018).

We argue that the main change in the halite unit, characterized by mixing of clastic material into the deep-basin deposits at the base of the Interbedded Evaporites~~,~~ correlates with the beginning of major sea-level drawdown and introduction of clastic material into the entire Mediterranean ~~basin~~Basin, from stage 2 of the MSC (5.6~~1~~ Ma) through the Upper Gypsum and Lago Mare stages in the marginal basins (5.~~53~~55-5.33 Ma; Argillaceous Evaporites in Fig. 12). During stage 2, sea-level drawdown eroded and redeposited the PLG gypsum into the marginal and intermediate parts of the basin (e.g., Lofi et al., 2011). The deep-basin expression ~~to~~ of this regression might be the fine-grained clastics, including older reworked fauna, reaching the Mediterranean~~'s~~ depocenters. However, to further test this idea~~,~~ and try to distinguish between stage 2 and 3 sediments, we compare biomarker distribution across the basin, and identify sedimentary cycles within the MSC of the Levant Basin.

5.2.3 Basin-wide transport of organic matter

The *n*-alkane distribution and CPI values of the Levant samples (Figs~~.~~ 7 and 8; Table 1) are similar to some extent to those obtained from marginal and onshore MSC successions (Vasiliev et al., 2017), and provide further support for the introduction of reworked and mixed material into the Levant during the deposition of the Interbedded Evaporites. The *n*-alkane distribution of Mediterranean MSC samples covering the entire 640-kyr-long MSC interval shows distinct dissimilarities between several marginal to intermediate-depth sections (Vasiliev et al., 2017): ~~the~~The Monte Tondo (Primary Lower Gypsum; MSC stage 1), Realmonte salt mine (Halite and Re-sedimented Lower Gypsum; MSC stage 2), and Eraclea Minoa (Upper Gypsum/Lago Mare; MSC stage 3). The Delphine well *n*-alkane distribution shows a higher abundance of short-chain homologues in the Levant relative to marginal sections (Vasiliev et al., 2017), likely due to the lower relative input of terrestrial organic matter in more distal depositional settings. Several similarities exist between both data sets. Vasiliev et al. (2017) reported CPI values of 3.0-7.9 ~~in~~ at Monte Tondo (stage 1), and 1.7-3.7 ~~in~~ at Eraclea Minoa (stage 3; Fig. 10). While CPI values were not reported from the halite samples of the Realmonte salt mine, Vasiliev et al. (2017) show two different types of organic matter: 1) autochthonous sediment associated with gypsum or halite deposited in place, and 2) allochthonous material associated with clastic sediments and transport. Marked similarities in CPI values are therefore noted between the Levant and marginal locations described by Vasiliev et al. (2017), with CPI values of 4.0-12.3 in the Main Halite interval (indicating stage 1), and 1.9-2.9 in the Interbedded Evaporites interval (indicating stages 2~~/~~-3) (Fig. 10).

Vasiliev et al. (2017) also suggest that dissimilarities in the biomarker and isotopic composition of stages 1 and 2, relative to stage 3 sediments, may be attributed to the outflow of Black Sea (i.e., Paratethys) waters and their mixing into the Mediterranean, which paved the way for Paratethyan 'Lago-Mare' type fauna. For instance, the distribution of *n*-alkanes and CPI values in stage 3 ~~in~~ at Eraclea Minoa are more evenly distributed and lower~~,~~ relative to those of stage 1 (~~Fig~~fig. 3 in Vasiliev et al., 2017). We report a similar distinction in the *n*-alkane distribution between the upper ~~Interbedded Evaporites~~clastic samples and underlying sediments (Table 1, Fig. 9). A much stronger odd-over-even predominance (i.e., higher CPI values) is observed in the Argillaceous Diatomites, together with more elevated long-chain over short-chain *n*-alkanes values (LCA/SCA; Table 1) and maturity parameters (Fig. 11; Table 2). This indicates more immature source rocks with significantly different sources of the organic matter in the Main Halite relative to the Interbedded Evaporites sediments (Bray and Evans, 1961; Scalan and Smith, 1970).

The distribution of stereoisomers of algal steranes and bacterial hopanes (Fig. 11; Table 2) reflects the transformation, or stereoisomerization from biological epimers to a more stable geological molecular configuration as a consequence of thermal alteration (Peters, 1986; Peters et al., 2005, 1980). The evidence for enhanced thermal maturity in the Interbedded Evaporites relative to the underlying deposits (Fig. 11; Table 2) is counterintuitive, as thermal maturity should increase with depth (Peters et al., 2005, 1980). Furthermore, the Interbedded Evaporites exhibit mixed signals that include high values of the C_{31} αβ S/R ratio (indicative of thermally mature organic matter) in addition to C_{31} hopanes with the ββ biological configuration (indicative of immature organic matter) (Fig. 11; Table 2). This aspect further supports the occurrence of organic -matter mixtures from differing ages and thermal histories, i.e., a higher proportion of allochthonous, thermally mature organic matter in the Interbedded Evaporites compared with the Main Halite and Pre-Evaporite samples. This interpretation is consistent with similar trends observed in early Paleogene (Sepúlveda et al., 2009) and Quaternary (Rashid and Grosjean, 2006) studies. Such trends may reflect an intensification of the hydrological cycle, and thus enhanced precipitation, continental runoff, and the transport of re-worked, and pre-aged, continental or marginally-derived organic matter during the deposition of the Interbedded Evaporites. Another mechanism through which transport can occur is dense shelf--water cascading (DSWC) transport of sediment and associated organic matter from marginal settings to deep Mediterranean basins, as reported to occur in the Mediterranean today (Canals et al., 2009). The interpretation of transport in these intervals is consistent with the occurrence of clastic material, larger sub-rounded minerals, and re-worked Cretaceous and Eocene foraminifera within samples from the Interbedded Evaporites, which also supports the presence of reworked, older sediments. Both Cretaceous and Eocene organic-rich source rocks are known around the

Mediterranean ~~basin~~ Basin (e.g., Almogi-Labin et al., 1993; Bayliss, 1973; Meilijson et al., 2014), and might represent sources of pre-aged weathered and transported organic matter, matching the apparent higher maturity measured from the organic-~~-~~matter extract of the Interbedded Evaporites sediments.

In summary, the similarities between our data and ~~that~~ of Vasiliev et al. (2017) suggest that organic geochemical analysis from the Dolphin well ~~can~~ might be used as regional chemostratigraphic markers to distinguish between Pre-Evaporites and Argillaceous Diatomites sediments, and the overlying Interbedded and Argillaceous Evaporites. A correlation between MSC stage 3 and the ~~Interbedded Evaporites~~upper part of theMSC in the Levant Basin has been previously proposed based on seismic interpretation and the sampling of shallower deposits (Druckman et al., 1995; Gvirtzman et al., 2017; Lugli et al., 2013). Here, we present evidence supporting the occurrence of stage 2 sea-~~-~~level drawdown or stage 3 and 'Lago-Mare'-type deposits in the deep domains of the Eastern Mediterranean. This includes increased supply of clastic material into the basin, reworked fauna, and chemostratigraphic markers (Figs~~.~~ 3, 9 and 10).

5.3 From cycles to astronomical tuning

Cyclostratigraphy and astronomical tuning of sediment sections, geochemical signals, and well-~~-~~log responses have been extensively used for stratigraphic interpretations of MSC deposits across the Mediterranean (Dela Pierre et al., 2014; Hilgen et al., 2007, 2000, 1995; Hilgen and Krijgsman, 1999; Hüsing et al., 2010, 2009, Krijgsman et al., 2001, 1999, 1997; Lugli et al., 2015; Manzi et al., 2015, 2013, 2012; Ochoa et al., 2015; Topper et al., 2014). The CIESM stratigraphic model of the MSC has halite deposited in stage 2 of the MSC, during four ~~insolation~~ precession cycles (e.g., Roveri et al., 2014a, with reference to Laskar et al., 2004; Fig.

12). These are part of the 32 precession-controlled cycles (Laskar et al., 2004) identified across the Mediterranean, with a periodicity of about 20 kyr per cycle, amounting to the 640 kyr time frame of the MSC. Manzi et al. (2015) proposed to tune the high-reflectivity intervals in the seismic section of the Levant (interpreted as clastic units; Gvirtzman et al., 2013a) to summer insolation maxima, and the transparent intervals (interpreted as halite) to summer insolation minima, within these four insolation cycles. By contrast, the study of the Pre-Evaporites in the Dolphin well by Meilijson et al. (2018) and the results of this study suggest that salt formation began around 5.97 Ma, i.e., more or less synchronously with the marginal deposition of the PLG. According to this age-model, the evaporitic sequence in the Levant Basin (Fig. 12) was deposited between 5.97 and 5.33 Ma, corresponding to a time span of ~640 kyr rather than 50 kyr, and encompassing 32 insolation cycles (Laskar et al., 2004). Our suggested scenario would imply an average cycle thickness of ~50 m, as the studied section is 1590 m thick.

Bandpass filtering of the Dolphin well logs resulted in the identification of 31 cycles, closely matching the 32 precession-controlled cycles (Laskar et al., 2004) in the interval between 5.97 and 5.33 Ma. However, this age model includes several assumptions: (1) the evaporite record at the studied site is complete with no hiatus, (2) it is largely undisturbed by salt tectonics, and (3) ~~that~~ the sedimentation rate is approximately constant, with no significant changes between the halite-rich intervals and clastic-diatomitic intervals. The Dolphin record lacks chronostratigraphic tie points and contains intervals in which the log data are erratic (Figs. 5, S2). Furthermore, the Dolphin well area appears deformed in the upper part of the section, and ~~missing~~ Unit 6 is missing (overlying the Interbedded Evaporites; Fig. 6). These sources of uncertainty suggest that the Dolphin well spectral analysis provides a first order approximation of the number of cycles, primarily across the lower part of the section. However, the large number of cycles observed in the Main Halite interval, if assumed to reflect precessional cycles, suggests a longer period of deposition than ~50 kyr. The Leviathan-1 well is much less deformed (Fig~~.~~s 5, 6) and has a thick interval of Unit 6 (Gvirtzman et al., 2013; 2017), similar to the sequence at the Aphrodite well (Manzi et al., 2018). It also presents a good fit between the seismic and the RE well~~-~~-log response~~,~~. The observed regularity ~~which~~ produced a filtered cycles curve (Fig. 5), which ~~. the filtered cycles have~~ reveals a good fit ~~to~~ with the well log ~~target~~ curve. ~~and a regularity that fits well the produced filtered cycles curve (Fig. 5).~~ We hypothesize that these cycles represent the 32 ~~insolation~~ precession cycles identified in MSC sections across the Mediterranean. This would imply that the Main Halite interval in the lower part of the studied section is equivalent to stage 1 (PLG) in marginal sections, as also proposed by Meilijson et al. (2018).

However, lacking chronostratigraphic tie points in the evaporitic section, an alternative explanation for the cyclicity observed in the well logs of the halite and the seismic profiles should be considered to reconcile the age model suggested by Manzi et al. (2018) for the Levant Basin. In this model the FBI unit, which represents the uppermost part of the ~~p~~Pre-E~~e~~vaporites in ~~, of~~ the Aphrodite well, corresponds to MSC stage 1 (the PLG; Manzi et al., 2018), ~~and~~ while the uppermost part of the section ~~correlates with~~corresponds to stage 3 (Unit 7; Gvirtzman et al., 2017). Following this model, the ~33 cycles identified within the Leviathan-1 MSC section (Figs~~.~~ 5, 7) correspond to the ~50 kyr estimated for the duration of stage 2 of the MSC (Roveri et al., 2014), and have therefore a cycle duration of ca. 1560 years. If we take into account the likely different sedimentation rates of the Argillaceous Diatomites facies, this period could correspond to the period inferred for the Dansgaard-Oescher events (1470 years), as observed during the second half of the last glacial (Schulz, 2002) (although see comments by Ditlevsen et al. (2007) and Lohmann and Ditlevsen (2018) on the validity and interpretation of these cycles). Alternatively, they could be explained by the Bond cycles, as observed for the North Atlantic during the Holocene (1500 years; Bond et al., 2001). Another alternative are the periods of ca. 1000 years corresponding to the so-called Eddy cycle observed in the ^{14}C record, which relate to variations in solar activity (Steinhilber et al., 2012). However, this last alternative is unlikely:~~, as~~ if the regular alternations in the halite would correspond to Eddy cycles, it implies that stage 2 of the MSC ~~only~~ lasted only ~32 kyr. This means that the climax stage of the MSC cannot encompass both glacial stages TG14 and 12 (Fig. 12), as is assumed in the CIESM model.

In the Realmonte salt mine in Sicily, 10-15 cm alternations in the salt have been interpreted as annual cycles (Manzi et al. 2012). Such sedimentation rates of ca. 10 cm/yr would imply that the 1,060 m thick Main Halite interval in the Levant could have been formed in a short time period of 10,600 years, although average sedimentation rate may be lower in the Argillaceous Diatomites. However, it is hard to reconcile such a short duration of deposition with the amounts of halite required to build up the thickness of the Levant Basin halite layer.

In the absence of a simple explanation for the cyclicity observed in the Dolphin well, we now consider its interpretation in relation to the different elements of the CIESM model for marginal MSC deposits. The CIESM (2008) consensus stratigraphic model for the MSC is strongly based on astronomical tuning of different MSC sections and includes the following division of the 32 orbital-related cycles identified during this time frame (Laskar et al., 2004): cycles 1-18 in stage 1 (PLG), 19-23 in stage 2 (RLG), 24-28 in stage 3.1 (lower part of Upper Gypsum), and 29-32 in stage 3.2 (the Lago ~~-~~Mare). The correlation between the Levant MSC well-~~-~~log-based astrochronology, the orbital target curves, and the chronology of shallow~~/~~ to marginal sections (CIESM, 2008) of the MSC indicates the following: (1) the Main Halite interval (3759-2800 m in the Leviathan-1 well) is bound between the Levant filtered cycles 1 through 19 (Fig. 12). A comparison with the current MSC chronology (CIESM, 2008; Roveri et al., 2014a) shows a correlation with the number of cycles in the interval between 5.97 and 5.6~~1~~ Ma from the base of the PLG (stage 1) to the base of the RLG (stage 2); (2) the Interbedded Evaporites interval (2800-2320 m) is bound between the Levant filtered cycles 19 through 28 (Fig. 12), which correlates to the number of cycles in in stage 2 (the RLG; 5.6~~1~~-5.~~53~~ 55 Ma; cycles 19-23), with ~~and~~ its top ~~is~~ known as the 'top salt' horizon, and the lower part of stage 3 (stage 3.1 the Upper Gypsum who's base is at 5.42 Ma). Thus, the lower part of the Interbedded Evaporites is also equivalent to stage 2 halite deposits recognized in intermediate basins, such as the Realmonte salt mine in Sicily; (3) at the upper part of the ~~section~~ Interbedded Evaporite and the Argillaceous Evaporites interval ~~is~~ are equivalent to ~~the continuation of~~ stage 3 of the MSC (2320-2090 m; Fig. 12), ending with the clastic Lago-Mare interval.

Following the suggestion of Meilijson et al. (2018) ~~of~~ for an early onset of halite deposition in the deep Mediterranean basins, similar claims were made by García-Veigas et al. (2018) based on sulfur stable-isotopes analysis of marginal and intermediate basin gypsum deposits. They hypothesize that the deep-basin halite deposits are not equivalent to one phase of deposition during stage 2 of the MSC, but rather comprise two to three phases of halite deposition, beginning with halite deposition during stage 1 of the MSC. Our astronomical tuning agrees with this idea by positioning the boundary between stage 1 and 2 of the MSC (2762 m in the Dolphin well, 2800 m in Leviathan-1) at the top of the Main Halite interval. Consequently, we propose that the Main Halite is equivalent to stage 1 gypsum deposits of the PLG, as indicated independently by the diatomite facies. The increase in clastic and re-worked faunal material into the basin fits well with our astrochronology, placing the Interbedded Evaporites within the time period of the Re-worked Lower Gypsum (stage 2 of the MSC). Sea-level drawdown promoted the scraping of the shelf, re-shaping of drainage and transport systems across the basin, and re-depositing of vast amounts of eroded ~~gypsum~~ sediment into the intermediate basins. It also delivered vast amounts of fine-grained material to the deep basins, as observed in the Interbedded Evaporites in the Levant Basin. Lastly, the identification of the *Discoaster quinqueramus* in Unit 5 (the Interbedded Evaporites) by Manzi et al. (2018) supports this conclusion, as this species went extinct towards the end of stage 2.

5.4 Implications of a new MSC chronology in the Mediterranean

While not conclusive, the integration of our different stratigraphic proxies supports an early and long-lasting deposition of deep-basin halite. The direct implication of this age-model is that halite was deposited in the deep Eastern Mediterranean when sea level was high and partial, episodic connection with the Atlantic still prevailed (Dela Pierre et al., 2014; Flecker and Ellam, 2006; Krijgsman et al., 2002; Roveri et al., 2014b), synchronously with gypsum deposition along the Mediterranean margins and intermediate basins (Ochoa et al., 2015). Our results do not exclude an evaporative drawdown (e.g., Lofi, et al., 2011; Rouchy and Caruso, 2006; Ryan, 2008) and lower sea level at the acme of the MSC during stage 2 (Ohneiser et al., 2015). The lack of sedimentological features within the monotonously clean halite, and our interpretation of long-lasting deep-water evaporite depositional settings, indicate that salt must have started to precipitate within a deep-basin deep-water environment, and not in shallow-waters. We propose that sea-level drawdown ~~actually~~ prompted enhanced transport of clastic sediments into the deep basin resulting ~~with~~ in the deposition of the Interbedded Evaporites unit, analog to the marginal deposition of the RLG. Studies of strontium isotopes from the Lower Evaporites (PLG, MSC stage 1) consistently report isotopic values close to those characteristic of the global ocean~~s~~

(Flecker and Ellam, 2006; Roveri et al., 2014b), and do not support an early desiccation model (Cita, 1976; Hsü, 1973). While advocating a different chronological model, our study is consistent with these interpretations and shows that halite deposition started during a time when Atlantic inflow was still evident.

A coeval initiation of basinal halite and marginal gypsum precipitation calls for a reevaluation of previous models for MSC development, as well as its effect on global ocean salinity and climate. We refer to the timing and persistence of halite deposition (which may have been an order of magnitude larger than previously thought), and also to the substantially lower rates of deposition of the deep-basin salt unit, from a previous assumption of 3,000 cm/kyr (according to CIESM chronology) to 250 cm/kyr as deduced ~~by~~ from our new age model. Although this assumes continuous precipitation and no dissolution, which we consider unlikely if the water is being relatively refreshed with additional seawater throughout deposition. The Levant chronostratigraphic model suggests that steady state of halite deposition was achieved and maintained earlier in the MSC than previously thought. Both halite and gypsum could have been precipitated ~~be~~ synchronously ~~precipitated~~, with their partitioning possibly governed by their different solubility product constants (K_{sp}) and ion availability. Furthermore, if we allow for an order of magnitude change in the time scale of halite precipitation, then the required sedimentation flux that removes sodium and chlorine from seawater is reduced. This exercise substantially reduces the total sea-level drawdown (Ryan, 2008) required to explain the deposition of a ~2 km-thick salt deposit. A further possible mechanism to explain the synchronous deposition of gypsum and halite in marginal and deeper parts of the basin, respectively, includes density stratification and down-shelf cascading of brines (Roveri et al., 2014c; Sirota et al., 2017). While salt-saturated shallow waters seem to have reached gypsum saturation values, brine formation might have continuously flowed down-shelf, in a similar manner as dense shelf-water cascading (DSWC) is observed today around the Mediterranean Basin (Canals et al., 2009, 2006). DSWC is associated with mass-transport complexes and submarine channels, and has a significant impact on the sediment and organic-matter supply from continental and shallow-marine settings to deep-sea ecosystems. Mass-balance calculations suggest that the input of dissolved organic carbon and suspended particulate organic carbon from ocean margins to the open ocean interior may be more than an order of magnitude greater than direct inputs of organic carbon produced near the ocean surface today (Bauer and Druffel, 1998). Similarly, highly saturated waters produced in an evaporitic Mediterranean may have produced vast quantities of brine accumulating in the deep depocenters. Brine formation may have been at least partly controlled by precession-induced increases in river runoff (Marzocchi et al., 2015), and potentially by surface inflow from the Paratethys (Karakitsios et al., 2017; Krijgsman et al., 2010). Salinity stratification is supported by geochemical evidence for the occurrence of low-salinity surface waters overlying deep brines at gypsum and halite saturation (Christeleit et al., 2015), as well as by the presence of brackish-water faunas of Paratethyan origin in the Lago-Mare phase (Stoica et al., 2016). Our data, including high concentrations of long-chain *n*-alkanes (Table 1) and high LCA/SCA values (Table 1), also support the occurrence of increased river runoff into the basin during the deposition of the Interbedded Evaporites.

Our interpretation of a deep-basin-deep-water model and early onset of halite, rejuvenates an idea that has been a focus of debate in the past (e.g., Garcia-Castellanos and Villaseñor, 2011; Lofi et al., 2011; Ryan, 2008; Schmalz, 1969). Simon and Meijer (2017) used a box-model setup to model the MSC events forced by Atlantic exchange and evaporative loss. This model demonstrated that a significantly stratified Mediterranean water column could have been established early in the crisis, while the duration of halite deposition must have taken longer than currently considered in the MSC stratigraphic consensus model. The synchronous formation of gypsum and halite in proximal and distal basins, respectively, could have occurred at different levels within the basin, with lower rates of halite sedimentation than previously thought. Our data supports the model by Simon and Meijer (2017) and calls to reevaluate Mediterranean MSC sections, while considering a possible early deposition of halite.

Sea--level drop during stage 2 of the MSC may have added more proximal basins to the regional deep-sea deposition of halite, which might explain why those intermediate-basin halite deposits correlate to the stage 2 RLG. Such a mechanism can explain the existence of marginal or intermediate-depth basins with relatively thin halite deposits, which only correlate with the Interbedded evaporites Evaporites interval in the Levant (Fig. 12), in which halite is still the dominant lithology. For example, the marginal Realmonte salt mine has a ~600 m thick halite sequence (Lugli et al., 1999; Roveri et al., 2014a) compared with the thick (>2 km) halite deposits in deep Mediterranean basins. In a similar manner, recent studies from the Dead Sea demonstrate downslope--flowing brines, in which the deep basinal areas accumulate the most brine and the marginal areas are influenced by fresher waters and hence subject to more dissolution (Sirota et al., 2016).

Being one of the largest and youngest salt giants formation episodes in Earth's history, the MSC is repeatedly used as a cornerstone for explaining evaporite deposition. Our new model, which includes the synchronous deposition of sulfates in the margins of the basin and halite at its center, calls for a re-evaluation of the mechanisms governing evaporite deposition in other salt-giant deposits in the geologic record. For example, in the Permian Zechstein-, similar to the Mediterranean, sulfates appear to have been limited to the margins while halite was deposited in the deeper parts of the basin (Richter-Bernburg, 1985). This is also the case for the Permian ~~aged~~ Delaware Basin in Texas and New Mexico, where clear inter-fingering between sulfates and halite are observed as brine concentrations oscillate (Anderson and Dean, 1995).

The alternating clastic and evaporitic sediments of the Interbedded Evaporites (Unit 5; Gvirtzman et al., 2013; 2017) include cycles 19-28, matching in its lower part the time frame of MSC stage 2, the RLG. Isolation from the Atlantic and significant sea~~-~~-level drawdown ~~is~~ are proposed as the formation mechanism for both the onshore deep subaerial canyons and offshore erosion surfaces across the Mediterranean (Lofi et al., 2011; Ryan, 1976; Ryan and Cita, 1978). Different models were proposed to explain the mechanisms behind erosion, transport, and re-deposition, such as early subaqueous large-scale mass-wasting processes occurring at the beginning of the MSC drawdown, subaerial rivers down-cutting by retrogressive action to adjust for their new base level, or marine abrasion as possible agent for late erosion (Lofi et al., 2011 and references therein). Regardless of the mechanism, clastic geometries are clear in MSC seismic sections and are partly controlled by local factors such as the dimension of the drainage basin, resulting in major differences between the Messinian sedimentary successions in the different areas of the Mediterranean. The whereabouts of the massive products of ~~this~~ these basin-wide erosional processes has been one of the MSC's enigmas (Ryan, 1976; Ryan and Cita, 1978; Lofi et al., 2011). The seismic facies defined as the Complex Unit (CU; Lofi et al., 2011) in the Western Mediterranean is either chaotic or roughly bedded, and is believed to account for some of the waste products. CU deposits are absent on the margin shelves, rarely observed on the upper slopes, and mainly ~~recovered~~ observed ~~at~~ along the ~~margin feet~~base of the slopes, either as fan~~-~~-shaped deposits at the Messinian river mouths or as poorly organized bodies elsewhere. This unit ~~makes~~ marks the transition between the eroded slopes and deep~~-~~-basin deposits (Lofi et al., 2011). The CU is positioned above or parallel to the Mobile Unit (the halite).

In summary, stage 2 of the MSC is characterized by massive sediment displacement, for which only a portion is accounted for. We propose that the Interbedded Evaporites (Unit 5; Gvirtzman et al., 2017) are part of this high-energy system and that the interbedding of clastics represents the deep-basin depocenters for the fine grained material at the distal part of the drainage system. These precession~~al~~-~~-~~controlled clastic incursions ~~were displaced~~reached into an evaporitic system, which in the deep basins has been depositing halite for ~360 kyr during stage 1 of the MSC. We argue that this idea could not be examined before due to lack of a sedimentary record from the deep basin and the difficulty of correlating marginal and deep-~~-~~basin units based on seismo-stratigraphy. The call for caution regarding the interpretation of MSC-~~-~~related offshore data was recently presented by Roveri et al. (2019). They pointed out that MSC units ~~having~~ with different age, nature and depositional setting~~s~~, may show similar seismic facies and geometries. On the other hand, the same unit~~s~~ may appear as belonging to different seismic facies, either with parallel and high-amplitude reflections or even transparent or chaotic reflectivity due to seismic interference patterns related to the dominant frequency. We therefore argue against lumping the different facies of the Interbedded Evaporites into a unified deep-basin halite deposit, disregarding its clastic nature, as done in past interpretations of the Levant Basin MSC section (e.g., Manzi et al., 2018). Here we offer new sedimentological analysis of the non-evaporitic facies, interpreted in the past as clastic deposits through seismic and well-~~-~~log interpretation (e.g., Feng et al., 2016). We argue that two different 'non-halite' deposits exist in the Levant deep MSC deposits: 1) ~~The~~ the mostly biogenic remains of diatoms (the Argillaceous

Diatomites) within the stage 1 Main Halite interval, and 2) ~~The~~ the clastic and reworked deposits of the Interbedded Evaporites/Argillaceous Evaporites belonging to stage 2 and 3 of the MSC.

Stage 3 of the MSC is generally characterized by reworking of shelf sediments and their occasional influx into the basin during renewed gypsum deposition. We position the base of stage 3 within the Interbedded Evaporites~~-~~ at cycle 23 (Figs~~.~~ 5, 6, ~~7~~12), pointing to a much thicker stage 3 section in the Levant ~~then~~ than in the model of Gvirtzman et al. (2017), Manzi et al. (2018), or Madof et al. (2019). Relying on the CIESM (2008) stratigraphic model, these separate studies position the halite into stage 2, and continue stage 2 until almost the top of the Levant MSC section. They position stage 3 at the topmost part of the section, represented only by Unit 7 - a thin anhydrite and shale unit (~~as~~ interpreted by well~~-~~-log data in the deep basin as no study has recovered samples from this interval thus far). These studies mainly differ in their interpretation of the stage 3 depositional environment, namely subaerial (Madof et al., 2019) or subaqueous (Gvirtzman ey al., 2017) dissolution~~/~~ and truncation. According to our depositional model (Fig. 12), Unit 6 belongs to stage 3 of the MSC (the Upper Gypsum and Lago Mare; CIESM, 2008), and the IMTS (Gvirtzman et al., 2017) or IES (Madof et al., 2019) unconformities in the Levant represent the transition between stage 3.1 (Upper Gypsum) and 3.2 (Lago Mare) of the MSC. The latter stage (3.2) was attributed to Unit 7 and perhaps also to parts of the overlying brackish Afiq Formation (Druckman et al., 1995) by Gvirtzman et al. (~~2018~~2017). The introduction of Paratethyan waters and sediment, termed Lago Mare deposits along the Paratethyan side of the Mediterranean, is also likely to have reached the deep basins. However, while those might have reached the Levant Basin, different local drainage systems are most likely the sources for the MSC stage 3 transported sediments in the Levant area. A local source for transported sediments is the Nile drainage and fan systems, identified as reaching further north~~-~~west, beyond the Dolphin and Leviathan wells, towards the Eratosthenes Seamount offshore Cyprus (Hawie et al., ~~2013b~~2013a, ~~2013a~~2013b). In addition, local drainage systems that may have supplied the transported sediments ~~observed~~ include the Afiq and Ashdod canyons (Bertoni and Cartwright, 2007; Druckman et al., 1995), and the southern Turkey and western Syria drainage systems proposed by Madof et al. (2019).

6. Conclusions

Over the past 50 years, models explaining the formation of offshore MSC deposits have remained hypothetical in the absence of a complete sedimentary record of the deep Mediterranean ~~basin~~Basin. The current study presents ~~results~~results from the offshore Dolphin and Leviathan-1 wells, which penetrated MSC evaporites ~~at~~ from 2~~,~~025 to 3~~,~~616 ~~m.b.s.l~~m, and from 2~~,~~090 to 3~~,~~759 ~~m.b.s.l~~m, respectively. Our results challenge some of the current models for the MSC~~,~~ regarding the synchronicity or diachronism of evaporite deposits across the Mediterranean ~~basin~~Basin, their composition, and controlling factors. A longer duration for halite deposition than previously assumed impacts our understanding of the biochemical and spatial constraints of this time period. While similar ideas have been previously raised (e.g., Van Couvering et al., 1976; Govers, 2009; Hardie and Lowenstein, 2004; Meilijson et al., 2018; Ryan, 2011; Simon and Meijer, 2017), we provide the first report on sedimentological data from the deep basin MSC halite deposits supporting the scenario of long-lasting salt deposition. We call for a re-evaluation of models based on a ~50 kyr-long deposition of halite in the deep basins. However, samples from the upper part of the deep MSC deposits in the Eastern Mediterranean are not ~~currently~~ yet available, while the existing sedimentary record drilled by the industry consists of well cuttings and not a continues core. The complexity revealed by this study makes a strong case for future scientific drilling efforts that can retrieve cores from different parts of the deep-basin halite deposits of the Mediterranean.

This study aimed at addressing the composition and key stratigraphic questions regarding the timing and correlation of MSC events in the deep Mediterranean. Our main findings can be summarized as follows:

1. The formation of thick halite deposits in the Levant Basin occurred in a deep-basin deep-water environment that began earlier than previously thought, during the PLG phase of gypsum precipitation ~~on~~ in the marginal basins~~s~~. This implies that a shallow desiccated scenario is not necessarily required to generate halite ~~-~~precipitation during the MSC. The presence of well-preserved marine planktonic diatoms within the massive halite deposits strongly supports a periodic connectivity between the Atlantic and the Eastern Mediterranean during halite deposition.
2. The exact timing for the end of deep-~~-~~basin halite precipitation is still unclear. Well-~~-~~log interpretation, cyclostratigraphy, and the astronomical tuning model presented here suggest that halite deposition continued at least until 5.45 Ma, and interbedded clastic material and evaporites (probably mainly gypsum/anhydrite) persisted until ca. 5.33 Ma.
3. The transition into the Interbedded Evaporites interval at 2~~,~~560 m at Dolphin and 2~~,~~800 m at Leviathan-1 marks a major shift in the mode of deposition. An increase in basin-ward transport of sediments is indicated by the high abundance of larger sub-rounded clastic grains such as quartz and plagioclase~~ minerals~~, clay, micrite, and reworked Cretaceous ~~and~~ to Eocene benthic and planktic foraminifera. Variable ~~ranges of organic- matter~~ thermal maturity indices also point to mixed sources of organic matter~~sediment~~. In general, biomarker indices in the Interbedded Evaporites resemble those measured

elsewhere in the Mediterranean Basin from strata with transported material and mixed sources. The transition from the Main Halite to the Interbedded Evaporites at 2~~,~~560 m most likely represents the transition between stage 1 and 2 of the MSC. The ~~massive~~ large amounts of clastic sediments in the Interbedded Evaporites are possibly an answer to one of the MSC enigmas~~,~~ regarding the location of the transported material related to the sea-level drawdown of stage 2 and the ~~closer~~ interruption of the connection with of the Atlantic Ocean.

4. During the MSC, high sea level and partial connectivity with the global ocean~~s~~ promoted the deposition of deep-basin deep-water halite, while see-level drawdown promoted deposition of reworked and transported material from the margins into deep Mediterranean basins.

Acknowledgments

The authors would like to thank Ratio Oil Exploration, Noble Energy, and Delek Energy for kindly providing data and permission to publish. This work was supported by the State of Israel Ministry of Energy, the Maurice Hatter Foundation, and by the Marie Curie Career Integration Grants (CIG) FP7-PEOPLE-2011-CIG under the GASTIME project framework. The work was also supported by the COST Action “Uncovering the Mediterranean salt giant” (MEDSALT) supported by COST (European Cooperation in Science and Technology). We are grateful to Emerson-Paradigm for software sponsorship. We would also like to thank Tanja Kouwenhoven for her contribution with foraminiferal analysis, Revital Bookman and Beverly Goodman for the use of laboratory equipment, Nimer Taha and Alexander Surdyaev for laboratory assistance with the XRD/XRF analysis and seismic interpretation, respectively. Nadia Dildar, Alexander Weber, and Ian Bishop are thanked for laboratory assistance for biomarker analysis and diatom taxonomy. We thank William B.F. Ryan, Andre Strasser, and an anonymous reviewer for suggestions which significantly improved the manuscript.

References

Alinat, J., Cousteau, J., 1962. Accidents de terrain en mer de Ligurie. Océanographie géologique et géophysique de la Mediterranee occidentale, 121. Centre national de la recherche scientifique, Paris.

Almogi-Labin, A., Bein, A., Sass, E., 1993. Late Cretaceous upwelling system along the Southern Tethys Margin (Israel): Interrelationship between productivity, bottom water environments, and organic matter preservation. Paleoceanography 8, 671–690. doi:10.1029/93PA02197

Anderson, R.Y., Dean, W.E., 1995. Filling the Delaware Basin: Hydrologic and Climatic Controls on the Upper Permian Castile Formation Varved Evaporite, in: Scholle, P.A., Peryt, T.M., Ulmer-Scholle, D.S. (Eds.), The Permian of Northern Pangea: Volume 2: Sedimentary Basins and Economic Resources. Springer Berlin Heidelberg, Berlin, Heidelberg, pp. 61–78. doi:10.1007/978-3-642-78590-0_4

Arnon, A., Selker, J.S., Lensky, N.G., 2016. Thermohaline stratification and double diffusion diapycnal fluxes in the hypersaline Dead Sea. Limnol. Oceanogr. 61, 1214–1231. doi:10.1002/lno.10285

Bauer, J.E., Druffel, E.R.M., 1998. Ocean margins as a significant source of organic matter to the deep open ocean. Nature 392, 20–23. doi:10.1038/33122

Bayliss, D.D., 1973. Micropalaeontology of sections Cenomanian to Middle Eocene West Bank of Jordan. London.

Bellaiche, G., Gennesseaux, M., Mauffret, A., Rehault, J.P., 1974. Prélèvements systématiqus et caractérisation des réflecteurs acoustiques: nouvelle étape dans la compréhension de la géologie de la Méditerranée occidentale. Marine Geology 16, M47–M56.

Berggren, W.A., Kennett, J.P., Srinivasan, M.S., 2006. Neogene Planktonic Foraminifera: A Phylogenetic Atlas. Micropaleontology. doi:10.2307/1485586

Bertoni, C., Cartwright, J.A., 2007. Major erosion at the end of the Messinian Salinity Crisis: Evidence from the Levant Basin, Eastern Mediterranean. Basin Res. 19, 1–18. doi:10.1111/j.1365-2117.2006.00309.x.

Bertoni, C., Cartwright, J.A., 2006. Controls on the basinwide architecture of late Miocene (Messinian) evaporites on the Levant margin (Eastern Mediterranean). Sediment. Geol. 188–189, 93–114. doi:10.1016/j.sedgeo.2006.03.019.

Biehl, B.C., Reuning, L., Strozyk, F., Kukla, P.A., 2014. Origin and deformation of intra-salt sulphate layers: An example from the Dutch Zechstein (Late Permian). Int. J. Earth Sci. 103, 697–712. doi:10.1007/s00531-014-0999-4

Blanc, P., 2000. Of sills and straits : a quantitative assessment of the Messinian Salinity Crisis. Deep. Res. I 47, 1429–1460.

Bond, G., Kromer, B., Beer, J., Muscheler, R., Evans, M.N., Showers, W., Hoffmann, S., Lotti-Bond, R., Hajdas, I., Bonani, G., 2001. Persistent Solar Influence on North Atlantic Climate During the Holocene. Science (80-.). 294, 2130–2136.

Borsetti,, A. M., Curzi, P. V., Landuzzi, V., Mutti, M., Ricci Lucchi, F., Sartori, R., Tomadin, L., Zuffa, G.G., 1990. Messinian and pre-Messinian sediments from ODP leg 107 Sites 652 and 654 in the Tyrrhenian Sea: sedimentological and petrographic study and possible comparisons with Italian sequences, in: Kastens, K. A., Mascle, J., et al. (Ed.), Proc. Ocean Drill. Program, 107 Sci. Results 107, 169–186. doi:10.2973/odp.proc.sr.107.161.1990.

Bourcart, J., Boillot, G., Cousteau, J.Y., Gennesseaux, M., Klimek, C., 1958. Les sediments profonds au large de la cote nicoise. Comptes Rendus de 1'Academie des Sciences Paris 147, 116.

Bray, E.E., Evans, E.D., 1961. Distribution of n-paraffins as a clue to recognition of source beds. Geochim. Cosmochim. Acta 22, 2–15. doi:10.1016/0016-7037(61)90069-2

Buchbinder, B., Zilberman, E., 1997. Sequence stratigraphy of Miocene-Pliocene carbonate-siliciclastic shelf deposits in the eastern Mediterranean margin (Israel): effects of eustasy and tectonics. Sediment. Geol. 112, 7–32.

Camerlenghi, A., Aoisi, V., Lofi, J., Hübscher, C, deLange, G., Flecker, R., Garcia-Castellanos, D., Gorini, C., Krijgsman, W., Lugli, S., Makovsky, Y., Manzi, V., McGenity, T., Pan, N., 2014. Uncovering a Salt Giant. Deep-Sea Record of Mediterranean Messinian Events (DREAM) multi-phase drilling project, in: EGU. Vienna, p. 1.

Canals, M., Danovaro, R., Heussner, S., Lykousis, V., Puig, P., Trincardi, F., Calafat, A., Durrieu de Madron, X., Palanques, A., 2009. Cascades in Mediterranean Submarine Grand Canyons. Oceanography 22, 26–43. doi:10.5670/oceanog.2009.03

Canals, M., Puig, P., de Madron, X.D., Heussner, S., Palanques, A., Fabres, J., 2006. Flushing submarine canyons. Nature 444, 354–357. doi:10.1038/nature05271

Christeleit, E.C., Brandon, M.T., Zhuang, G., 2015. Evidence for deep-water deposition of abyssal Mediterranean evaporites during the Messinian salinity crisis. Earth Planet. Sci. Lett. 427, 226–235. doi:10.1016/j.epsl.2015.06.060

CIESM, 2008. The Messinian Salinity Crisis from mega-deposits to microbiology - A consensus report. N° 33. CIESM Work. Monogr. 7–10.

Cita, M.B., 1976. Biodynamic effects of the messinian salinity crisis on the evolution of planktonic foraminifera in the mediterranean. Palaeogeogr. Palaeoclimatol. Palaeoecol. 20, 23–42. doi:10.1016/0031-0182(76)90023-7

Cita, M.B., Ryan, W.B.F., Kidd, R.B., 1978. Sedimentation rates in neogene deep-sea sediments from the mediterranean and geodynamic implications of their changes, in: Initial Reports of the Deep Sea Drilling Project. pp. 991–1002.

Cita, M.B., Santambrogio, S., Melillo, B., Rogate, F., 2006. Messinian Paleoenvironments: New Evidence from the Tyrrhenian Sea (ODP Leg 107). Proc. Ocean Drill. Program, 107 Sci. Results 107, 211–227. doi:10.2973/odp.proc.sr.107.161.1990.

Clauzon G., Suc, J.P., Gautier, F., Berger, A., Loutre, M.F., 1996. Alternate interpretation of the Messinian salinity crisis, controversy resolved? Geology, 24, 363-366. Doi: 10.1130/0091-7613

Cornet, C., 1968. Le graben médian (zone A) de laMéditerranée occidentale pourrait etre pontien. Sommaire Societé Géologique de France 149.

Couto, D. Do, Popescu, S., Suc, J., Melinte-dobrinescu, M.C., Barhoun, N., Gorini, C., Jolivet, L., Poort, J., Jouannic, G., Auxietre, J., 2014. Lago Mare and the Messinian Salinity Crisis : Evidence from the Alboran Sea Lago Mare and the Messinian Salinity Crisis : Evidence from the Alboran Sea (S . Spain). Mar. Pet. Geol. 52, 57–76. doi:10.1016/j.marpetgeo.2014.01.018

Van Couvering, J.A., Berggren, W.A., Drake, R.E., Aguirre, E., Curtis, G.H., 1976. The terminal Miocene event. Mar. Micropaleontol. 1, 263–286.

Debenedetti, A., 1982. The problem of the origin of the salt deposits in the mediterranean and of their relations to the other salt occurrences in the neogene formations of the contiguous regions. Mar. Geol. 49, 91–114.

Dela Pierre, F., Clari, P., Natalicchio, M., Ferrando, S., Giustetto, R., Lozar, F., Lugli, S., Manzi, V., Roveri, M., Violanti, D., 2014. Flocculent layers and bacterial mats in the mudstone interbeds of the Primary Lower Gypsum unit (Tertiary Piedmont basin, NW Italy): Archives of palaeoenvironmental changes during the Messinian salinity crisis. Mar. Geol. 355, 71–87. doi:10.1016/j.margeo.2014.05.010

Derin, B., 2000. Stratigraphic and environments of deposition of Or South 1075–2090 m. Ramat Gan, Derin Consulting & Micropaleontological Services LTD, Internal Isramco Consultant Report 2/00.

Ditlevsen, P.D., Andersen, K.K., Svensson, A., 2007. The DO-climate events are probably noise induced: Statistical investigation of the claimed 1470 years cycle. Clim. Past 3, 129–134. doi:10.5194/cp-3-129-2007

Driussi, O., Maillard, A., Ochoa, D., Lofi, J., Chanier, F., Gaullier, V., Briais, A., Sage, F., Sierro, F., Garcia, M., 2015. Messinian Salinity Crisis deposits widespread over the Balearic Promontory: Insights from new high-resolution seismic data. Mar. Pet. Geol. 66, 41–54. doi:10.1016/j.marpetgeo.2014.09.008

Druckman, Y., Buchbinder, B., Martinotti, G.M., Tov, R.S., Aharon, P., 1995. The buried Afiq Canyon (eastern Mediterranean, Israel): a case study of a Tertiary submarine canyon exposed in Late Messinian times. Mar. Geol. 123, 167–185. doi:10.1016/0025-3227(94)00127-7

Ensminger, A., Joly, G., Albrecht, P., 1978. Rearranged steranes in sediments and crude oils. Tetrahedron Letters. 1575–1578. doi:https://doi.org/10.1016/S0040-4039(01)94608-8

Feng, Y.E., Yankelzon, A., Steinberg, J., Reshef, M., 2016. Lithology and characteristics of the Messinian evaporite sequence of the deep Levant Basin, Eastern Mediterranean. Mar. Geol. 376, 118–131. doi:10.1016/j.margeo.2016.04.004

Flecker, R., Ellam, R.M., 2006. Identifying Late Miocene episodes of connection and isolation in the Mediterranean-Paratethyan realm using Sr isotopes. Sediment. Geol. 188–189, 189–203. doi:10.1016/j.sedgeo.2006.03.005

Flecker, R., et al., 2015. Evolution of the Late Miocene Mediterranean-Atlantic gateways and their impact on regional and global environmental change. *Earth-Science Reviews,* 150**,** 365–392.

Frey-Martınez, J., Hall, B., Cartwright, J., Huuse, M., 2007. Clastic Intrusion at the Base of Deep-water Sands: A Trap-forming Mechanism in the Eastern Mediterranean. Sand Inject. Implic. Hydrocarb. Explor. Prod. AAPG Mem. 87 49–63. doi:10.1306/1209849M873255

Garcia-Castellanos, D., Villaseñor, A., 2011. Messinian salinity crisis regulated by competing tectonics and erosion at the Gibraltar arc. Nature 480, 359–363. doi:10.1038/nature10651

García-Veigas, J., Cendón, D.I., Gibert, L., Lowenstein, T.K., Artiaga, D., 2018. Geochemical indicators in Western Mediterranean Messinian evaporites: Implications for the salinity crisis. Mar. Geol. 403, 197–214. doi:10.1016/j.margeo.2018.06.005

Gardosh, M., Druckman, Y., Buchbinder, B., Rybakov, M., 2008. The Levant Basin Offshore Israel: Stratigraphy, Structure, Tectonic Evolution and Implications for Hydrocarbon Exploration - revised edition. Geological Survey of Israel report GSI/4/2008.

Garrison, R.E., Schreiber, B.C., Bernoulli, D., Fabricius, F.H., Kidd, R.B.., Mélières, F., 1978. Sedimentary Petrology and Structures of Messinian Evaporitic Sediments in the Mediterranean Sea, Leg 42A, Deep Sea Drilling Project, in: Initial Reports of the Deep Sea Drilling Project 42, No. 1. pp. 571–612.

Geletti, R., Zgur, F., Del Ben, A., Buriola, F., Fais, S., Fedi, M., Forte, E., Mocnik, A., Paoletti, V., Pipan, M., Ramella, R., Romeo, R., Romi, A., 2014. The Messinian Salinity Crisis: New seismic evidence in the West-Sardinian Margin and Eastern Sardo-Provencal basin (West Mediterranean Sea). Mar. Geol. 351, 76–90. doi:10.1016/j.margeo.2014.03.019

Gennari, R., Manzi, V., Angeletti, L., Bertini, A., Ceregato, A., Faranda, C., Gliozzi, E., Menichetti, E., Rosso, A., Roveri, M., Taviani, M., 2013. A shallow water record of the onset of the Messinian salinity crisis in the Adriatic foredeep (Legnagnone section, Northern Apennines).NU SC. Palaeogeogr. Palaeoclimatol. Palaeoecol. doi:10.1016/j.palaeo.2013.05.015

Govers, R., 2009. Choking the Mediterranean to dehydration: The Messinian salinity crisis. Geology 37, 167–170. doi:10.1130/G25141A.1

Gvirtzman, Z., Manzi, V., Calvo, R., Gavrieli, I., Gennari, R., Lugli, S., Reghizzi, M., Roveri, M., 2017. Intra-Messinian truncation surface in the Levant Basin explained by subaqueous dissolution. Geology 45, 4–7. doi:10.1130/G39113.1

Gvirtzman, Z., Reshef, M., Buch-leviatan, O., Ben-avraham, Z., 2013a. Intense salt deformation in the Levant Basin in the middle of the Messinian Salinity Crisis. Earth Planet. Sci. Lett. 379, 108–119. doi:10.1016/j.epsl.2013.07.018

Gvirtzman, Z., Reshef, M., Buch-Leviatan, O., Ben-Avraham, Z., 2013b. Intense salt deformation in the Levant Basin in the middle of the Messinian Salinity Crisis. Earth Planet. Sci. Lett. 379, 108–119. doi:10.1016/j.epsl.2013.07.018

Hall, J.K., Udintsev, G.B., Odinikov, Y.Y., 1994. The bottom relief of the Levantine Sea, in Geologic Structure of the Northeastern Mediterranean. Krasheninnikov, V. A., Hall, J.K., pp. 5–32, Historical Productions-Hall Ltd., Jerusalem.

Hall, J.K., Lippman, S., Gardosh, M., Tibor, G., Sade, A.R., Sade, H., 2015. A New Bathymetric Map for the Israeli EEZ: Preliminary Results. State of Israel, Ministry of National

Infrastructure Energy and Water, Jerusalem.

Hardie, L.A., Lowenstein, T.K., 2004. Did the Mediterranean Sea Dry Out During the Miocene? a Reassessment of the Evaporite Evidence From Dsdp Legs 13 and 42a Cores. J. Sediment. Res. 74, 453–461. doi:10.1306/112003740453

Hawie, N., Deschamps, R., Nader, F.H., Gorini, C., 2013a. Sedimentological and stratigraphic evolution of northern Lebanon since the Late Cretaceous: implications for the Levant margin and basin. doi:10.1007/s12517-013-0914-5

Hawie, N., Gorini, C., Deschamps, R., Nader, F.H., Montadert, L., Granjeon, D., Baudin, F., 2013b. Tectono-stratigraphic evolution of the northern Levant Basin (offshore Lebanon). Mar. Pet. Geol. 48, 392–410. doi:10.1016/j.marpetgeo.2013.08.004

Hernández-Molina F.J, et al., 2014. Onset of Mediterranean outflow into the North Atlantic. Science 344, 1244–1250. doi: 10.1126/science.1251306

Hilgen, F., Kuiper, K., Krijgsman, W., Snel, E., Laan, E. Van Der, van der Laan, E., 2007. Astronomical tuning as the basis for high resolution chronostratigraphy: The intricate history of the Messinian Salinity Crisis. Stratigraphy 4, 231–238.

Hilgen, F.J., Bissoli, L., Iaccarino, S., Krijgsman, W., Meijer, R., Negri, A., Villa, G., 2000. Integrated stratigraphy and astrochronology of the Messinian GSSP at Oued Akrech (Atlantic Morocco). Earth Planet. Sci. Lett. 182, 237–251. doi:10.1016/S0012-821X(00)00247-8

Hilgen, F.J., Krijgsman, W., 1999. Cyclostratigraphy and astrochronology of the Tripoli diatomite formation (pre-evaporite Messinian, Sicily, Italy). Terra Nov. 11, 16–22. doi:10.1046/j.1365-3121.1999.00221.x

Hilgen, F.J., Krijgsman, W., Langereis, C.G., Lourens, L.J., Santarelli, A., Zachariasse, W.J.,

1995. Extending the astronomical (polarity) time scale into the Miocene. Earth Planet. Sci. Lett. 136, 495–510. doi:10.1016/0012-821X(95)00207-S

Hsü, K.J., 1973. The desiccated deep-basin model for the Messinian events, in: Drooger, C.W. (Ed.), Messinian Events in the Mediterranean. North-Holland Publ. Co., Amsterdam, pp. 60–67.

Hsü, K .J., Ryan, W.B.F., Schreiber, B.C., 1973. Petrography of a halite sample from hole 134 - balearic abyssal plain, in: Initial Reports of the Deep Sea Drilling Project 13, No. Part 2. pp. 708–711.

Hsü, K.J., Montadert, L., Bernoulli, D., Bizon, G., Cita, M., Erickson, A., Fabricius, F., Garrison, R.E., Kidd, R.B., Mélières, F., Müller, C., Wright, R.C., 1978a. Site 374: Messina Abyssal Plain, in: Initial Reports of the Deep Sea Drilling Project: DSDP Volume XLII Part 1. p. 43. doi:10.2973/dsdp.proc.42-1.105.1978

Hsü, K.J., Montadert, L., Bernoulli, D., Bizon, G., Cita, M., Erickson, A., Fabricius, F., Garrison, R.E., Kidd, R.B., Mélières, F., Müller, C., Wright, R.C., 1978b. Sites 375 and 376: Florence Rise, in: Initial Reports of the Deep Sea Drilling Project: DSDP Volume XLII Part 1. p. 86.

Hüsing, S.K., Cascella, A., Hilgen, F.J., Krijgsman, W., Kuiper, K.F., Turco, E., Wilson, D., 2010. Astrochronology of the Mediterranean Langhian between 15 . 29 and 14 . 17 Ma. Earth Planet. Sci. Lett. 290, 254–269. doi:10.1016/j.epsl.2009.12.002

Hüsing, S.K., Kuiper, K.F., Link, W., Hilgen, F.J., Krijgsman, W., 2009. The upper Tortonian-lower Messinian at Monte dei Corvi (Northern Apennines, Italy): Completing a Mediterranean reference section for the Tortonian Stage. Earth Planet. Sci. Lett. 282, 140–157. doi:10.1016/j.epsl.2009.03.010

Karakitsios, V., Cornée, J.J., Tsourou, T., Moissette, P., Kontakiotis, G., Agiadi, K., Manoutsoglou, E., Triantaphyllou, M., Koskeridou, E., Drinia, H., Roussos, D., 2017. Messinian salinity crisis record under strong freshwater input in marginal, intermediate, and deep environments: The case of the North Aegean. Palaeogeogr. Palaeoclimatol. Palaeoecol. 485, 316–335. doi:10.1016/j.palaeo.2017.06.023

Keogh, S.M., Butler, R.W.H., 1999. The Mediterranean water body in the late Messinian: interpreting the record from marginal basins on Sicily. J. Geol. Soc. London. 156, 837–846. doi:10.1144/gsjgs.156.4.0837

Krijgsman, W., Blanc-Valleron, M.M., Flecker, R., Hilgen, F.J., Kouwenhoven, T.J., Merle, D., Orszag-Sperber, F., Rouchy, J.M., 2002. The onset of the Messinian salinity crisis in the Eastern Mediterranean (Pissouri Basin, Cyprus). Earth Planet. Sci. Lett. 194, 299–310. doi:10.1016/S0012-821X(01)00574-X

Krijgsman, W., Fortuin, A.R., Hilgen, F.J., Sierro, F.J., 2001. Astrochronology for the Messinian Sorbas basin (SE Spain) and orbital (precessional) forcing for evaporite cyclicity. Sediment. Geol. 140, 43–60. doi:10.1016/S0037-0738(00)00171-8

Krijgsman, W., Garces, M., Agusti, J., Raffi, I., Taberner, C., Zachariasse, W.J., 2000. The “Tortonian salinity crisis” of the eastern Betics (Spain). Earth Planet. Sci. Lett. 181, 497–511. doi:10.1016/S0012-821X(00)00224-7

Krijgsman, W., Hilgen, F.J., Negri, A., Wijbrans, J.R., Zachariasse, W.J., 1997. The Monte del Casino section (Northern Apennines, Italy): A potential Tortonian/Messinian boundary stratotype? Palaeogeogr. Palaeoclimatol. Palaeoecol. 133, 27–47. doi:10.1016/S0031-0182(97)00039-4

Krijgsman, W., Hilgen, F.J., Raffi, I., Sierro, F.J., Wilson, D.S., 1999. Chronology, causes and progression of the Messinian salinity crisis. Nature 400, 652–655. doi:10.1038/23231.

Krijgsman, W., Meijer, P.T., 2008. Depositional environments of the Mediterranean "Lower Evaporites" of the Messinian salinity crisis: Constraints from quantitative analyses. Mar. Geol. doi:10.1016/j.margeo.2008.04.010

Krijgsman, W., Stoica, M., Vasiliev, I., Popov, V. V., 2010. Rise and fall of the Paratethys Sea during the Messinian Salinity Crisis. Earth Planet. Sci. Lett. 290, 183–191. doi:10.1016/j.epsl.2009.12.020.

Lange, G.J. De, Krijgsman, W., 2010. Messinian salinity crisis: A novel unifying shallow gypsum / deep dolomite formation mechanism. Mar. Geol. 275, 273–277. doi:10.1016/j.margeo.2010.05.003

Laskar, J., Robutel, P., Joutel, F., Gastineau, M., Correia, A.C.M., Levrard, B., 2004. A long-term numerical solution for the insolation quantities of the Earth. Astron. As-trophys. Astron. Astrophys. 428, 261–285. doi:10.1051/0004-6361:20041335

Leila, M., Kora, M.A., Ahmed, M.A., Ghanem, A., 2016. Sedimentology and reservoir characterization of the Upper Miocene Qawasim Formation, El-Tamad Oil Field onshore Nile Delta, Egypt. Arab. J. Geosci. 9, 1–13. doi:10.1007/s12517-015-2088-9

Lofi, J., Camerlenghi, A., 2014. Messinian Salinity Crisis - DREAM (Deep-sea Record of Mediterranean Messinian events) drilling projects Messinian Salinity Crisis - DREAM (Deep-sea Record of Mediterranean Messinian events) drilling projects, in: EGU. Vienna, p. 1.

Lofi, J., Sage, F., Deverchere, J., Loncke, L., Maillard, A., Gaullier, V., Thinon, I., Gillet, H., Guennoc, P., Gorini, C., 2011. Refining our knowledge of the Messinian salinity crisis records in the offshore domain through multi-site seismic analysis. Bull. la Soc. Geol. Fr. 182, 163–180. doi:10.2113/gssgfbull.182.2.163

Lohmann, J., Ditlevsen, P.D., 2018. Random and externally controlled occurrences of Dansgaard-Oeschger events. Clim. Past 14, 609–617. doi:10.5194/cp-14-609-2018

Lugli, S., Gennari, R., Gvirtzman, Z., Manzi, V., Roveri, M., Schreiber, B.C., 2013. Evidence of clastic evaporites in the canyons of the Levant Basin (Israel): implications for the Messinian Salinity Crisis. J. Sediment. Res. 83, 942–954. doi:10.2110/jsr.2013.72

Lugli, S., Manzi, V., Roveri, M., Schreiber, B.C., 2015. The deep record of the Messinian salinity crisis: Evidence of a non-desiccated Mediterranean Sea. Palaeogeogr. Palaeoclimatol. Palaeoecol. 433, 201–218. doi:10.1016/j.palaeo.2015.05.017

Lugli, S., Schreiber, B.C., Triberti, B., 1999. Giant polygons in the Realmonte Mine (Agrigento, Sicily); evidence for the desiccation of a Messinian halite basin. J. Sediment. Res. 69, 764–771. doi:10.2110/jsr.69.764

McArthur, J. M., Howarth, R. J., Shield, G. A., 2012. Chapter 7: Strontium Isotope Stratigraphy. In The Geologic Time Scale, eds. F. M. Gredstein, J. G. Ogg, M. D. Schmotz & G. M. Ogg, 1144 Elsevier.

Madof, A.S., Bertoni, C., Lofi, J., 2019. Discovery of vast fluvial deposits provides evidence for drawdown during the late Miocene Messinian salinity crisis. Geology 47, 171–174. doi:10.1130/G45873.1

Manzi, V., Gennari, R., Hilgen, F., Krijgsman, W., Lugli, S., 2013. Age refinement of the Messinian salinity crisis onset in the Mediterranean. doi:10.1111/ter.12038

Manzi, V., Gennari, R., Lugli, S., Persico, D., Reghizzi, M., Roveri, M., Schreiber, B.C., Calvo, R., Gavrieli, I., Gvirtzman, Z., 2018. The onset of the Messinian salinity crisis in the deep Eastern Mediterranean basin. Terra Nov. 38, 42–49. doi:10.1111/ter.12325

Manzi, V., Gennari, R., Lugli, S., Roveri, M., Scafetta, N., Charlotte, B., 2012. High-frequency cyclicity in the Mediterranean Messinian evaporites: evidence for solar-lunar climate forcing. J. Sediment. Res. 82, 991–1005. doi:10.2110/jsr.2012.81

Manzi, V., Lugli, S., Roveri, M., Dela Pierre, F., Gennari, R., Lozar, F., Natalicchio, M., Schreiber, B.C., Taviani, M., Turco, E., 2015. The Messinian salinity crisis in Cyprus: A further step towards a new stratigraphic framework for Eastern Mediterranean. Basin Res. 28, 207–236. doi:10.1111/bre.12107

Manzi, V., Lugli, S., Roveri, M., Schreiber, B.C., 2009. A new facies model for the Upper Gypsum of Sicily (Italy): Chronological and palaeoenvironmental constraints for the Messinian salinity crisis in the Mediterranean. Sedimentology 56, 1937–1960. doi:10.1111/j.1365-3091.2009.01063.x

Manzi, V., Lugli, S., Roveri, M., Schreiber, B.C., Gennari, R., 2011. The Messinian "Calcare di Base" (Sicily, Italy) revisited. Bull. Geol. Soc. Am. 123, 347–370. doi:10.1130/B30262.1

Marzocchi, A., Lunt, D.J., Flecker, R., Bradshaw, C.D., Farnsworth, A., Hilgen, F.J., 2015. Orbital control on late Miocene climate and the North African monsoon: Insight from an ensemble of sub-precessional simulations. Clim. Past 11, 1271–1295. doi:10.5194/cp-11-1271-2015

Meilijson, A., Ashckenazi-Polivoda, S., Ron-Yankovich, L., Illner, P., Alsenz, H., Speijer, R.P., Almogi-Labin, A., Feinstein, S., Berner, Z., Püttmann, W., Abramovich, S., 2014. Chronostratigraphy of the Upper Cretaceous high productivity sequence of the southern Tethys, Israel. Cretac. Res. 50. doi:10.1016/j.cretres.2014.04.006

Meilijson, A., Steinberg, J., Hilgen, F., Bialik, O.M., Waldmann, N.D., Makovsky, Y., 2018. Deep-basin evidence resolves a 50-year-old debate and demonstrates synchronous onset of Messinian evaporite deposition in a non-desiccated Mediterranean. Geology 46, 4–7.

Müller, D.W., Mueller, P.A., 1991. Origin and age of the Mediterranean Messinian evaporites: implications from Sr isotopes. Earth Planet. Sci. Lett. doi:10.1016/0012-821X(91)90039-K

Nam, M., Görür, N., Flecker, R., Sak, M., Tüno, C., Ellam, R., Krijgsman, W., Vincent, S., Dikba, A., 2006. Paratethyan–Mediterranean connectivity in the Sea of Marmara region (NW Turkey) during the Messinian. Sediment. geo 188–189, 171–187. doi:10.1016/j.sedgeo.2006.03.004

Netzeband, G.L., Hübscher, C.P., Gajewski, D., 2006. The structural evolution of the Messinian evaporites in the Levantine Basin. Mar. Geol. 230, 249–273. doi:10.1016/j.margeo.2006.05.004

Ochoa, D., Sierro, F.J., Lofi, J., Maillard, A., Flores, J.A., Suarez, M., 2015. Synchronous onset of the Messinian evaporite precipitation: First Mediterranean offshore evidence. Earth Planet. Sci. Lett. 427, 112–124. doi:10.1016/j.epsl.2015.06.059

Ogniben, L., 1957. Petrografia della Serie Solfifera Siciliana e considerazioni geologiche relative. Memorie Descriptive della Carta Geologica d'Italia 33, 1–275.

Ohneiser, C., Florindo, F., Stocchi, P., Roberts, A.P., DeConto, R.M., Pollard, D., 2015. Antarctic glacio-eustatic contributions to late Miocene Mediterranean desiccation and reflooding. Nat. Commun. 6, 8765. doi:10.1038/ncomms9765

Peters, K.E., A.E. Kontorovich, J.M.M., 1993. Geochemistry of selected oils and rocks from the central portion of the west Siberian Basin, Russia. Am. Assoc. Pet. Geol. Bull. 77, 87–863.

Peters, K.E., 1986. Guidelines for Evaluating Petroleum Source Rock Using Programmed Pyrolysis. Am. Assoc. Pet. Geol. Bull. 70, 318–329. doi:10.1306/94885688-1704-11D7-8645000102C1865D

Peters, K.E., Rohrback, B.G., Kaplan, I.R., 1980. Laboratory-simulated thermal maturation of

Recent sediments. Phys. Chem. Earth 12, 547–557. doi:10.1016/0079-1946(79)90136-8

Peters, K.E., Walters Clifford C, Moldowan, J.M., 2005. The Biomarker Guide, Biomarkers and Isotopes in Petroleum Exploration and Earth Histroy, Volume 2. Cambridge. doi:10.1017/s0016756806212056

Rashid, H., Grosjean, E., 2006. Detecting the source of Heinrich layers: An organic geochemical study. Paleoceanography 21. doi:10.1029/2005PA001240

Reiche, S., Hübscher, C., Beitz, M., 2014. Fault-controlled evaporite deformation in the Levant Basin, Eastern Mediterranean. Mar. Geol. 354, 53–68. doi:10.1016/j.margeo.2014.05.002

Richter-Bernburg, G., 1996. Zechstein-Anhydrite: Fazies und Genese, Geologisches Jahrbuch. Reihe A, Allgemeine und regionale Geologie Bundesrepublik Deutschland und Nachbargebiete, Tektonik, Stratigraphie, Paläontologie. Bundesanstalt für Geowissenschaften und Rohstoffe.

Roberts, G., Peace, D., 2007. Hydrocarbon plays and prospectivity of the Levantine basin, offshore Lebanon and Syria from modern seismic data. GeoArabia 12, 99–124.

Rouchy, J.M., Caruso, A., 2006. The Messinian salinity crisis in the Mediterranean basin : A reassessment of the data and an integrated scenario. Sediment. Geol. 188–189, 35–67. doi:10.1016/j.sedgeo.2006.02.005

Roveri, M., Flecker, R., Krijgsman, W., Lofi, J., Lugli, S., Manzi, V., Sierro, F.J., Bertini, A., Camerlenghi, A., De Lange, G., Govers, R., Hilgen, F.J., Hübscher, C., Meijer, P.T., Stoica, M., 2014a. The Messinian Salinity Crisis: Past and future of a great challenge for marine sciences. Mar. Geol. 352, 25–58. doi:10.1016/j.margeo.2014.02.002

Roveri, M., Gennari, R., Ligi, M., Lugli, S., Manzi, V., Reghizzi, M., 2019. The synthetic seismic expression of the Messinian salinity crisis from onshore records: implications for shallow- to deep-water correlations. Basin Res.. doi:10.1111/bre.12361

Roveri, M., Lugli, S., Manzi, V., Gennari, R., Schreiber, B.C., 2014b. High-resolution strontium isotope stratigraphy of the messinian deep Mediterranean basins: Implications for marginal to central basins correlation. Mar. Geol. 349, 113–125. doi:10.1016/j.margeo.2014.01.002

Roveri, M., Manzi, V., Bergamasco, A., Falcieri, F.M., Gennari, R., Lugli, S., Schreiber, B.C., 2014c. Dense shelf water cascading and messinian canyons: A new scenario for the mediterranean salinity crisis. Am. J. Sci. 314, 751–784. doi:10.2475/05.2014.03

Rullkötter, J., R.M., 1988. Natural and artificial maturation of biological markers in a Toarcian shale from northern Germany, in: Novelli, L.M. and L. (Ed.), Advances in Organic Geochemistry 1987. Oxford Pergamon Press, pp. 639–645.

Ryan, W.B.F., 2011. Geodynamic responses to a two-step model of the Messinian salinity crisis. Bull. la Soc. Geol. Fr. 182, 73–78. doi:10.2113/gssgfbull.182.2.73

Ryan, W.B.F., 2008. Modeling the magnitude and timing of evaporative drawdown during the Messinian salinity crisis. Stratigraphy 5, 227–243.

Ryan, W.B.F., 1978. Messinian badlands on the southeastern margin of the Mediterranean Sea. Mar. Geol. 27, 349–363. doi:10.1016/0025-3227(78)90039-7

Ryan, W.B.F., 1976. Quantitative evaluation of the depth of the western Mediterranean before, during and after the late Miocene salinity crisis. Sedimentology 23, 791–813.

Ryan, W.B.F., 1973. Geodynamic implications of the Messinian crisis of salinity, in: Drooger, D.W. (Ed.), Messinian Events in the Mediterranean. Elsevier, Amsterdam, pp. 26–38.

Ryan, W.B.F., Cita, M.B., 1978. The nature and distribution of Messinian erosional surfaces - Indicators of a several-kilometer-deep Mediterranean in the Miocene. Mar. Geol. doi:10.1016/0025-3227(78)90032-4

Ryan, W.B.F., Hsü, K.J., Cita, M.B., Dumitrica, P., Lort, J., Maync, W., Nesteroff, W.D., Pautot, G., Stradner, H., 2007. DSDP Volume XIII: 6. Balearic Rise - Site 124. The Shipboard Scientific Party. doi:10.2973/dsdp.proc.13.1973

Ryan, W.B.F., Stanley, D.J., Hersey, J.B., Fahlquist, D.A., Allan, T.D., 1971. The tectonics and geology of the Mediterranean Sea. In: Maxwell, A.E. (Ed.), The Sea. Wiley- Interscience, New York, pp. 387–492.

Scafetta, N., Milani, F., Bianchini, A., Ortolani, S., 2016. On the astronomical origin of the Hallstatt oscillation found in radiocarbon and climate records throughout the Holocene. Earth-Science Rev. 162, 24–43. doi:10.1016/j.earscirev.2016.09.004

Scalan, E.S., Smith, J.E., 1970. An improved measure of the odd-even predominance in the normal alkanes of sediment extracts and petroleum. Geochim. Cosmochim. Acta 34, 611–620. doi:10.1016/0016-7037(70)90019-0

Schmalz, R.F., 1969. Deep-Water Evaporite Deposition: A Genetic Model. Am. Assoc. Pet. Geol. Bull. 53, 798–823. doi:10.1306/5D25C7FD-16C1-11D7-8645000102C1865D

Schulz, M., 2002. On the 1470-year pacing of Dansgaard-Oeschger warm events. Paleoceanography 17, 4-1-4–9. doi:10.1029/2000PA000571

Schulz, M., Mudelsee, M., 2002. REDFIT: Estimating red-noise spectra directly from unevenly spaced paleoclimatic time series. Comput. Geosci. 28, 421–426. doi:10.1016/S0098-3004(01)00044-9

Selli, R., 1954. Il Bacino del Metauro. Giornale di Geologia 24, 1–294.

Sepúlveda, J., Wendler, J.E., Summons, R.E., Hinrichs, K.U., 2009. Rapid Resurgence of Marine Productivity After the Cretaceous-Paleogene Mass Extinction. Science (80-.). 326, 129–132.

Sierro, F.J., Hilgen, F.J., Krijgsman, W., Flores, J.A., 2001. The Abad composite (SE Spain): A Messinian reference section for the Mediterranean and the APTS. Palaeogeogr. Palaeoclimatol. Palaeoecol. 168, 141–169. doi:10.1016/S0031-0182(00)00253-4

Simon, D., Marzocchi, A., Flecker, R., Lunt, D.J., Hilgen, F.J., Meijer, P.T., 2017. Quantifying the Mediterranean freshwater budget throughout the late Miocene: New implications for sapropel formation and the Messinian Salinity Crisis. Earth Planet. Sci. Lett. 472, 25–37. doi:10.1016/j.epsl.2017.05.013

Simon, D., Meijer, P.T., 2017. Salinity stratification of the Mediterranean Sea during the Messinian crisis: A first model analysis. Earth Planet. Sci. Lett. 479, 366–376. doi:10.1016/j.epsl.2017.09.045

Sirota, I., Ali, A., Lensky, N.G., 2016. Seasonal variations of halite saturation in the Dead Sea. Water Resour. Res. 52. doi:10.1002/2014WR016618

Sirota, I., Enzel, Y., Lensky, N.G., 2017. Temperature seasonality control on modern halite layers in the Dead Sea: In situ observations. Bull. Geol. Soc. Am. 129, 1181–1194. doi:10.1130/B31661.1

Sonnenfeld, P., Finetti, I., 2011. Messinian Evaporites in the Mediterranean: A Model of Continuous Inflow and Outflow, in: Geological Evolution of the Mediterranean Basin. doi:10.1007/978-1-4613-8572-1-17

Sonnenfeld, P., Hudec, P.P., 1983. Clay laminations in Halite: Their Cause and Effect, in: Sixth International Syposyum on Salt. pp. 51–56.

Steinberg, J., Gvirtzman, Z., Folkman, Y., 2010. New age constraints on the evolution of the Mt Carmel structure and its implications on a Late Miocene extensional phase of the Levant continental margin. J. Geol. Soc. London. 167, 203–216. doi:10.1144/0016-76492009-089

Steinberg, J., Gvirtzman, Z., Folkman, Y., Garfunkel, Z., 2011. Origin and nature of the rapid late Tertiary filling of the Levant Basin. Geology 39, 355–358. doi:10.1130/G31615.1

Steinhilber, F., Abreu, J.A., Beer, J., Brunner, I., Christl, M., Fischer, H., Heikkila, U., Kubik, P.W., Mann, M., McCracken, K.G., Miller, H., Miyahara, H., Oerter, H., Wilhelms, F., 2012. 9,400 Years of Cosmic Radiation and Solar Activity From Ice Cores and Tree Rings. Proc. Natl. Acad. Sci. 109, 5967–5971. doi:10.1073/pnas.1118965109

Steinhorn, I., 1983. In situ salt precipitation at the Dead Sea. Limnol. Oceanogr. 28, 580–583. doi:10.4319/lo.1983.28.3.0580

Stiller, M., Gat, J.R., Kaushansky, P., 1997. Halite Precipitation and Sediment Deposition As Measured in Sediment Traps Deployed in the Dead Sea: 1981-1983. Dead Sea lake its settings 161–170.

Stoica, M., Krijgsman, W., Fortuin, A., Gliozzi, E., 2016. Paratethyan ostracods in the Spanish Lago-Mare: More evidence for interbasinal exchange at high Mediterranean sea level. Palaeogeogr. Palaeoclimatol. Palaeoecol. 441, 854–870. doi:10.1016/j.palaeo.2015.10.034

ten Haven, H.L., de Leeuw, J.W., Schenck, P.A., 1985. Organic geochemical studies of a Messinian evaporitic basin, northern Apennines (Italy) I: Hydrocarbon biological markers for a hypersaline environment. Geochim. Cosmochim. Acta 49, 2181–2191.

Tomas, C.R., 1996. Identifying Marine Phytoplankton, Academic Press Inc. San Diego. doi:10.1016/S0025-3227(97)81154-1

Topper, R. P. M., Flecker, R., Meijer, P., Wortel, M. J. R., 2011. A box model of the Late Miocene Mediterranean Sea: implications from combined 87Sr/86Sr and salinity data. Paleoceanography, 26.

Topper, R.P.M., Lugli, S., Manzi, V., Roveri, M., Meijer, P.T., 2014. Precessional control of Sr ratios in marginal basins during the Messinian Salinity Crisis? Geochemistry, Geophys. Geosystems 15, 1926–1944. doi:10.1002/2013GC005192

van den Berg, B.C.J., Sierro, F.J., Hilgen, F.J., Flecker, R., Larrasoaña, J.C., Krijgsman, W., Flores, J.A., Mata, M.P., Bellido Martín, E., Civis, J., González-Delgado, J.A., 2015. Astronomical tuning for the upper Messinian Spanish Atlantic margin: Disentangling basin evolution, climate cyclicity and MOW. Glob. Planet. Change 135, 89–103. doi:10.1016/j.gloplacha.2015.10.009

Vasiliev, I., Mezger, E.M., Lugli, S., Reichart, G., Manzi, V., Roveri, M., 2017. How dry was the Mediterranean during the Messinian salinity crisis ? Palaeogeogr. Palaeoclimatol. Palaeoecol. 471, 120–133. doi:10.1016/j.palaeo.2017.01.032

Supplementary Figures

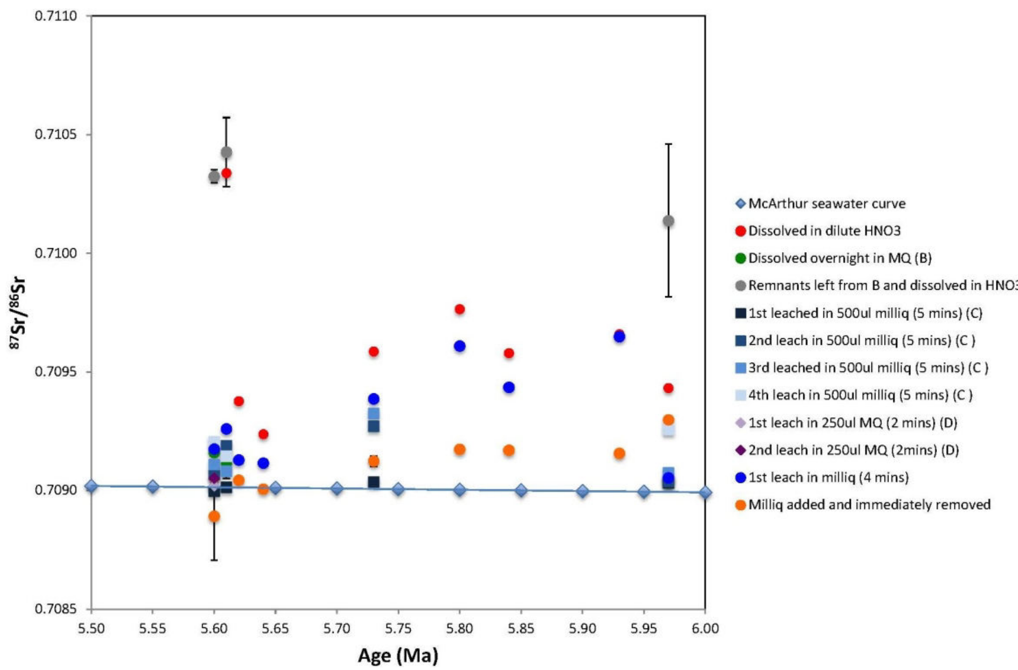

Figure S1. Strontium stable isotope analysis

Results obtained by the different protocols used for strontium stable isotope analysis with respect to the McArthur et al. (2012) seawater curve. Note the large discrepancies between the results obtained by the different methods used, indicating a highly probable contamination from the drilling mud used during the retrieval of the halite cuttings samples.

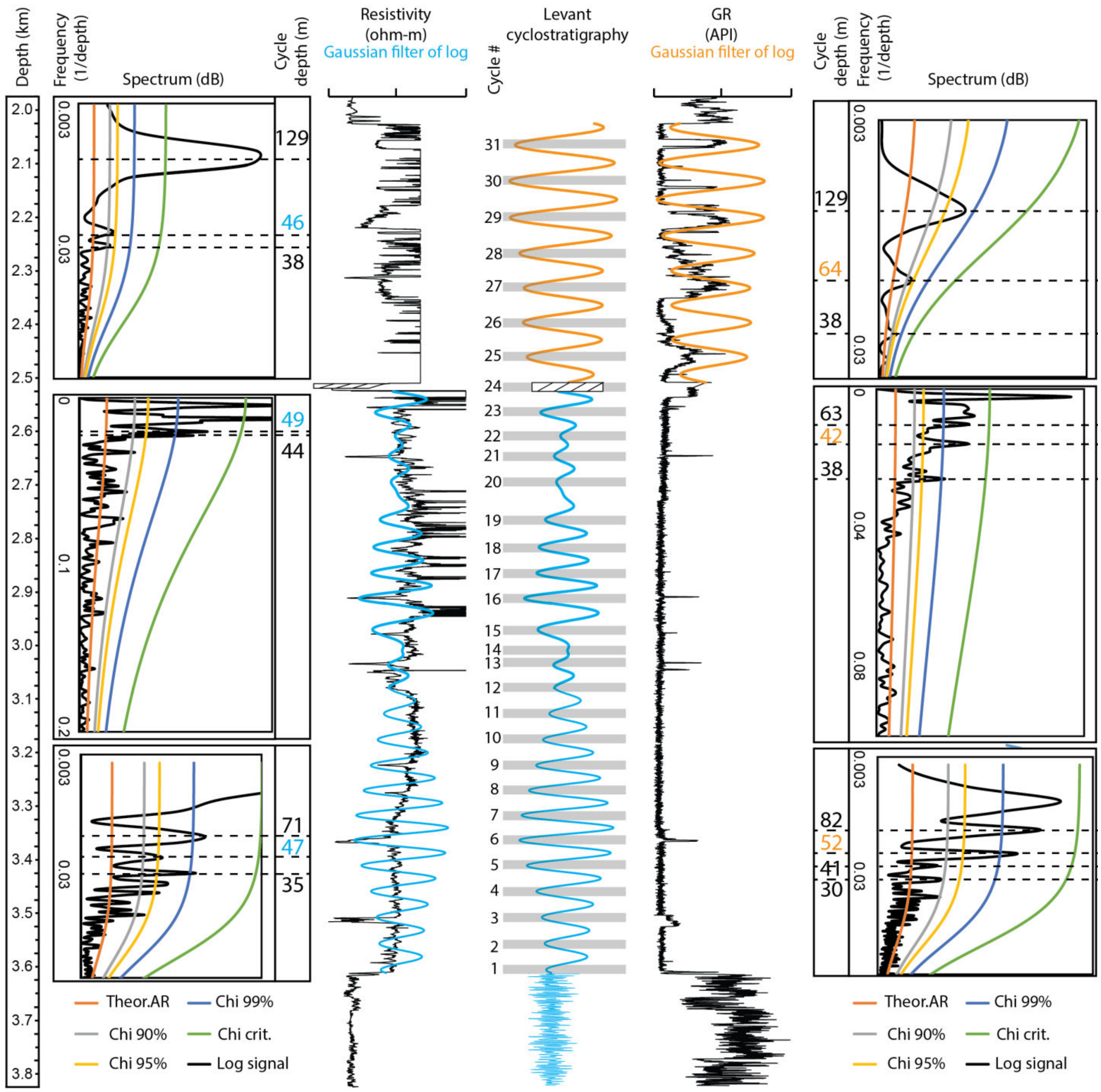

Figure S2. Spectral analysis of the Dolphin well-log curves.

Data shown are the spectral analysis of the resistivity (blue, left) and gamma ray (orange, right) well log curves using REDFIT spectral analysis procedure in Matlab, PAST and Analyseries software. Each log is bounded by respective REDFIT (left of resistivity and right of gamma ray logs) and the combined optimal cyclostratigraphy (center). The REDFIT procedure fits the time series to a red noise model null hypothesis (Theor. AR), produces 'false-alarm' parametric approximations (chi^2 of 90%, 95%, and 99%) and a 'critical false-alarm' level (chi crit.). REDFIT analyses were run by intervals, defined according to the logs expression as follows: from the base to 3175 m, from 3175 to 2560 m, and from 2560 m to the top of the evaporitic bed.

Chronology with a pinch of salt: integrated stratigraphy of Messinian evaporites in the deep Eastern Mediterranean reveals long--lasting halite deposition during Atlantic connectivity

Aaron Meilijson[a,b,*], Frits Hilgen[c], Julio Sepúlveda[b], Josh Steinberg[d], Vanessa Fairbank[e], Rachel Flecker[e], Nicolas D. Waldmann[f], Sarah A. Spaulding[g,h], Or M. Bialik[f], F. Garrett Boudinot[b], Peter Illner[i], and Yizhaq Makovsky[a,f]

[a]The Hatter Department of Marine Technologies, Charney School of Marine Sciences, University of Haifa, Mount Carmel, 31905 Haifa, Israel.

[b]Organic Geochemistry Laboratory, Department of Geological Sciences and Institute of Arctic and Alpine Research (INSTAAR), University of Colorado Boulder, Boulder, Colorado 80309, USA.

[c]Stratigraphy/Paleontology, Faculty of Geosciences, Utrecht University, Budapestlaan 4, 3584 CD Utrecht, the Netherlands.

[d]Ratio Oil Exploration, Tel Aviv, Israel.

[e]BRIDGE, School of Geographical Sciences, Bristol University, University Road, Bristol BS8 1SS, United Kingdom.

[f]The Dr. Moses Strauss Department of Marine Geosciences, Charney School of Marine Sciences, University of Haifa, Mount Carmel, 31905 Haifa, Israel.

[g]Institute of Arctic and Alpine Research (INSTAAR), University of Colorado Boulder, Boulder Colorado 80309, USA.

[h]United States Geological Survey, University of Colorado Boulder, Boulder Colorado 80309, USA.

[i]Institute for Mineralogy and Geochemistry, Karlsruhe University, 76131 Karlsruhe, Germany

[*]Correspondence to: Dr. Aaron Meilijson email: aaron.meilijson@colorado.edu Tel: +972-505666926

Abstract

The Messinian Salinity Crisis (MSC; 5.97-5.33 Ma) is considered to be an extreme environmental event driven by changes in climate and tectonics, which affected global ocean salinity and shaped the biogeochemical composition of the Mediterranean Sea. Yet, after more than 50 years of research, MSC stratigraphy remains controversial. Recent studies agree that the transition from the underlying pre-evaporite sediments to thick halite deposits is conformal in the deep Eastern Mediterranean basin. However, the age of the base and the duration of halite deposition are still unclear. Also disputed is the nature of the intermediate and upper MSC units, which are characterized as periods of increased clastic deposition into the Eastern Mediterranean based on marginal outcrops and seismic data. We provide a multidisciplinary study of sedimentary, geochemical, and geophysical data from industrial offshore wells in the Levant Basin, which recovered a sedimentary record of deep-basin Mediterranean evaporites deposited during the MSC. In combination with previous observations of the MSC throughout the Mediterranean Basin, our results promote the need for a new chronological model. Remarkably, the one-kilometer-thick lower part of the evaporitic unit is composed of essentially pure halite, other thanexcept for a thin transitional anhydrite layer at its base. The halite is undisturbed and homogeneous, lacking diverse features apparent in more proximal sections, indicating a deep-sea depositional environment. We confirm find that distinct, meters-thick non-evaporitic intervals interbedded with the halite, previously thought to be clastic layers, are indeed diatomites. While XRD analysis confirms an increase in clastic components in these sediments, they are composed primarily of well-preserved marine and freshwater planktonic diatoms. The occurrence of marine planktonic diatoms in these intervals indicates the input of Atlantic waters into the Mediterranean Basin during the deposition of the massive halite unit. Seismic stratigraphy and well-log cyclostratigraphy further support deep basin halite deposition, which started about 300 kyr earlier than widely assumed (~5.97 Ma). We propose that halite deposition in the deep Mediterranean took place during stage 1 of the MSC, rather than being limited to the short 50 kyr MSC acme when sea-level was presumably at its lowest. Thus, brine formation, salt precipitation, and faunal extinction occurred at least in part in a deep, non-desiccated basin, with a restricted yet open Mediterranean-Atlantic connection that allowed inflow of oceanic water. We observe an increase in heavy minerals and reworked fauna within the clastic-evaporitic, Interbedded Evaporites of the basinal MSC section, and argue that these settings correspond in the deep basins with a significant sea-level drawdown during stage 2 of the MSC, as observed in the marginal sections. This correlation is corroborated by astrochronology and chemostratigraphic markers, such as the distribution of *n*-alkanes and biomarker-based thermal maturity indices.

The Levant deposits indicate that high sea-level and partial connectivity with global oceans promoted the deposition of deep-basin deep-water halite, while sea-level drawdown promoted deposition of reworked and transported material from the margins into deep Mediterranean basins. This ~~review~~ study modifies the current understanding of the mechanisms governing salt deposition throughout the MSC with implications for other evaporitic events in the geologic record.

Keywords: Messinian Salinity Crisis, Mediterranean, deep-basin, evaporites, stratigraphy, sedimentology

Highlights

- After 50 years of research and over 10,000 publications, Messinian Salinity Crisis chronology is still debated
- We analyze a detailed sedimentary and geophysical record from the deep Levant Messinian halite
- Lithological, stratigraphic, and chemical signals indicate precipitation of halite 300 kyr earlier then presumed
- Halite was deposited in a deep-basin deep-water environment synchronously with gypsum deposition ~~in~~ on the margins
- Sea-level drawdown during the MSC acme in the Mediterranean promoted the deposition of reworked material in deep basins

Chronology with a pinch of salt: integrated stratigraphy of Messinian evaporites in the deep Eastern Mediterranean reveals long-lasting halite deposition during Atlantic connectivity

Aaron Meilijson[a,b,*], Frits Hilgen[c], Julio Sepúlveda[b], Josh Steinberg[d], Vanessa Fairbank[e], Rachel Flecker[e], Nicolas D. Waldmann[f], Sarah A. Spaulding[g,h], Or M. Bialik[f], F. Garrett Boudinot[b], Peter Illner[i], and Yizhaq Makovsky[a,f]

[a]The Hatter Department of Marine Technologies, Charney School of Marine Sciences, University of Haifa, Mount Carmel, 31905 Haifa, Israel.

[b]Organic Geochemistry Laboratory, Department of Geological Sciences and Institute of Arctic and Alpine Research (INSTAAR), University of Colorado Boulder, Boulder, Colorado 80309, USA.

[c]Stratigraphy/Paleontology, Faculty of Geosciences, Utrecht University, Budapestlaan 4, 3584 CD Utrecht, the Netherlands.

[d]Ratio Oil Exploration, Tel Aviv, Israel.

[e]BRIDGE, School of Geographical Sciences, Bristol University, University Road, Bristol BS8 1SS, United Kingdom.

[f]The Dr. Moses Strauss Department of Marine Geosciences, Charney School of Marine Sciences, University of Haifa, Mount Carmel, 31905 Haifa, Israel.

[g]Institute of Arctic and Alpine Research (INSTAAR), University of Colorado Boulder, Boulder Colorado 80309, USA.

[h]United States Geological Survey, University of Colorado Boulder, Boulder Colorado 80309, USA.

[i]Institute for Mineralogy and Geochemistry, Karlsruhe University, 76131 Karlsruhe, Germany
[*]Correspondence to: Dr. Aaron Meilijson email: aaron.meilijson@colorado.edu Tel: +972-505666926

Abstract

The Messinian Salinity Crisis (MSC; 5.97-5.33 Ma) is considered an extreme environmental event driven by changes in climate and tectonics, which affected global ocean salinity and shaped the biogeochemical composition of the Mediterranean Sea. Yet, after more than 50 years of research, MSC stratigraphy remains controversial. Recent studies agree that the transition from the underlying pre-evaporite sediments to thick halite deposits is conformal in the deep Eastern Mediterranean basin. However, the age of the base and the duration of halite deposition are still unclear. Also disputed is the nature of the intermediate and upper MSC units, which are characterized as periods of increased clastic deposition into the Eastern Mediterranean based on marginal outcrops and seismic data. We provide a multidisciplinary study of sedimentary, geochemical, and geophysical data from industrial offshore wells in the Levant Basin, which recovered a sedimentary record of deep-basin Mediterranean evaporites deposited during the MSC. In combination with previous observations of the MSC throughout the Mediterranean Basin, our results promote the need for a new chronological model. Remarkably, the one-kilometer-thick lower part of the evaporitic unit is composed of essentially pure halite, except for a thin transitional anhydrite layer at its base. The halite is undisturbed and homogeneous, lacking diverse features apparent in more proximal sections, indicating a deep-sea depositional environment. We find that distinct, meters-thick non-evaporitic intervals interbedded with the halite, previously thought to be clastic layers, are indeed diatomites. While XRD analysis confirms an increase in clastic components in these sediments, they are composed primarily of well-preserved marine and freshwater planktonic diatoms. The occurrence of marine planktonic diatoms in these intervals indicates the input of Atlantic waters into the Mediterranean Basin during the deposition of the massive halite unit. Seismic stratigraphy and well-log cyclostratigraphy further support deep basin halite deposition, which started about 300 kyr earlier than widely assumed (~5.97 Ma). We propose that halite deposition in the deep Mediterranean took place during stage 1 of the MSC, rather than being limited to the short 50 kyr MSC acme when sea level was presumably at its lowest. Thus, brine formation, salt precipitation, and faunal extinction occurred at least in part in a deep, non-desiccated basin, with a restricted yet open Mediterranean-Atlantic connection that allowed inflow of oceanic water. We observe an increase in heavy minerals and reworked fauna within the clastic-evaporitic, Interbedded Evaporites of the basinal MSC section, and argue that these settings correspond in the deep basins with a significant sea-level drawdown during stage 2 of the MSC, as observed in the marginal sections. This correlation is corroborated by astrochronology and chemostratigraphic markers, such as the distribution of *n*-alkanes and biomarker-based thermal maturity indices.

The Levant deposits indicate that high sea level and partial connectivity with global oceans promoted the deposition of deep-basin deep-water halite, while sea-level drawdown promoted deposition of reworked and transported material from the margins into deep Mediterranean basins. This study modifies the current understanding of the mechanisms governing salt deposition throughout the MSC with implications for other evaporitic events in the geologic record.

Keywords: Messinian Salinity Crisis, Mediterranean, deep-basin, evaporites, stratigraphy, sedimentology

Highlights

- After 50 years of research and over 10,000 publications, Messinian Salinity Crisis chronology is still debated
- We analyze a detailed sedimentary and geophysical record from the deep Levant Messinian halite
- Lithological, stratigraphic, and chemical signals indicate precipitation of halite 300 kyr earlier then presumed
- Halite was deposited in a deep-basin deep-water environment synchronously with gypsum deposition on the margins
- Sea-level drawdown during the MSC acme in the Mediterranean promoted the deposition of reworked material in deep basins

1. Introduction

An international and multidisciplinary group of scientists have recently joined efforts to organize the challenging endeavor of drilling through the thick Messinian evaporites found in deep Mediterranean basins (IODP pre-Proposal P857B DREAM; Camerlenghi et al., 2014; Lofi and Camerlenghi, 2014). The targeted deep basin evaporites reach up to 3 km in thickness (Hsü, 1973) and are thought to have resulted from restricted connectivity of the Mediterranean Basin to the Atlantic Ocean that led to the Messinian Salinity Crisis (MSC). It has been suggested that deposition of the MSC salt giant has greatly affected the global oceans by sequestering 5% (Ryan, 1973; 2008) to 10% (Garcia-Castellanos and Villaseñor, 2011) of their salt content into the Mediterranean. Also, by contributing warm, saline water to northern latitudes, the MSC influenced Atlantic Meridional Overturning Circulation and, consequently, global climatic shifts (Hernández-Molina et al., 2014). Among the major stratigraphically-driven findings of modern geoscience, the MSC stands alone as being supported by an 'outrageously under-sampled stratigraphic record' (CIESM, 2008). For several decades, focused investigation of the MSC within various interdisciplinary studies was aimed at understanding the mechanisms governing its timing, paleogeography, and the inter-relationship between external forcing and physical systems response. However, while the deep-basin halite was penetrated in its uppermost part (Fig. 1), the prohibitive risk and high drilling cost of recovering cores through the entire deep-basin MSC unit has resulted in a critical lack of data. Scientific drilling of the deep Mediterranean basins has been repeatedly called for in order to test and validate different hypotheses regarding the MSC in the deep Mediterranean basins (CIESM, 2008; Dela Pierre et al., 2014; Gvirtzman et al., 2017; Manzi et al., 2015, 2018; Meilijson et al., 2018), but has yet to be achieved.

The MSC came into awareness and was documented as early as the 1950's, when massive evaporite outcrops in the peri-Mediterranean were identified as co-occurring around the end of the Miocene (Selli, 1954; Ogniben, 1957). However, the MSC magnitude and extent became clear only when seismic imaging penetrated the massive diapiric and stratified salt bodies of the Mediterranean Sea, reaching more than 2 km in thickness and stretching across vast parts of the basin (e.g., Bourcart et al., 1958; Alinat and Cousteau, 1962; Cornet, 1968; Ryan et al., 1971; Bellaiche et al. 1974; Ryan, 1976). One of the oldest controversies related to the MSC concerns the magnitude and timing of sea-level lowering and desiccation, where several models for evaporite formation have been suggested. Some have proposed that salt was precipitated in deep basins under a deep-water environment (Schmalz, 1969; Debenedetti, 1982; Sonnenfeld and Finetti, 2011), while other scenarios promoted a desiccated shallow-water environment (Hsu, 1973). A hybrid model was proposed, with early brine formation in the deep Mediterranean, preceding substantial drawdown, followed by massive salt precipitation during gateway closure (Ryan, 2008; Garcia-Castellanos and Villaseñor, 2011; Lofi et al., 2011). Clauzon et al. (1996) recognized the occurrence of shallow-water first cycle gypsum beds of the same age in many localities in the western and eastern Mediterranean. Based on this observation they presented a 2-step model, in which the surface of the Mediterranean Sea remained close to the global ocean level during the early part of the crisis, and deep-basin evaporites formed following sea-level drop of the subsequent step. Based on this model, Ryan (2011) described the geodynamic response of the basin to each of these steps: 1) Significant deepening of the basins by isostatic load due to an increase in weight of the brine layer. 2) As the basins dried out, the loss of weight of the water led to regional isostatic uplift that permanently closed the prior inlets.

Van Couvering et al. (1976) were the first to propose a similar 2-step model, which also portrays an early deposition of halite in the deep basins: (1) An initial deep-water phase marked by refluxive concentration of brines and controlled by a tectonically elevated sill, during which evaporites and associated sediments accumulated simultaneously near the surface in marginal areas (gypsum) and within great saline water bodies in the depths of the basin (halite). (2) A terminal phase of total isolation, caused by an eustatic sea-level drop, during which erosion and desiccation features were developed that fit the "deep-basin, shallow-water" model. However, this model was later abandoned in favor of what developed into the CIESM (2008) workshop consensus stratigraphic model, which was elaborated in the extensive review of the MSC by Roveri et al. (2014a) and widely cited.

The CIESM (2008) stratigraphic model of the MSC is based on correlation of Mediterranean evaporite sequences deposited in marginal to intermediate basins, and their isotopic signatures (Keogh and Butler, 1999; Müller and Mueller, 1991; Flecker and Ellam, 2006). While the division of MSC units differs slightly in terminology between the CIESM (2008) model and the widely used review of the MSC presented by Roveri et al. (2014a), they both stem from the same stratigraphic concepts, and are jointly referred to here as the ‘consensus model’ for MSC chronology. These studies demonstrate that partial connectivity with the Atlantic Ocean persisted throughout the first phase of gypsum deposition, lasting for ~370 kyr and known as MSC phase 1: Primary Lower Gypsum [PLG], 5.97–5.6 Ma.

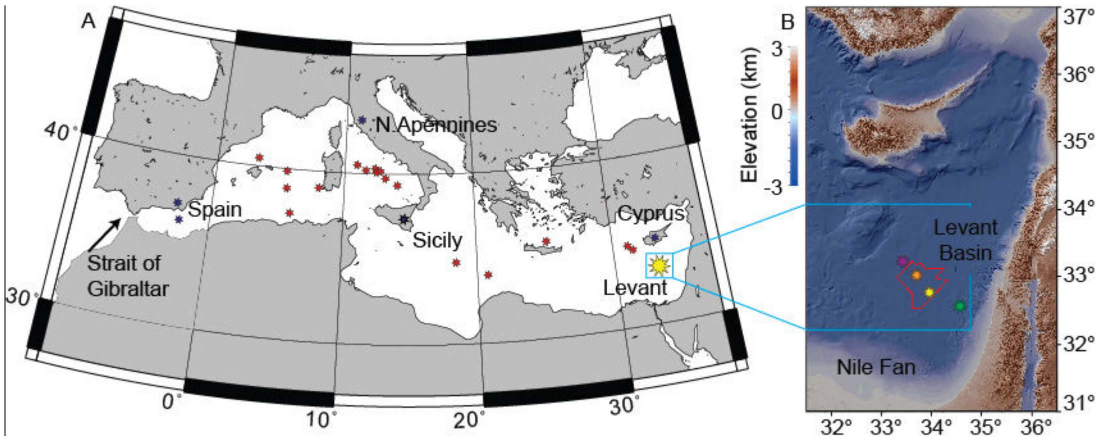

Figure 1. Map of the Mediterranean Sea marking the study area and referenced sections. **A.** Map of Mediterranean Sea marking study area (yellow star); main referenced sections (blue stars); and Deep Sea Drilling Project and Ocean Drilling Program wells (red stars), which penetrated MSC halite deposits only at their uppermost part. **B.** A shaded relief map of the Levant Basin and surrounding area (Hall et al., 1994, 2015). Red polygon outlines the three-dimensional seismic cube referred to in this study. Well locations marked by stars: Aphrodite-1 (purple star), Leviathan-1 (orange), Dolphin (yellow), and Sara (Green).

During the PLG, euxinic shales and dolostones were thought to have been deposited in the deep basins in parallel to gypsum deposition in the proximal settings (Lange and Krijgsman, 2010). However, using sonic and resistivity logs and samples from cuttings of the 497-Muchamiel oil-industry well, Ochoa et al. (2015) observed all 14 of the known first-stage gypsum beds present in the Sorbas Basin, offshore southeast Spain, deep (875 -965 m) below the present-day sea level. This observation was regarded opposite to previous assumptions that only shales would be present in this interval of the deep basins (CIESM, 2008; Roveri et al., 2014a).

The thick salt unit was interpreted as being accumulated during the succeeding MSC acme, a short period of ~50 kyr known as MSC phase 2: Resedimented Lower Gypsum [RLG], 5.6–5.55 Ma (although its top is often marked at 5.53 Ma in different cyclostratigraphic schemes (e.g., Roveri et al., 2014a; Manzi et al., 2015) due to the ‘Messinian gap’, during which Messinian erosion and/or deposition of resedimented gypsum and halite occurred). A model depicting the desiccation of the Mediterranean during stage 2 was proposed to explain its formation over such a short period of time. This model entails a massive sea-level drawdown and consequent removal and re-deposition of the PLG gypsum, and a seasonal or long-term deposition of halite in intermediate to deep-water basins. Lastly, the third phase of the MSC was defined within the Upper Evaporites or Gypsum sequences (UG), which include clastic or brackish sediments culminating in the Lago-Mare deposits (5.55-5.33 Ma). The latter consist of several units with 7-10 sedimentary cycles identified in the Upper Gypsum of Italy overlying erosional surfaces and angular unconformities, and underlying Pliocene sediments (Hilgen et al., 2007; Krijgsman et al., 2010; Roveri et al., 2014a). A recent review of different Lago-Mare deposits depicts that three main pulses of seaward-transport occurred within the time-interval 5.64-5.33 Ma, and suggests abandonment of previous concepts dealing with a unique chronostratigraphic unit, favoring several episodes of flooding (Couto et al., 2014). Nonetheless, the first influx of Paratethyan organisms, identified through the dinoflagellate cyst record near Malaga within a fan delta, was found overlying the intra-Messinian truncation surface (IMTS) (Couto et al., 2014).

Recent industrial activities targeting hydrocarbon reservoirs in the Eastern Mediterranean Basin provide the scientific community with unparalleled seismics, well logs, and cuttings across the salt interval. The current work takes advantage of these industrial data to address two critical issues regarding Messinian stratigraphy in the deep Eastern Mediterranean Basin, which impact our basic understanding of this event: (1) To evaluate the composition, age and duration of evaporite deposition in the Eastern Mediterranean. (2) To characterize, interpret, and stratigraphically position the sediments overlying the IMTS (as in Gvirtzman et al., 2017), termed here the Interbedded and Argillaceous Evaporites. Here, we report previously unknown features and lithology of the deep basin MSC and, by using a multi-disciplinary approach, we provide further interpretation of their stratigraphy.

2. MSC deposits in the Levant

Feng et al. (2016) analyzed jointly well-log measurements and a pervasive seismic dataset, and demonstrated that the seismically transparent layers composing the majority of the Messinian evaporite deposits across the deep Levant Basin are composed of pure halite. The reflective layers appearing within the halite (Figs 2, 3) were interpreted as bundles of thin clay layers interbedded in the halite background, having a cumulative thickness of 25-40 m. Feng et al. (2016) also reported high-amplitude fan structures on the deepest internal reflectors, which may suggest transport mechanisms. Later, Gvirtzman et al. (2017) argued against a complete desiccation of the Eastern Mediterranean, following the seismic identification of the IMTS at ~100 m below the Messinian-Zanclean boundary in the Levant Basin. Based on interpretion of well logs and correlation to shallower-water wells, Gvirtzman et al. (2017) suggested that the post-truncation Messinian unit is different from the underlying salt deposits and mostly consists of shale, sand and anhydrite. Lastly, two separate studies (Manzi et al., 2018; Meilijson et al., 2018) have investigated the sediments underlying the evaporites, based on data from different wells within the Levant Basin. Both studies address the stratigraphy of the Pre-Evaporites and are aimed at providing an indication for the age of the base of the halite in the deep Eastern Mediterranean, represented on seismic data in the region as the ‘N’ reflection (Ryan, 1978; Bertoni and Cartwright, 2007). Establishing the age and duration of the deep-basin halite is perhaps the most enigmatic aspect of MSC research. Both recent studies test the CIESM stratigraphic model of the MSC (CIESM, 2008; Dela Pierre et al., 2014; Roveri et al., 2014a).

Manzi et al. (2018) and Meilijson et al. (2018) report several similar findings, such as the seismic interpretations regarding the conformity of the base of the evaporites, and thus refuting the occurrence of a long hiatus at the base of the evaporites. In addition, both studies indicate little deformation of the Levant Pre-Evaporite interval and a continuous record of the Tortonian to Messinian sediments. Still, different observations reported in these studies have led to continued uncertainty concerning the age and duration of salt deposition.

Meilijson et al. (2018) considered two alternatives for the age of the base evaporites in the deep basins: (1) during stage 1 (PLG) of the MSC at around 5.9 Ma, or (2) at around 5.6 Ma during stage 2 (RLG) of the MSC, as is described in the CIESM stratigraphic model (CIESM, 2008; Roveri et al., 2014a). The latter would imply a major hiatus of ~370 kyr (missing the PLG equivalent unit) at the base of the salt, or alternatively that the PLG is expressed as a very thin interval in the uppermost Pre-Evaporites unit. A hiatus in the deep basin has not been identified, but rather a visible lateral continuity of seismic reflectors below and at the boundary itself (Meilijson et al., 2018). This finding is consistent with published regional seismic sections (Feng et al., 2016; Manzi et al., 2018; Roberts and Peace, 2007) and elsewhere in the deep domain of the Mediterranean (Lofi et al., 2011). Thus, Meilijson et al. (2018) concluded that the studied section is in fact conformal and halite began to precipitate around the onset of the PLG in the marginal basins, predating the CIESM consensus for halite deposition by ~300 kyr.

Manzi et al. (2018) reported that in the Aphrodite-2 well (Fig. 1), which is the deepest location along their four-well cross-section, a complete absence of foraminifera occurs from 3959 m upwards, 28 m below the first occurrence of anhydrite, and 33 m from the base of halite deposition. They interpret this foraminifera barren interval (FBI) as corresponding to the Non-Distinctive Zone (NDZ) marking the onset of the MSC (5.971 Ma) in marginal settings (Gennari et al., 2013; Manzi et al., 2013). Manzi et al. (2018) proposed that this interval represents the deep basin expression of the PLG, followed by halite deposition during stage 2 of the MSC at around 5.6 Ma. This FBI is argued by them to be further substantiated by a prominent peak of *Sphenolitus abies* at 3961 m, closely followed by a decrease in the number of species of calcareous nannofossils. The FBI was also identified by Manzi et al. (2018) in the Myra well, which is situated in a more proximal position, 90 km SW to the Aphrodite well. Farther landward to the west, the FBI is no longer recognized in the Sara well, where the Aphrodite well equivalence of about 60 m underlying the base of the evaporites is missing. This observation indicates that the Dolphin well should also include an equivalent FBI, as it is positioned between the Myra well, and closer to the latter (Fig. 1). However, such an FBI is not present in the Dolphin well, in which the samples include a relatively open-marine foraminiferal assemblage up to the uppermost sample available for analysis, representing the interval 0-9 m below the base of the evaporites (Meilijson et al., 2018). Thus, the MSC timing and events are still debated after more than 50 years of research and over 10,000 publications.

In recent years, different studies have been leaning towards new and very different ideas regarding MSC chronology, and thus the mechanisms controlling the deposition of salt giants in deep sea basins. Ochoa et al. (2015) demonstrated synchronous deposition of evaporites in marginal and intermediate basins. Simon and Meijer (2017) modeled stratification in the Mediterranean during the MSC and raised the possibility of a much earlier onset of halite in the deep basins. Finally, García-Veigas et al. (2018) even went so far as to draw a model for an early onset of halite, yet added a question mark next to this assumption due to lack of proof for this claim (their fig. 12). Here, we address this debate on the chronology of MSC events in the Mediterranean by examining the recovery of deep-basin evaporites from the Levant Basin for stratigraphic indicators that can promote a better understanding of MSC chronology.

The MSC (CIESM, 2008; Roveri et al., 2014a) is expressed in the southeastern Levant Basin margins as a thick evaporitic sequence (locally named the Mavqiim Formation), as well as clastic evaporite deposits along local topographical lows (Buchbinder and Zilberman, 1997; Druckman et al., 1995; Lugli et al., 2013). The MSC deposits in the deep Levant Basin have been identified through seismic data, and interpreted as mainly consisting of halite, reaching a thickness of ~2 km in the central part of the basin and pinching out upslope towards its southeastern margin (Bertoni and Cartwright, 2007, 2006; Feng et al., 2016; Gardosh et al., 2008; Netzeband et al., 2006; Steinberg et al., 2011). The halite sequence base and top are generally imaged as pronounced high-amplitude seismic reflections, known as the N and M reflectors, respectively (Ryan, 1978). Up-dip, the evaporitic sequence thins below seismic resolution and is entirely represented by the M reflector (e.g., Steinberg et al., 2010). The nomenclature of the MSC section in the Levant Basin is currently based on the regional identification of a number of key markers within seismic sections across the basin, with several divisions presented by different studies: division of the section into 6 or 7 units (Gvirtzman et al., 2013b, 2017; Lugli et al., 2013), or into ME 1-4 (Messinian evaporites) and MC 1 and 2 (Messinian clastics; Feng et al., 2016). In this manuscript we refer to the unit numbers (Gvirtzman et al., 2017, 2013b) and ME/MC units (Feng et al., 2016), corresponding seismically to the lithostratigraphic descriptions and division of the Dolphin well sediments.

Several studies have shown that the seismic records of the MSC greatly differ between the Western and Eastern Mediterranean basins, and argued that it is impossible to properly correlate individual sub-units (Lofi et al., 2011). Some authors have also questioned the possible diachronism between both basins (Blanc, 2000; Ryan, 2008). However, the Levant has been for many years at the center of debate regarding the evolution of the MSC across the entire

Mediterranean Basin. An example for such a long-term debate includes the formation of the vast drainage systems at the Mediterranean margins and the deposition, or re-deposition, of gypsum within them. An important type location for this debate is the Afiq canyon along the continental margin of Israel. The presence of evaporite layers at different levels along the Afiq canyon was brought as one of the first evidence for a substantial Messinian sea-level drawdown (800 m sea-level drop; Druckman et al., 1995). However, these deposits were recently argued to result from evaporite recycling through slope mass-wasting, a phenomena suggested to characterize the upper parts of the MSC throughout the Mediterranean (Lugli et al., 2013). The wells investigated in this study were drilled in the Levant Basin, and may represent local conditions rather than account for the entire Mediterranean Basin. However, by recovering one of the most extensive evaporite deposits of the MSC, the analysis of these wells bears key implications for unraveling the MSC across the entire Mediterranean.

3. Methodology

This study is based on the combined analyses of well cuttings, 3D pre-stack depth-migrated reflection seismics, and well-log data of two deep-water industry wells recently drilled in the Levant Basin (Fig. 1). We have also used a time-migrated 2-D seismic survey acquired by TGS-Nopec Geophysical Company in 2000, and the 3-D depth-migrated Pelagic seismic survey acquired by CGG-Veritas in 2009. Lithological and biostratigraphic data presented in this study are from the Dolphin well (N 3628144.05 m, E 575444.97 m), drilled by the Leviathan partnership at a water depth of 1500 m and penetrating the 1590 m thick Messinian evaporite section at depths of 2026-3616 m below sea level. The second studied well is the Leviathan-1 (N 3653455.35 m, E 553663.40 m), also drilled by the Leviathan partnership at a water depth of 1644 m and penetrating the 1694 m thick Messinian evaporite section at depths of 2090-3784 m below sea level. The record presented in this study supplements the 350 m section immediately below the base of the halite shown in Meilijson et al. (2018). Samples were curated and archived in both the Organic Geochemistry Laboratory at the University of Colorado (organic extracts) and the Department of Marine Geosciences, Leon Charney School of Marine Sciences, University of Haifa.

Drilled cutting returns are available starting down from a depth of 2535 m and 2497 m in the Dolphin and Leviathan-1 wells, respectively. The Pre-Evaporites interval of the Dolphin (Meilijson et al., 2018) and Leviathan wells was sampled every 3 m. The evaporite interval was sampled every ~9 m, with a total of 123 samples from the Dolphin well. Due to standard drilling activities, many fallouts of clastic deposits occur downhole from the lower part of the Interbedded Evaporite unit to the upper part of the Main Halite unit, appearing as an interval of clastic deposits in the XRD log of the Dolphin well from 2560 to 2675 m. Well-log data does not respond to this high-clastic content (i.e., high RE log values and low GR log values), and so does not show a shift from halite deposition. This observation confirms that the clastic material arrive from the unit above, as drilling fallouts into the halite interval. While not in-situ, these fallouts, together with the well logs, allow us to interpret the distinct lithological transition that occurs at the boundary between the Main Halite and Interbedded Evaporites unit. However, these fallouts might also originate from the Argillaceous Evaporites unit above.

Individual cutting bits were separated by their lithology under a microscope, cleaned with deionized water and 10% hydrochloric acid, dried, and then crushed in an agate pestle and mortar. Fine powders were pressed and used for bulk mineralogical X-ray diffractogram (XRD) analysis using a Rigaku 600 MiniFlex X-Ray Diffractometer with a CuKα source at 30kV / 15-mA from 3° to 70°. Mineralogical compositions of assemblages were determined using the

ICDD PDF2 mineral database references. Next, fine powders were pressed in Teflon crucibles with X-Ray transparent mylar (which was replaced between samples). Each sample was then analyzed using a Nitton X-Ray XL3 GOLDD+ Fluorescence apparatus for elemental composition.

Samples found to be bearing microfossils were investigated for their faunal assemblages, which included washing and picking foraminifera from the Pre-Evaporites (detailed in Meilijson et al., 2018) and the preparation of smear slides for the study of the diatomites interbedded within the halite. For the latter, samples were weighed, treated several times with 10% HCl for carbonate removal, and 30% hydrogen peroxide for organic matter removal, and then loaded onto glass slides. A total of 50 diatom valves were counted and identified from 10 samples. Diatoms were characterized by their habitat preferences: planktonic vs. benthic, and marine vs. freshwater.

We also studied the distribution of selected biomarkers (i.e., *n*-alkanes, algal steranes, and bacterial hopanes) from different intervals to gain insight into variations in organic matter sources and thermal alteration. Rock cuttings were cleaned and handled with solvent-rinsed metal tweezers, a Dremmel 8220 wire-brush tip, spatulas, and combusted aluminum foil, and then powdered with a solvent-rinsed agate mortar and pestle. Approximately 5-10 grams of sample were extracted using a Dionex Accelerated Solvent Extractor (ASE 200; 100 ºC; 2,000 psi) and a mixture of dichloromethylene:methanol 9:1 (v:v) until no more color was observed (typically 3-6 extractions). Each extraction cycle included heating of the cell for 5 minutes, static mode for 5 minutes, and flushing for 2 minutes time. A cocktail of internal standards containing 500 ng of D4 C_{29} $\alpha\alpha\alpha$ (20R)-Ethylcholestane, and 1,000 ng of each 3methyl heneicosane, D14 pTerphynyl, 1-nonadecanol, behenic acid methylester (Docosanoic acid), and 2methyl octadecaonoic acid, was added to samples before extraction for quantitation purposes. Total lipid extracts (TLEs) were combined and evaporated under a gentle nitrogen flow using a Turbovap. Elemental sulfur was removed using HCl-activated copper shots. TLEs were then filtered through small Pasteur pipettes filled with combusted glass wool and sand to remove impurities and any copper-sulfide residues. Asphaltenes were separated from maltenes by precipitation in hexanes at 4^{0}C for 3 hours, followed by centrifugation at 2000 rpm (3x). Maltenes were later separated into five different lipid classes by liquid chromatography on small Pasteur pipettes filled with silica gel. Aliphatic (F1) and aromatic (F2) hydrocarbons were recovered with hexane (3/4 dead volumes) and hexane:dichloromethylene 8:2 (v:v; 4 dead volumes), respectively. The more polar fractions (F3, F4, F5) were eluted using dichloromethylene, dichloromethylene:EtOAc 1:1, and EtOAc (v:v, 4 dead volumes), respectively. Aliphatic hydrocarbons were analyzed on full scan and selected reaction monitoring (SRM) modes via gas chromatography – triple quadrupole-mass spectrometry (GC-QQQ-MS) using a Thermo Trace 1310 Gas Chromatograph interphase to a TSQ Evo 8000 triple quadrupole mass spectrometer (GC-QQQ-MS) equipped with a split-less PTV injector and electron impact ion source. Helium was used as a carrier gas with a flow rate of 1.2 ml min^{-1}. Chromeleon 7 was used for data integration. Aliphatic hydrocarbons were separated using a 60-meter DB-1MS GC column (60 m, 0.25 mm I.D., 0.25 μm film thickness; Agilent Technologies). For FS analysis, sampled were injected at 60°C and then the PTV was heated to 300°C at 14.5°C/second. The GC oven temperature program was: 60°C (2 min) to 150°C at 15°C min^{-1}, to 315 (held 24 min) at 3°C min^{-1}. The total GC program was 90 minutes. MS conditions were: 300°C ion source at 70eV electron energy, 50uA emission current, and 15V electron lens voltage. The mass range was 50-600 m/z with a dwell time of 0.2 seconds per scan. For SRM analysis, the GC oven temperature program was: 60°C (0 min) to 220°C at 15°C min^{-1}, to 315°C (held 25 min) at 3°C min^{-1}. The total GC program was 68 minutes. Samples were injected at 65°C and then the PTV temperature was heated to 400°C at 3 °C min^{-1}. MS conditions were: ion source temperature of 250°C; transfer line temperature of 320°C, electron energy of 70eV, electron lens voltage of 35V, and emission current of 35uA. Peak scanning windows ranged from 0.6 to 1 minute for 147 timed transitions for regular and methylated steranes and hopanes, and their stereoisomers.

4. Evidence from the Levant Basin for an early onset of halite deposition in a deep-water environment

4.1 Lithologic composition of the Levant deep-sea salt-giant

4.1.1 Pre-Evaporites

This interval is detailed in Meilijson et al. (2018). Here we provide a generalized summary, followed by a more elaborate account of the overlying evaporites of the deep Levant Basin. The Pre-Evaporite interval in the Dolphin well (3850-3616 m; Fig. 2) is seismically characterized by sub-horizontal and sub-parallel continuous high-amplitude reflections, implying a stratified and relatively undeformed marine succession (Meilijson et al., 2018). It is composed of fine-grained clastic-micritic and carbonate bathypelagic sediments, primarily gray to dark gray or greenish calcareous soft to hard shale, with several thin layers of white to light gray hard limestone, and light gray very fine to fine-grained unconsolidated sandstone. Diverse assemblages of nannofossils, benthic and planktic foraminifera are recognized within this interval.

Figure 2. The MSC succession of the Dolphin well in the deep Levant Basin.
A juxtaposed simplified display of the primary proxies used to characterize the Dolphin well section (five central columns), and our depositional (left) and lithological (right) interpretations.

The attributes are (left to right): the faunal composition; the seismic response, with transparent intervals representing predominantly evaporites and high-amplitude reflections representing clastic beds (a seismic trace (center) emphasizes relative intensity of the seismic phases); XRD mineralogy, showing the relative abundance of halite (bright) vs. non-halite (dark; 'marine clastics'), where the uppermost clastic interval (<2650 m) represents fallouts from the Interbedded Evaporites; the gamma ray (GR - API units) and resistivity (RE - log ohm-m units) logs, color coded based on the characteristic responses to halite and clastics. The lithological interpretation is color coded as in the attribute columns. Planktonic foraminiferal (PF) bio-events in blue circles correspond to the following ages: 1- 7.72, 2- 7.24, 3- 6.72, 4- 6.36, and 5- 6.13 Ma (Meilijson et al., 2018).

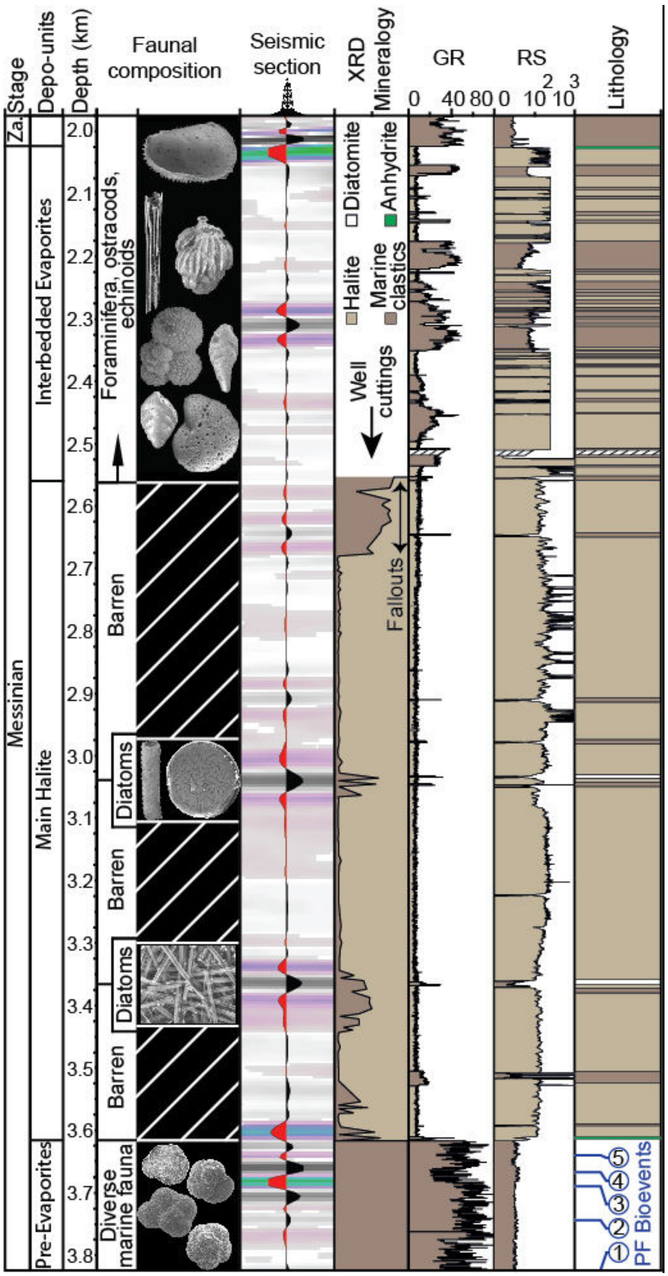

Za.
Stage
Depo-units
Depth (km)
Faunal composition
Seismic section
XRD Mineralogy
GR
RS
Lithology
0 40 80
0 10 10^2 10^3
Messinian
Interbedded Evaporites
Main Halite
Pre-Evaporites
Foraminifera, ostracods, echinoids
Barren
Diatoms
Diverse marine fauna
Diatomite
Anhydrite
Halite
Marine clastics
Well cuttings
Fallouts
PF Bioevents
2.0
2.1
2.2
2.3
2.4
2.5
2.6
2.7
2.8
2.9
3.0
3.1
3.2
3.3
3.4
3.5
3.6
3.7
3.8

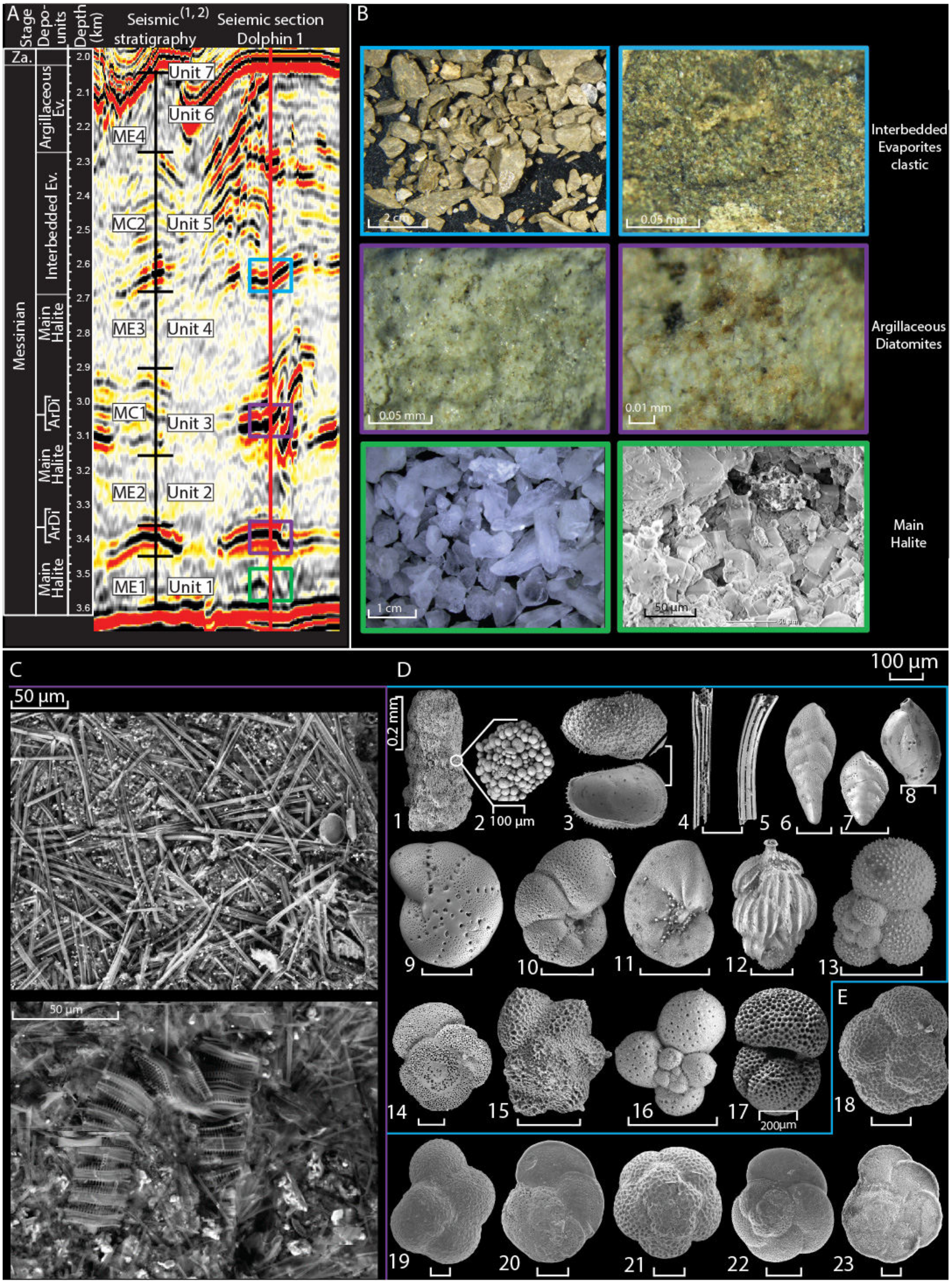
A
Stage
Depo-units
Depth (km)
Seismic(1, 2) stratigraphy
Seiemic section Dolphin 1
Za.
Argillaceous Ev.
Interbedded Ev.
Main Halite
ArDi
Main Halite
ArDi
Main Halite
Messinian
2.0
2.1
2.2
2.3
2.4
2.5
2.6
2.7
2.8
2.9
3.0
3.1
3.2
3.3
3.4
3.5
3.6
ME4
MC2
ME3
MC1
ME2
ME1
Unit 7
Unit 6
Unit 5
Unit 4
Unit 3
Unit 2
Unit 1
B
2 cm
0.05 mm
Interbedded Evaporites clastic
0.05 mm
0.01 mm
Argillaceous Diatomites
1 cm
50 µm
Main Halite
C
50 µm
50 µm
D
100 µm
0.2 mm
100 µm
1
2
3
4
5
6
7
8
9
10
11
12
13
14
15
16
17
200µm
E
18
19
20
21
22
23

Figure 3. Seismic stratigraphy, common lithologies, and SEM imaging of the studied section. **A.** The seismic profile crossing the sampled Dolphin well position and its division into the MSC depositional units, compared to previously published seismic stratigraphy of the deep Levant MSC ((1) Feng et al., 2016; (2) Gvirtzman et al., 2017). ArDi - Argillaceous Diatomites; Ev. - Evaporites. Color coded rectangles corresponding to lithologies described in (B). **B.** images of the three main facies recognized in the Levant evaporite section: the homogeneous Main Halite (green rectangle) made of pure halite as seen in hand specimen (left) and SEM imagery of cubic cleavage (right), corresponding with subdued internal seismic reflectivity in (A); Argillaceous Diatomite beds (purple rectangle), represented by high amplitude reflections in (A); and Interbedded Evaporites (blue rectangle) identified as brown marine clastics, characterized by interchanging low and high amplitude reflections in (A). **C.** Selected SEM images from the densely packed and very well preserved diatoms from the diatomite facies. **D.** Selected SEM images of the >63 μm size fraction of the washed residue from the Interbedded Evaporites unit clastic sediments (P.1-17) showing: large grains of framboidal pyrite (P.1-2), well-preserved ostracod valves (P.3), sea urchin spines (P.4-5), benthic foraminifera (P.6-12), and planktic foraminifera (P.13-17). **E.** SEM images of the planktic foraminifera used for the biostratigraphic age model (Meilijson et al., 2018) of the Pre-Evaporites (P.18-23): *Neogloboquadrina* sp. (P.18), *Sphaeroidinellopsis seminulina* (P.19), *Globorotalia miotumida* (P.20), *Globoquadrina altispira* (P.21), *Globorotalia scitula* (P.22); *Globorotalia menardii*-4 (P.23). All scales are 100 μm unless indicated otherwise.

Shale samples are organic-rich (>1 wt.% TOC) and reach peak values of 4 wt.% TOC immediately underlying the base of evaporite deposition (Meilijson et al., 2018). Lower values of gamma ray (GR) are associated with silt/carbonate-rich sediments, while higher GR corresponds to shale/organic-rich sediments (Fig. 2).

4.1.2 Main Halite

Here we reference our lithologic interpretation to the recently defined seismic stratigraphy of the Levant MSC (Units 1-6; Gvirtzman et al., 2013), and ME1-4 for the transparent and MC1-2 for the high reflectivity intervals (Feng et al., 2016) (Fig. 3). Different velocity models reported high seismic velocities of 4200-4400 m/s (Gvirtzman et al., 2013a), 3850-4240 m/s (Reiche et al., 2014), and 4400-4600 m/s (Feng et al., 2016) for the seismic transparent layers, interpreted as representing the halite facies. Here we advocate this interpretation by providing the first semi-quantitative XRD analysis (Fig. 4) of well cuttings spanning the transparent high velocity layers.

The Main Halite unit in the vicinity of the Dolphin (3616- 2755 m) and Leviathan-1 (3759-2800 m) wells is characterized by low seismic reflectivity, which is internally interrupted by several main high reflectivity bands (Figs 5, 6). These instances are clearly recognized in the well logs (Fig 2, 5), and represent a different facies within the hypersaline deposits described below. Using XRD analysis coupled with SEM (Fig. 4), we conclude that the transparent intervals are indeed composed of nearly pure (>90%) halite (Fig. 4), with minor quantities of anhydrite, magnesite and barite. Anhydrite is also present as a relatively thin bed (<3 m) at the base of the Main Halite section, where it represents the transition to the Main Halite. Anhydrite further appears in the upper, more clastic part of the section (Fig. 2), as is also reported from the same stratigraphic interval by Gvirtzman et al. (2017). The halite is clear to milky white with a firm to very hard macrocrystalline structure (Fig. 3), while the anhydrite minerals are white, soft to firm, nodular and amorphous to massive. A sharp transition from the Pre-Evaporites to halite is marked by a decrease in GR well log counts from 53 API to 12 API as well as a sharp increase in the RE well log reaching 10,000 ohm (Fig. 2; see also Feng et al., 2016).

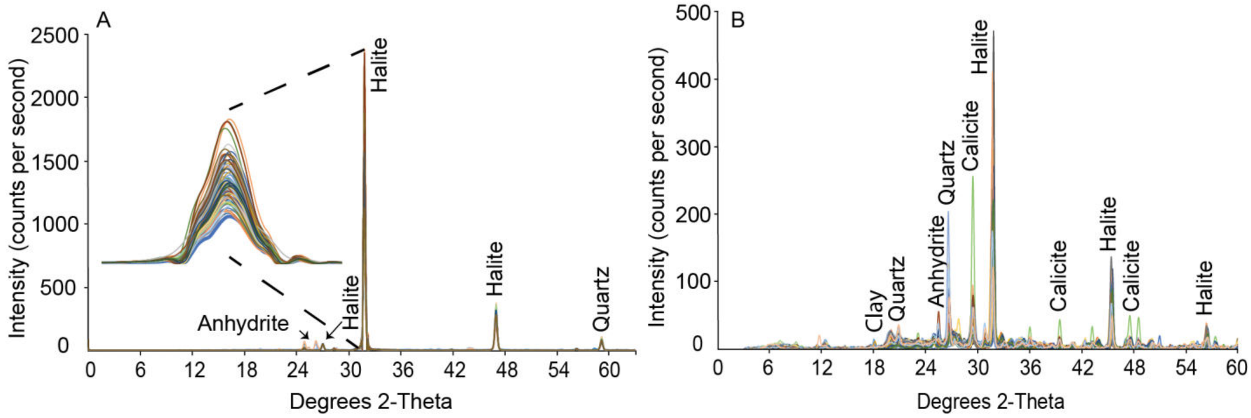

Figure 4. X-ray diffraction results

A. Overlaid (color coded) XRD analysis of 89 halite samples from the Dolphin well produced diffractograms, which are practically identical. The main halite peak is zoomed for emphasis. **B.** Higher variability is recorded both in peak location and intensity when analyzing samples from the non-evaporitic marine sediments, sampled along the section between the depth of 3,616 m to 2560 m.

These values remain relatively constant within the halite deposits, although inter-halite variations are observed, mainly on the RE log. The pronounced high-amplitude reflection at ca. 3520 m (Dolphin well; Figs 2, 3), also recognized as an increase in the GR well logs, represents a short-term return to the clastic Pre-Evaporites facies although with low abundance and poorly preserved foraminiferal content. This interval is not part of the Argillaceous Diatomites facies.

4.1.3 Argillaceous Diatomites

Distinct reflective layers appear within the seismic transparent halite expressions, correlating with relatively lower velocity zones in the seismic velocity models developed for the deep Levant Basin MSC strata (e.g., 3800-4000 m/s in Gvirtzman et al. (2013); 3650-4030 m/s in Reiche et al. (2014)). These reflective layers are easily identified across the study area (Figs 5, 6).

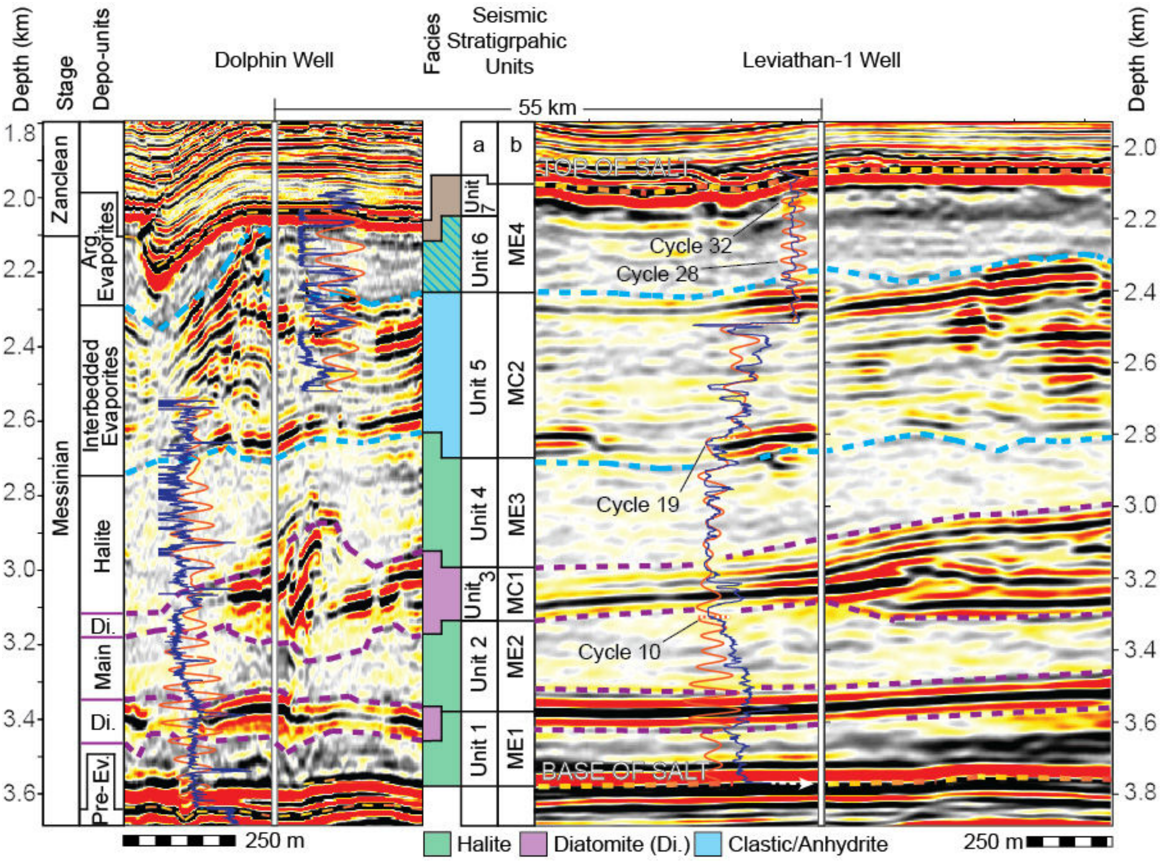

Figure 5. Geophysical data and seismic stratigraphy of the Dolphin and Leviathan-1 wells. Depth-migrated sections crossing the Dolphin (left) and Leviathan-1 (right) wells (marked by a vertical white line). Overlaid on the sections are the well logs (blue curve left to the well), and the filtered well-log cycles superimposed on the target curves (orange). The depth and lithostratigraphic units (this work) related with the sampled Dolphin well are displayed on the left, and the depth related with the Leviathn-1 well is displayed on the right. Data columns in the middle are seismic-stratigraphic units from (a) Gvirtzman et al. (2013, 2017), and (b) Feng et al. (2016). Note the relatively deformed area of the Dolphin well relative to the more conformal vicinity of the Leviathan-1 well.

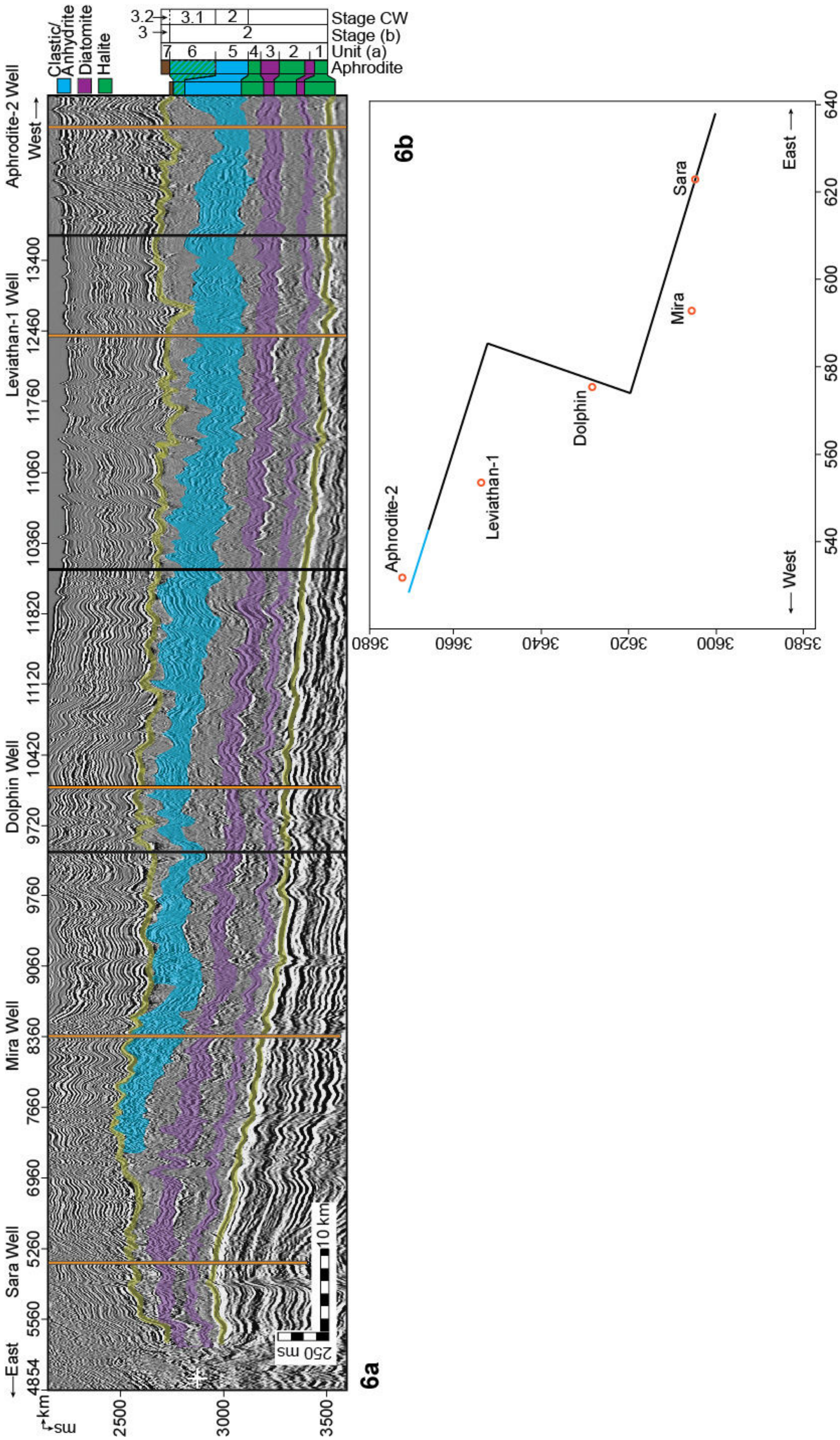
6a
6b
Stage CW
Stage (b)
Unit (a)
Aphrodite
Clastic/ Anhydrite
Diatomite
Halite
Aphrodite-2 Well
Leviathan-1 Well
Dolphin Well
Mira Well
Sara Well
West
East
10 km
250 ms
Aphrodite-2
Leviathan-1
Dolphin
Mira
Sara

Figure 6. A composite seismic section linking the commercial wells across the Levant Basin. A composite time-migrated seismic section (a), and location map (b), combining three 2D traverses of the TGS survey (dark line) with a transect through the Pelagic 3D volume (blue line) across the Levant Basin, all plotted at a common scale with a vertical exaggeration of ca. x10. Orange vertical lines note the positions of the wells discussed in the text, while black lines note the section stiches, primarily at turning points. The wells are projected laterally onto the seismic profiles by up to 10 km (in the case of the Leviathan-1 well). Note the similar relative spatial thickness of the diatomite beds (purple) in comparison with the largely varying thickness of the Interbedded Evaporites (blue). Stage CW (current work); Stage (b) (Manzi et al., 2018); Unit (a) (Gvirtzman et al., 2013; 2017).

In the Dolphin well, this seismic facies includes five seismic high-reflectivity bands, corresponding to peaks in the GR and troughs in the RE well logs, appearing within the Main Halite interval between 3375 and 2560 m (Fig. 2). Using a GR value of 20 API as an upper cutoff value for determining the location and thickness of these intervals results in estimated bed thicknesses of 0.9-2.4 m (Fig. 2). Of the 1,056 m Main Halite interval in the Dolphin well, the non-halite sediments form a regional cumulative thickness of 25-40 m (see also Feng et al., 2016; Gvirtzman et al., 2013). At the macro-scale, the content of these layers appears as light gray to white, soft to firm, porous, and occasionally fibrous. SEM imaging and smear-slide analyses indicate that the rock-mass is made of densely packed, very well-preserved, and intact diatoms (Fig. 3), and fine-grained terrigeneous sediments (Fig. 4). No other transported or local faunal remains were recognized. Identified diatoms include abundant marine planktonic genera, such as *Coscinodiscus*, *Asteromphalus*, and *Actinoptychus* (*sensu* Tomas, 1996).

XRD analysis from available samples of these high-amplitude intervals confirms the log data response and shows an increase in terrigeneous grains, mainly composed of quartz, calcite, some clay minerals, and low amounts of anhydrite, dolomite and magnesite (Fig. 4). Halite appears within these samples in a high relative abundance, reaching 45% (Figs 2, 4).

Due to the nature of well cuttings, samples from these intervals were only retrieved from the two thickest beds, at 3367.7 m of the Dolphin well with a thickness of 2.4 m, and the two adjacent beds at 3047 and 3034 m with a cumulative thickness of 2.1 m. These intervals are also represented by bands of much higher seismic reflectivity than the thin (1.2-1.4 m), overlying intervals at 2910 and 2646.5 m. Consequently, the two upper intervals might be the same diatomite facies, or only represent marine clastic sediments.

4.1.4 Interbedded Evaporites

This facies is represented in the seismic sections by high-amplitude reflections interbedded with nearly transparent intervals with weak internal reflections (Fig. 3), interpreted in previous studies to represent an alternation of clastic sediments and evaporites (Gvirtzman et al., 2013a; Feng et al., 2016). More recently, Gvirtzman et al. (2017) and Manzi et al. (2018) presented further evidence based on well logs from deep-basin wells in the region (Aphrodite), or by correlation to more proximal well sections (Hannah-1), showing that this interval mostly consists of shale, sand, anhydrite, and halite. The Interbedded Evaporites unit correlates to Unit 5 in Gvirtzman et al. (2013). It covers 2560-2025 m in the Dolphin well, and 2548-2276 m in the Leviathan-1 well. The GR well log in the Leviathan-1 well indicates 3 to 20 m thick clastic beds, interbedded with evaporites varying in thickness from 6 to 30 m. A relatively large diameter wellbore used while drilling this interval might have reduced the GR signal and thinner clastic beds might not have been detected.

Due to drilling limitations, the material made available from this interval is partial, and the only sampled sequence consists of the lowermost part above 2560 m in the Dolphin well. We consider grains from this interval as fallouts from the Interbedded Evaporites unit, confirmed by the absence of any indications for a clastic interval in the well-log and seismic data from the top of the Main Halite interval, were these grains appear. The samples are made of hard, light to dark brown sandy shales (Fig. 3). The grain composition of the >63 μm washed residue is very different compared to the underlying Main Halite or Argillaceous Diatomite facies. It contains a higher amount of sub-rounded larger sand grains compared to the diatomite facies, different types of pyrite including large agglutination of pyritohedrons reaching several mm in size, and a diverse faunal composition (Fig. 3). The latter includes few mollusk fragments, ostracods, echinoid spines and a relatively rich assemblage of benthic and planktic foraminifera (Fig. 3). The most common foraminifera are different *Globigerinoides* species, *Orbulina universa* and *Sphaeroidinellopsis seminulina* (younger than 15 Ma; Berggren et al., 2006). Older Cretaceous to Eocene foraminifera species are also present, indicating reworking processes, most likely from exposed basin margins. These include *Parasubbotina pseudobulloides* (Daninan-Selandian; Fig. 3.D.13), *Plummerita hantkeninoides* (Maastrichtian; Fig. 3.D.15), and *Subbotina triloculinoides* (Paleocene; Fig. 3.D.17). While no overlying samples exist, this interval was logged and a reliable lithological interpretation is presented by extrapolating the coupling between sample analysis (XRD and micropaleontology) and the log data from the lower to the upper part of the section (Fig. 2). The clastic input is estimated from the geophysical data as ~40% of the 535 m thick unit in the Dolphin well. However, due to local deformations in the Dolphin well area, the Interbedded Evaporites are displaced and their top is reached at the top of the MSC section.

Comparison with Manzi et al. (2018) suggests that Unit 6 is not represented in the Dolphin well but that Unit 5 marks the top of the section (Fig. 5). However, seismic and well-log interpretation indicates that in the Leviathan-1 well another ~200 m of evaporites appear above the Interbedded Evaporites, which corresponds to Unit 6 in Manzi et al. (2018). There, the Interbedded Evaporites (Unit 5) are 260 m thinner than in the Dolphin well (Fig. 5). This discrepancy is presumably the result of post-depositional halokinetic deformation and imbrication of Unit 5 in the Dolphin well, as imaged in the seismic data (Fig. 5).

4.1.5 Argillaceous Evaporites

This interval was not sampled in any of the Levant Basin studies and its interpretation is only based on the interpretation of seismic and well-log data. In the Leviathan-1 well this interval covers the uppermost part of the evaporites between 2090 and 2320 m (Fig. 5). The transparent reflective character of this interval in the seismic section includes cyclic darker bands. The unit appears to be composed of clastic sediments, probably clays, silts and sands, which are characterized by GR values of 7 to 15 API. Intervals of ca. zero GR are interpreted as argillaceous anhydrite. Gvirtzman et al. (2013; 2017), Feng et al. (2017), and Manzi et al. (2018) refer to this interval as Unit 6, which is generally lumped with the underlying halite as part of the evaporite unit. Regionally, the presence of Unit 6 is limited to the westernmost and deeper areas of the basin, while it is truncated to completely removed landward to the east (Fig. 6). The amount of truncation on Unit 6 gradually increases eastwards, eroding also Units 5-2 at the eastern parts (Gvirtzman et al., 2013, Feng et al., 2017; the current study). Both the Dolphin and the Leviathan wells are within the deeper areas in which Unit 6 is present, but due to local deformations it might be underrepresented in the Dolphin well. A 5 m clastic and anhydrite bed defines the top of this unit, marked by a nearly transparent seismic interval in the Leviathan-1 well, as indicated by a sharp drop in GR and drilling penetration rate relative to the overlying Pliocene sediments. This anhydrite interval is most likely part of Unit 7 in Gvirtzman et al. (2018), or the Nahal Menashe in Madof et al. (2019).

4.2 Chronology of halite deposition and well log frequency analysis

In order to attain a direct age control on the duration of halite deposition, the halite samples were washed and inspected for microfossils, prepared as smear slides, and examined under SEM in search for the preservation of eukaryotic life in the evaporites, which failed.

We also measured the Sr-isotopic composition of evaporite samples in order to compare them with the well-established Sr isotope stratigraphy constructed from elsewhere in the Mediterranean (e.g., Topper et al., 2011; Roveri et al., 2014; Flecker et al., 2015). This published dataset shows that Sr-isotope data from stage 1 lie mainly within error of the ocean-water curve (McArthur et al., 2012), suggesting that the Mediterranean was connected to the global ocean during the initial phases of the MSC (e.g., Roveri et al., 2014; Flecker et al., 2015). During stages 2 and 3 the Mediterranean's Sr record diverges from ocean-water values towards much lower ratios that reflect a substantially smaller connection to the global ocean and dominance of fresh-water sources such as the Nile, Rhone, and input from the Paratethys, particularly during the Lago Mare phase (e.g., Roveri et al., 2014; Flecker et al., 2015). Sr-isotope data from the lowest Pliocene are again within error of ocean-water values, indicating an abrupt transition back to full connectivity after the MSC (e.g., Roveri et al., 2014; Flecker et al., 2015). Despite the wide geographical distribution of the Mediterranean samples from which this published Sr-isotope stratigraphy has been constructed, the pattern appears to be consistent, indicating that the controlling factor was Mediterranean-Atlantic exchange and that the Mediterranean behaved as a single basin throughout the MSC (Flecker et al., 2015). However, the dataset does not include samples from these deep-water Eastern Mediterranean sites as they were previously not available; it therefore makes sense to compare new analyses from these locations with the existing Sr-chemostratigraphic scheme.

Halite is highly soluble and it is therefore challenging to clean samples prior to analysis. We used the basic method described in Gvirtzman et al. (2017) and Manzi et al. (2018), with additional eleven different techniques (Fig. S1, Table S1) for attempting to isolate the halite crystals from any contaminant phases coating the samples such as clay or industrial drilling additives. The data generated for each of the nine different samples analyzed is highly variable, ranging from a few values within error of Late Miocene ocean water (McArthur et al., 2012), to substantially higher values (Fig. S1, Table S1). There is no consistency between the data generated and the technique used for dissolving the halite (Fig. S1, Table S1), suggesting that we have not been able to reliably isolate the halite from contaminant phases coating the crystals by any of the methods used. We therefore conclude that none of this data should be considered as representing a primary record of Eastern Mediterranean water at this time.

Similar high values have been reported for halite from other industrial wells in the Levant Basin (Gvirtzman et al., 2017; Manzi et al., 2018). Manzi et al. (2018) attributed the anomalously high values to “local, diverse, short-term Sr input”, but did not specify what this input might be. One possibility is that these published halite values from industrial cuttings may, like our data, be contaminated. We conclude that a robust Sr-isotope record for the deep-basin halite deposits will only be achieved either by establishing a reliable method for removing contaminant phases or by recovering halite samples without the use of industrial drilling fluids, e.g., through scientific drilling (Camerlenghi et al., 2014).

Next, we attempted to construct a chronostratigraphic framework for the Levant MSC deposits based on astrochronological tuning. We carried out spectral analysis of GR and RE well-logs to correlate the Levant MSC section to astronomical target curves, and the more proximal to onshore Mediterranean MSC deposits. REDFIT spectral analyses (Schulz and Mudelsee, 2002) of the Dolphin and Leviathan-1 well-log data from the base to the top of the evaporite unit (3616-2025 m in the Dolphin well, divided into three intervals for spectral analysis; Fig. S2) indicates statistically significant, periodical signals in the RE and GR logs. However, the GR produces a weaker signal than the RE log within the massive halite intervals. This is expected, as pure halite does not contain the elements U, Th, and K and their decay series responsible for natural GR radiation emitted by rocks. However, several examples indicate how different log responses occur within halite sequences. For example, inner-halite variations such as thin clay laminae caused by microstratification within the brines might occur (Sonnenfeld, 1983). Alternatively, thin sulphate layers (Biehl et al., 2014) have also been shown to produce log-responses.

Each of the analyzed log segments is characterized by several frequency peaks exceeding the chi 95% confidence interval (Fig. S2). Each segment was bandpass filtered according to these frequencies, and the fit of the filtered version to the original well-log was examined, ultimately selecting the best-fit result for subsequent analysis. Both logs are composed of significant and approximately overlapping periodical frequencies, with an average cycle thickness of ~50 m (Fig. S2). While the RE log appears to be more attuned to inner-halite variations in the Main Halite interval, the GR log is more consistent and provides a more reliable fit to the well log target curve in the units above 2833 m. Consequently, the Dolphin well cyclostratigraphy is constructed from information derived from the GR and RE logs that cover the lower and upper parts of the section (Fig. S2). The lower part of the Main Halite interval (cycles 1-11; Fig. S2) is not very well represented by the Gaussian filter, with some five cycles that fit well with the target curve. The upper part of the Main Halite interval is best filtered by using the RE log with a bandwidth of 49 m (cycles 12-24; Fig. S2). The cycles within the upper part of the section in the Interbedded Evaporite interval are picked up relatively clearly by the GR log (cycles 25-32; Fig. S2). However, as the Dolphin well section from the Interbedded Evaporites and above experienced significant deformation (Figs 5, 6), the well-log cyclostratigraphy of the upper part of the studied section is not reliable in this well.

Several frequency peaks exceeding the chi 95% confidence interval were also identified in the Leviathan-1 well-log analysis, where deformation is reduced and Unit 6 is represented (Figs 5, 6). The RE log was cleaned from outlier spikes and used for bandpass filtering. The original log includes several short intervals in which values range from 10's or 100's of ohm*m to extremely high 18,000+ ohm*m values, masking cyclic trends in the data. Figure 5 shows the cleaned RE log overlain on the seismic data. There is a much-improved fit between the log and filtered cycles, relative to the Dolphin well, with only a few examples of a misfit between the two. A good fit is also generally apparent between the seismic signal and the well-log response. The Main Halite interval includes 19 cycles, in which cycles 4 and 5 are within the first Argillaceous Diatomite beds, and cycles 11-13 are within the second. The cycles within the Interbedded Evaporite interval are picked up relatively clearly by the RE log (cycles 19-27; Fig. 5). In the Argillaceous Evaporites in the uppermost part of the studied section in the Leviathan-1 well, the RE log response fits with banding in the seismic data, which is also picked by bandpass filtering (cycles 27-33; Fig. 5).

Consequently, bandpass filtering of the well logs results in ~33 cycles from the base to the top of the evaporite sequence in the Levant Basin. In the next two sections, we present different findings supporting the occurrence of lithological cycles along the studied section, followed by the astrochronologic interpretation of these cycles in the discussion section.

4.3 Cyclicity of seismic reflective phases

Modern high-quality 3D seismic imagery represents a new frontier for astronomical calibration, potentially adding a chronological time-frame for seismic stratigraphy. However, in most marine settings, precession-scaled cycles are registered at a thicknesses-to-cycles ratio which has a much higher resolution than the seismic data. Yet, several studies show a good match between the number of precession-induced astronomic cycles and the number of positive vs. negative seismic phases within MSC deposits (Driussi et al., 2015; Geletti et al., 2014). This is explained by the considerably higher sedimentation rates that characterize evaporite deposits, relative to the much lower rates typical of normal-marine clastic or carbonate deposition. The higher sedimentation rates result in an improved alignment between the spacing, or resolution, of lithologic variations and the resolution of the seismic imagery. As orbital forcing was repeatedly identified as determining lithological variations during the MSC (e.g., Krijgsman et al., 1999; Ochoa et al., 2015; Roveri et al., 2014a; Sierro et al., 2001; van den Berg et al., 2015), seismic data recording these variations can be used with caution for strengthening the well-log astronomical tuning-based age models. This is not the case for the Pre-Evaporites in this area, which deposited at an average sedimentation rate of 11.4 cm/kyr and a cycle thickness of around 2-3 m, as shown by Meilijson et al. (2018). This thickness is below the resolution of the seismic data. Here, we use the seismic 3D data for additional validation of our results from well-log curves based on REDFIT spectral analysis and bandpass-filtering within the Main Halite and overlying intervals.

In practice, the seismic tuning analysis was performed by counting the number of reflectivity phases on three different sections where wells were drilled within the 3D geophysical dataset of the study area (Figs 1, 7). Yet, as halokinetic deformation affected the Levant deep-basin evaporites, and particularly their upper units (Gvirtzman et al., 2013a), spatial variations are expected even considering a scenario of regionally uniform deposition. Such variations in the number and thickness of cycles are indeed observed when comparing different seismic sections, reflecting the local variabilities (Fig. 7). In total, a consistent number of ~30 reflectivity cycles is identified in different locations, which is in agreement with the cyclicity identified through well-log spectral analysis.

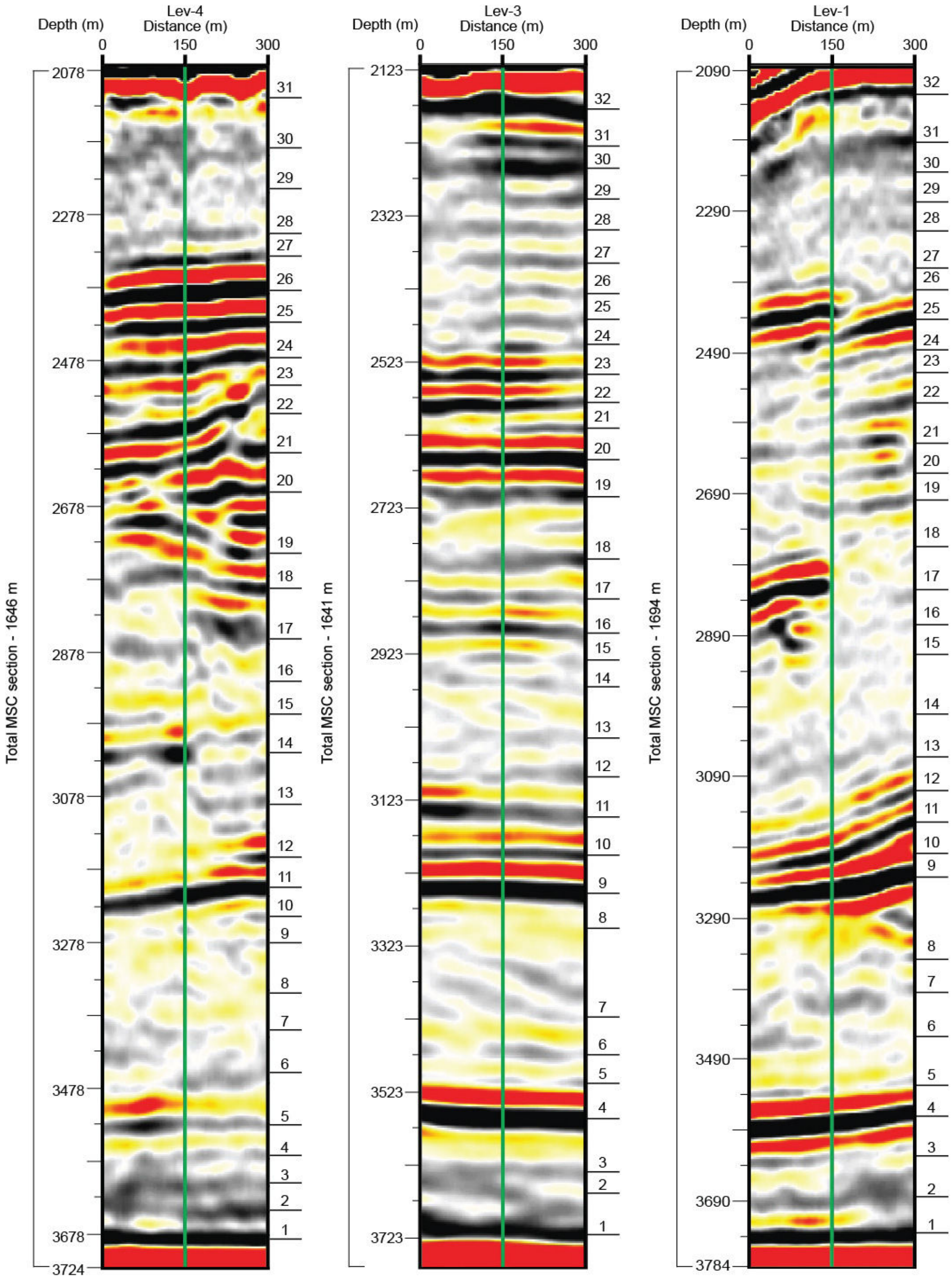

Figure 7. Seismo-cyclostratigraphy of three seismic profiles around wells in the study area.

Three depth-migrated profiles that are aligned with wells in the central Levant. Black lines with numbers on the right hand side of each seismic profile represents a reflectivity phase (black) cycle count along the section. Left bar show actual depth for each section and the total depth from base to top of the MSC section in each well.

4.4 Elemental variations within evaporite samples

The wellbore cuttings do not allow recognition of macro-scale sedimentological features, which may reflect the cyclicity identified in the well logs and seismic data within the halite sequence. Tuning of marginal MSC sections has been done based on lithological transitions, such as branching selenite to massive selenite, or chaotic deposits to clastic evaporites in stages 1-3 (e.g., Roveri et al., 2014a), or diatomite-shale-carbonate transitions in the Pre-Evaporites (Ochoa et al., 2015; Sierro et al., 2001). Here, we explore whether minor inner-halite chemical variability down-section can account for the filtered cycles and variable log response within apparently massive and homogenous halite. Other Miocene intervals of homogeneous lithology have also been shown to contain cyclic changes in the chemical composition of the sediments (van den Berg et al., 2015), which are assumed to represent shifts in the depositional environment. We hypothesize that these variations, if present in deep Mediterranean basins, could correspond to: 1) variations in riverine runoff and associated influx of clastic material into the basin, and/or 2) shifts in the degree of evaporation determining the type of deposited evaporites. Both of these drivers can be related to orbital forcing (Marzocchi et al., 2015; Simon et al., 2017).

We observe a relatively low correlation (R^2=0.46; Fig. 8A) between Fe and K in the Levant halite samples, which is not in agreement with the occurrence of continentally-derived material transported to the Eastern Mediterranean. In contrast, a high elemental correlation (R^2=0.91; Fig. 8B1) is observed between S and Ca, which confirms that low and variable amounts of minerals rich in $CaSO_4$ (i.e., gypsum and anhydrite) represent an integral part of evaporite deposition in the Main Halite of the deep Levant Basin.

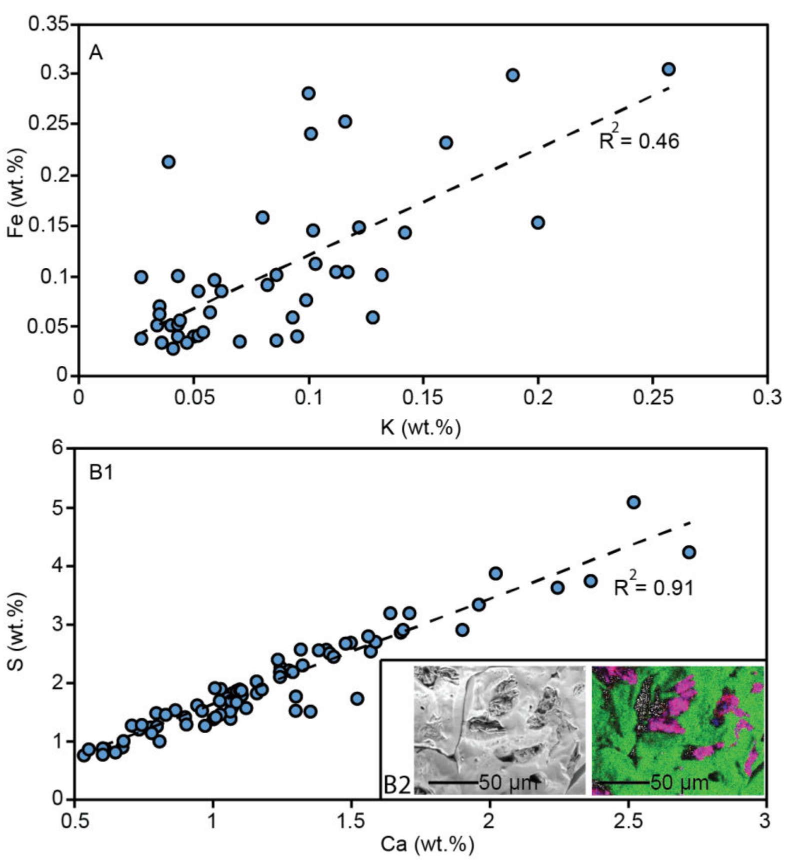

Figure 8. X-ray fluorescence elemental analysis of the Levant evaporites

Results of XRF elemental analysis are shown for 77 halite samples for specific elemental composition. (A) Note the low correlation between iron and potassium, while (B1) shows a high sulfur to calcium correlation. The high correlation between sulfur and calcium is corroborated by SEM-EDS imagery and element maps (halite sample from 3058 m; (B2)) showing the distribution of Na (green), Ca (blue) and S (red), indicating the occurrence of gypsum microcrystals (purple; B2) within cavities of the larger and much more common halite crystals.

This notion is further confirmed by the recognition of calcium sulfate microcrystals minerals within the halite cuttings (Fig. 8B-2). Note that not all halite crystals include a similar precipitation of calcium sulfates in small pores. We suggest that shifts in the amount of gypsum or anhydrite deposition along the section might correspond with the cycles obtained by well-log spectral analysis.

4.5 Organic geochemistry as a stratigraphic marker

Biomarker data allow us to identify sources of sedimentary organic matter preserved in the cuttings as well as to gain insights into its thermal history. We observed distinct differences in the biomarker distribution found in the Pre-Evaporites, the Argillaceous Diatomites within the Main Halite deposits, and the overlying Interbedded Evaporites interval. The *n*-alkanes range from *n*-C_{16} to *n*-C_{38} (Table 1, Fig. 9), and their distribution varies between samples. For example, while short- and long-chain alkanes are more predominant in the Pre-Evaporites and the Argillaceous Diatomites, mid-chain alkanes are more prominent in the Interbedded Evaporites. Additionally, the carbon preference index (CPI) of long-chain *n*-alkanes, which portrays the degree of oddity in the distribution of the different *n*-alkanes, varies around 5-7 in the Pre-Evaporites, 4-12.3 in the Main Halite (Argillaceous Diatomites) interval, and around 1.9-2.9 in the Interbedded Evaporites (Table 1; Fig. 10). The Argillaceous Diatomites also contain the lowest Pr/Ph ratios (Table 1, Fig. 10) compared to other samples. The relative abundance of long-chain *n*-alkanes (C_{25}–C_{35}) is more elevated within the Argillaceous Diatomites and Pre-Evaporite. This is reflected in the ratio of long chain (C_{25}-C_{37}) to short chain (C_{16}-C_{21}) *n*-alkanes, which maximize in the Argillaceous Diatomites (1.9), followed by the Interbedded Evaporites (1.6) and the Pre-Evaporites (1.2). The C_{31} *n*-alkane commonly is the most dominant homologue.

Selected hopane- and sterane-based thermal maturity indices (Table 2; Fig. 11; Peters and Moldowan, 1993; Rullkötter and Marzi,1988; Peters et al., 2005) also indicate major differences between samples from the Pre-Evaporites and Argillaceous Diatomites, relative to those from the lower part of the Interbedded Evaporites. As summarized in Table 2, the diatomite facies exhibit the lowest thermal maturity values, to be followed by the Pre-Evaporites, while much more mature indices are reached in the overlying Interbedded Evaporites. This is clearly indicated by the presence of hopanes with the biological ββ configuration, in addition to low values of the C_{31} S/R hopanes ratio and the C_{28} ααα 20S/20R steranes ratio, and more elevated values of the C_{30} βα/αβ hopanes ratio in immature samples (Fig. 11). Additionally, the Argillaceous Diatomites samples exhibit a lack of re-arranged steranes compared to the overlying and underlying intervals (Fig. 11; Table 2).

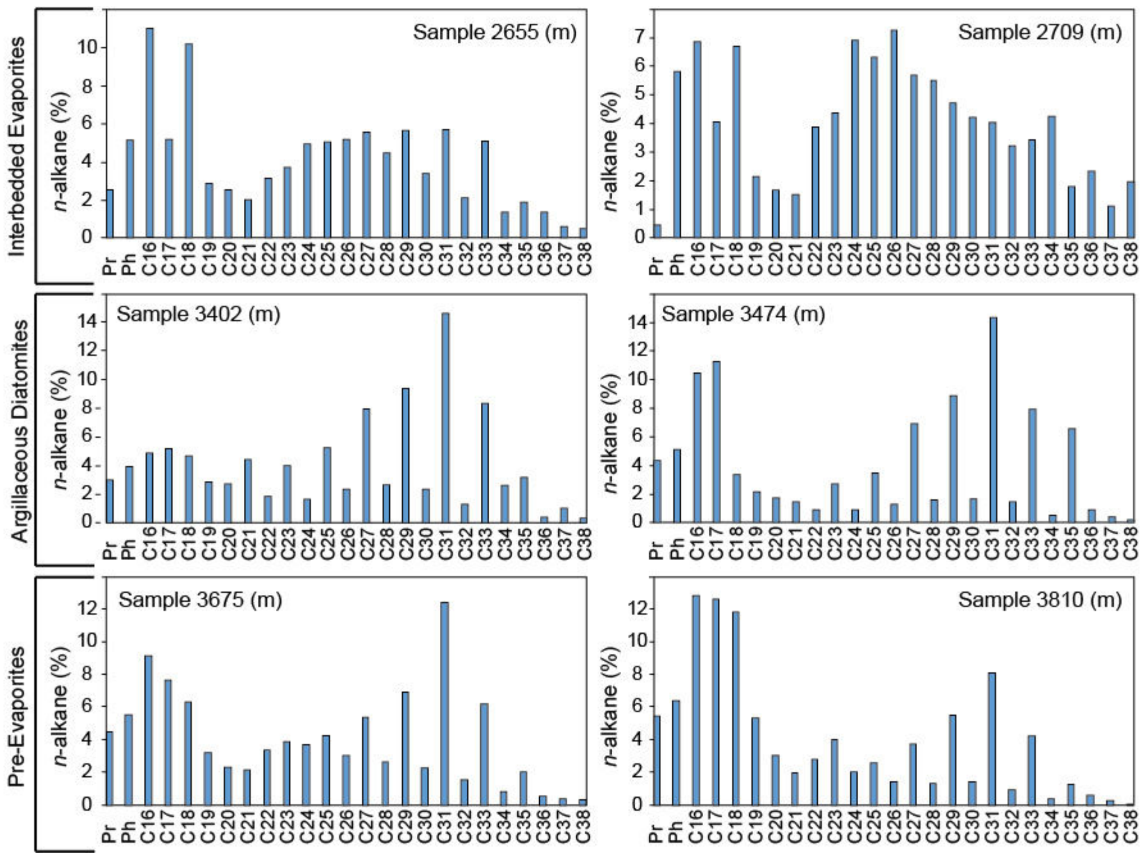

Figure 9. n-alkane distribution in non-halite intervals.

Two samples from each depositional unit (left and right columns) show the relative abundance of pristane (Pr), phytane (Ph), and C_{16}-C_{38} *n*-alkanes. Note the odd-over-even carbon-number predominance of long-chain *n*-alkanes in the Argillaceous Diatomites (center) and Pre-Evaporites (lower) relative to the overlying Interbedded Evaporites. Also observe the higher CPI, i.e., the distribution of *n*-alkanes, in the Pre-Evaporites and Argillaceous Diatomites relative to the Interbedded Evaporites, and higher relative abundance of medium-long chained compounds.

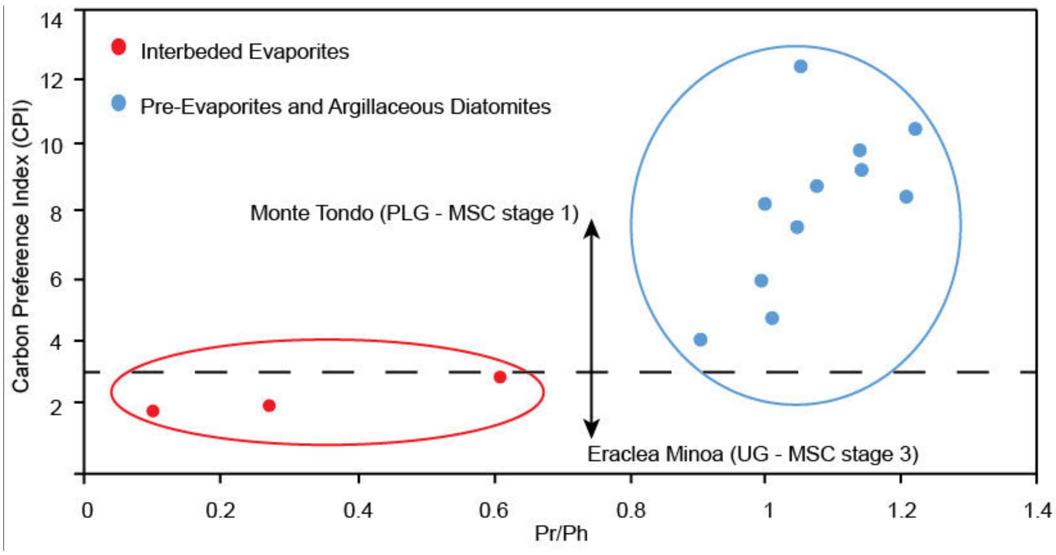

Figure 10. Pristane/phytane ratio to carbon preference index (CPI) plot.

Legend indicates the strata of plotted samples. Horizontal dashed line indicates the separation of CPI values of marginal section across the MSC reported by Vasiliev et al. (2017). Note that the samples from the Interbedded Evaporites plot in the area of values measured in stage 3 of the MSC (Vasiliev et al., 2017), while the lower samples from the Levant plot in the area of MSC stage 1. Also note the separation in Pr/Ph values between the Interbedded Evaporites relative to the Pre-Evaporites and Argillaceous Diatomites.

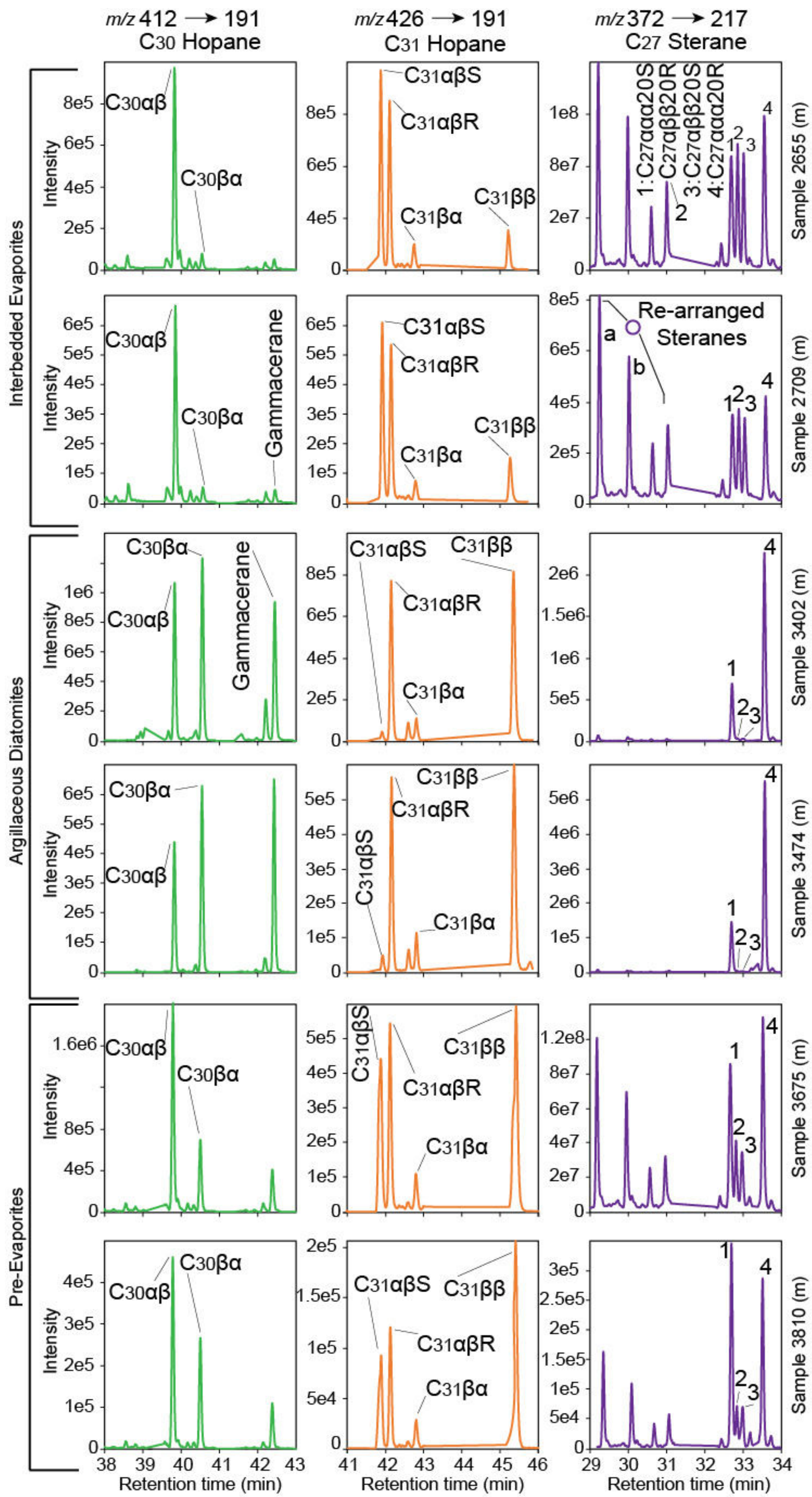

m/z 412 → 191
C30 Hopane
m/z 426 → 191
C31 Hopane
m/z 372 → 217
C27 Sterane
Interbedded Evaporites
Argillaceous Diatomites
Pre-Evaporites
Intensity
C30αβ
C30βα
Gammacerane
C31αβS
C31αβR
C31βα
C31ββ
1:C27ααα20S
2:C27αββ20R
3:C27αββ20S
4:C27ααα20R
Re-arranged Steranes
Sample 2655 (m)
Sample 2709 (m)
Sample 3402 (m)
Sample 3474 (m)
Sample 3675 (m)
Sample 3810 (m)
Retention time (min)

Figure 11. Distribution of selected bacterial hopanes and algal steranes.

Two samples from each depositional unit (left and right columns) were investigated for the distribution of aliphatic hydrocarbons using selective reaction monitoring (SRM) analysis. Each sample (numbered on the right) includes a chromatogram for three given SRM transitions: 412 → 191 (C_{30} Hopane); 426 → 191 (C_{31} Hopane); 372 → 217 (C_{27} Sterane). The C_{27} rearranged steranes are marked as (a) $C_{27}\beta\alpha$ 20S and (b) $C_{27}\beta\alpha$ 20R. High ratios of $C_{31}\alpha\beta$S/R hopanes and $C_{27}\alpha\alpha\alpha$S/R steranes, along with low values of $C_{31}\beta\beta/\alpha\beta$ and $C_{30}\beta\beta/\alpha\beta$ hopane ratios, indicate a higher, yet mixed, maturity of the organic matter preserved in the Interbedded Evaporite shale samples compared to samples from the Pre-Evaporites and Argillaceous Diatomites. The underlying diatomite facies sediments are immature in nature, while the Pre-Evaporite shale samples exhibit mixed signatures (e.g., high $C_{31}\beta\beta/\alpha\beta$ hopanes and C_{27} $\alpha\alpha\alpha$S/R steranes).

5. Discussion

5.1 Deep-sea halite depositional environment

The halite in the Dolphin well appears to be a pure, homogeneous layer, indicating a monotonous deposition of halite in the deep Levant Basin. Transmitted-light microscopy and SEM analysis of halite crystals (<0.5 cm) throughout the section reveals no distinct sedimentological variations. XRD analysis also confirms a uniform, halite-dominated mineralogical composition (Fig. 4). Gypsum microcrystal were observed within several halite crystals as seen in SEM-EDS (Fig. 8B-2), and elemental variations supporting shifts in the relative amounts of calcium sulfates deposited along the halite part of the section were apparent in XRF analysis (Fig. 8). However, we found no features similar to the lithological variations reported from the Realmonte salt mine (Lugli et al., 1999) or the intermediate depth halite of the Balearic Basin (Site 134; Lugli et al., 2015), such as cumulates of halite plates settled out from a stratified water column, plate cumulates in a shallowing-upward sequence containing kainite layers, or cumulates of skeletal hoppers with chevron overgrowths. The above conclusion might be biased due to the usage of well cutting, possibly not allowing to recognize these features. However, the mm-scale variations in the salt deposits shown by Lugli et al. (2015) should have been recognizable in the halite well cuttings. The lack of comparative features between the marginal halite and the Levan deep-basin halite is also evident when comparing the halite samples in the Dolphin well and halite deposits penetrated by DSDP drilling. There is a clear distinction between the featureless Dolphin halite and the halite interbedded with detrital sand and small anhydrite nodules recovered at DSDP Site 134 offshore Sardinia in the margins of the western Mediterranean (Hsü et al., 1973). The halite sampled in Site 134 is banded similarly to the Sicily halite reported by Lugli et al. (1999), with alternative cloudy and translucent beds.

Similarly, the banded halite and polyhalite at DSDP Sites 374, 375 and 376 in the Eastern Mediterranean (Garrison et al., 1978) does not resemble the homogenous halite recovered in the Dolphin well. The homogeneous nature of the halite observed in the Dolphin well suggests continuous deep-sea deposition, in comparison to halite deposition in the shallower marginal basins.

Modern analogs for ancient deep-water halite depositional environments are scarce. An exception is the hypersaline Dead Sea, in which active precipitation of halite occurs within the deepest parts of the basin (Arnon et al., 2016; Sirota et al., 2016, 2017; Steinhorn, 1983; Stiller et al., 1997). The Dead Sea floor is divided into two principal environments: a deep, hypolimnetic lake floor, and a shallow, epilimnetic lake floor (Sirota et al., 2016, 2017). Halite continuously precipitates with seasonal variations influencing the type of halite formation on the deeper hypolimnetic lake floor. However, the shallow epilimnetic lake floor is also subject to seasonal variations, which produce annual unconformities related to halite deposition and dissolution. The epilimnion part of the lake is undersaturated during the summer and halite is dissolved, while winter is characterized by a heavily supersaturated water column and halite is crystallized (Sirota et al., 2016). Summer is associated with higher loss of water by evaporation from the lake compared to the winter. Sirota et al. (2016) argue that the seasonal halite deposition cycle in the Dead Sea epilimnion is controlled by the decrease in the saturation with increasing temperature, which overcomes the effect of enhanced summer evaporation. The hypolimnion is supersaturated and halite is crystallized throughout the year, with higher supersaturation and higher crystallization rates during winter. During summer, the undersaturated epilimnion dissolves halite, forming highly saturated dense solutions. These solutions flow to the hypolimnion, which becomes supersaturated and crystallizes halite. This process results in focusing of halite deposits in the deep hypolimnetic parts of the evaporitic sea, and thinning of the shallow epilimnetic deposits occurs (Sirota et al., 2016, 2017). The Dead Sea modern analogue provides a mechanism for explaining the great thickness of the deep Mediterranean MSC halite deposit. A similar model might have applied during the MSC, with halite dissolution in the marginal and intermediate basin evaporites, and focusing and thickening of halite deposition in the deeper parts of the basin, as also partly proposed by Roveri et al. (2014c).

5.2 Stratigraphic markers in deep basin MSC deposits

5.2.1 Deep-basin diatomites as environmental and lithostratigraphic markers

As no chronostratigraphic indicators were found in the studied section, we aim to use the litho-chemical analysis performed on the Dolphin well samples to identify lithostratigraphic and chemostratigraphic markers that may serve as tie-points for establishing an age model for the deep basin MSC deposits (Fig. 12). In this context, the occurrence of diatomites within the Main Halite unit provides a primary observation. Diatomites are known to occur within Pre-Evaporite and PLG intervals in some of the marginal sections (Dela Pierre et al., 2014; Hilgen et al., 2007; Hilgen and Krijgsman, 1999; Krijgsman et al., 2001; Manzi et al., 2011; Roveri et al., 2014a), and more rarely within stage 3 Upper Gypsum deposits (e.g., Eraclea Monia section; Manzi et al., 2009). Diatom-rich aggregates within laminated layers, appearing as mudstone intervals interbedded within the PLG deposits of the Piedmont basin, were used by Dela Pierre et al. (2014) to establish the existence of normal-marine (not brackish or hypersaline) waters during deposition of non-evaporitic intervals during stage 1 of the MSC. Here we show that open-marine planktonic diatom taxa abundant in the Piedmont during the PLG (e.g., *Coscinodiscus* sp. and *Thalassionema longissimi*) are also abundant or closely related to abundant species within the Dolphin assemblage.

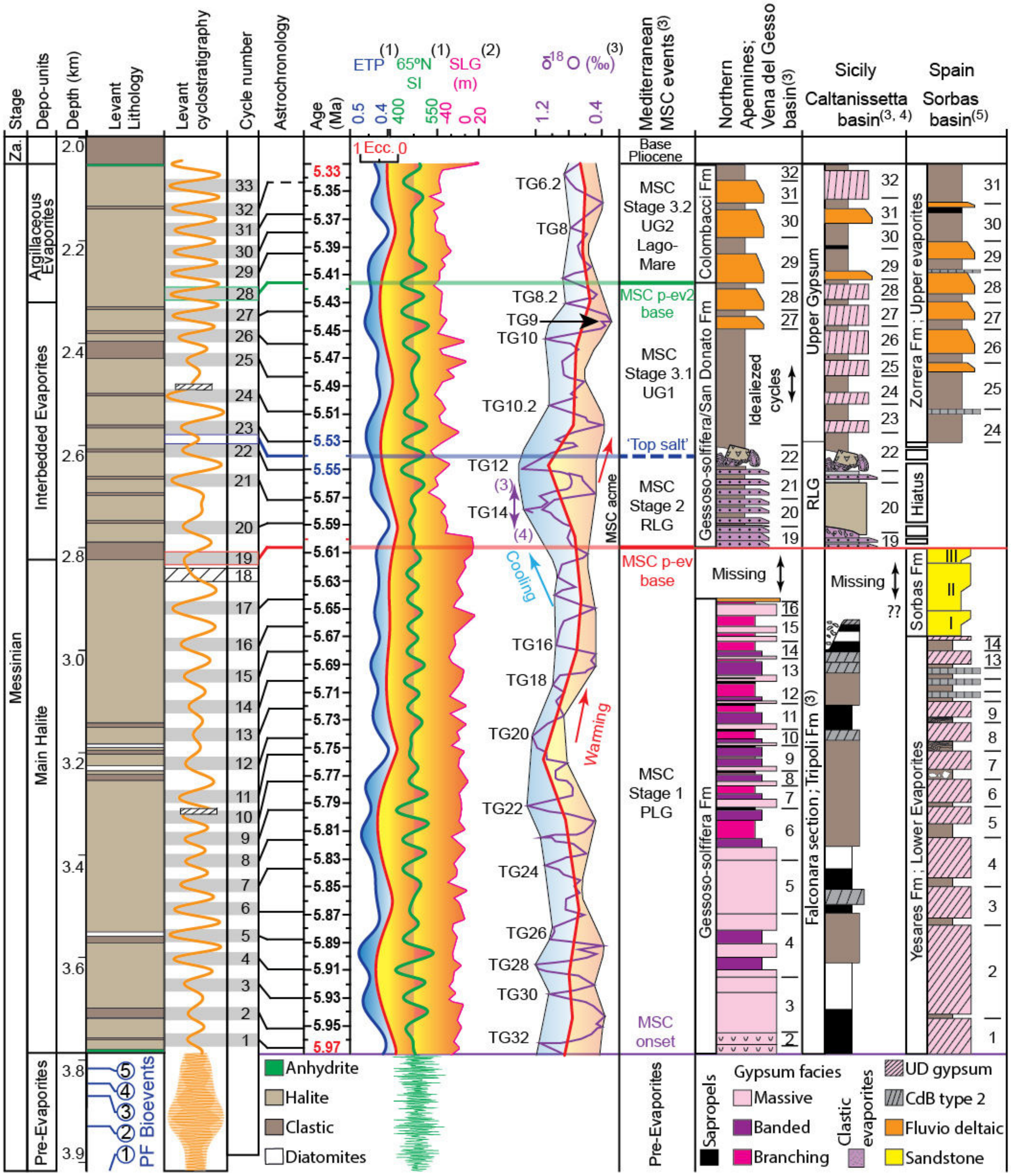

Figure 12. Astronomical age model and regional correlation of the Levant MSC

The Levant interpreted lithology (left, from Fig. 2), biostratigraphic reference levels (PF – planktic foraminifera, below) and filtered well-log model (Fig. 5) determine a cyclostratigraphic *model, resulting with 33 cycles for the Levant MSC (shaded cycles). Note the significantly lower cycle frequency in the Pre-Evaporites (2.3 m compared to 51 m per-cycle), due to the much higher sedimentation rates in the evaporites interval. This cyclostratigraphic model is tuned to astronomic target curves (center) of ETP (blue; calculated as eccentricity (Ecc; red) + obliquity - precession ((1) Laskar et al., 2004), 65°N summer insolation (65°N SI; green) (Laskar et al., 2004), and marginal MSC deposits (right columns) based on astronomical calibrated ages and cycles identified across the Mediterranean ((1) Laskar et al., 2004; (3) Roveri et al., 2014a, CIESM (2008); (4) Manzi et al., 2011; (5) Krijgsman et al., 2001). The drop in sea level (SLG; sea level Gibraltar; (2) Ohneiser et al. 2015) corresponding to glacial peaks TG12-14 ($\delta^{18}O$; as summariezed in Roveri et al. (2014)) marks the top of the Main Halite unit. The shift to post-evaporitic and clastic deposits of MSC stage 3 (Hilgen et al., 2007; Krijgsman et al., 2001; Laskar et al., 2004; Roveri et al., 2014), through a stepwise deglaciation associated with sea-level rise (TG12-9), is here astronomically tuned to enhanced clastic deposition in the Interbedded Evaporites and Argillaceous Evaporites units of the Levant.*

To date, there are no reports of diatomites, or a diatom-rich assemblage in stage 2 of the MSC across the Mediterranean. Based on the taxonomic similarities between the deep and marginal planktonic marine diatom assemblages, we propose that the Levant diatomites constitute a temporal lithostratigraphic marker. If we follow the interpretation for the occurrence of planktic marine diatoms as indicators of partial connectivity with the Atlantic Ocean (Dela Pierre et al., 2014; Hüsing et al., 2009; Krijgsman et al., 2000), then their appearance interbedded within the halite in the Levant suggests that deposition of the halite layer occurred at a time of at least partial, periodic Atlantic connectivity, most likely during deposition of the PLG on the margins (5.97-5.6 Ma).

5.2.2 Allochthonous grains in the Interbedded Evaporites-Argillaceous Evaporites and stages 2-3 of the MSC

The abrupt change that marks the onset of enhanced clastic input in the Interbedded Evaporites in the Levant Basin, together with endemic and reworked Eocene and Cretaceous foraminifera into the basin, matches other similar episodes reported from the MSC in the Mediterranean. Primarily, these are the clastic-rich deposits that result in the deposition of the Reworked Lower Gypsum (stage 2) and the Upper Gypsum and Lago-Mare deposits (stage 3) on the margins. These clastic deposits, including a similar abundance of minerals and reworked fauna, are not only reported from marginal sections (e.g., Lofi et al., 2011; Roveri et al., 2014), but also from cores of deeper parts of the basin (e.g., Site 124 in the Western Med (Ryan et al., 2007), Site 654 in the Tyrrhenian Sea (Borsetti et al., 1990), and from Sites 374 and 376 in the Eastern Mediterranean (Cita et al., 2006; Hsü et al., 1978a, 1978b)).

DSDP Sites 375 and 376 at the Florence Rise in the Eastern Mediterranean recovered nannofossil marlstones and dolomitic marlstones of latest Miocene age, overlying a gypsum with marlstone sequence (Hsü, et al., 1978b). The gypsum with marlstone, which are interpreted as deposits of a shallow subaqueous environment, are followed downwards by anhydrite and halite at Site 376 and are collectively recognized as the upper part of the Mediterranean evaporites. The interbedded gypsum contains reworked Cretaceous, Paleogene and lower/middle Miocene foraminifera and nannofossils, similar to the fauna identified in the clastic interval of the Interbedded Evaporites in the Dolphin well. The reworked fauna from Florence Rise are common to abundant in the bedded evaporites and rare to absent in the overlying Pliocene and underlying Tortonian and Serravallian (Hsü, et al., 1978b), indicating a distinctive phase of reworked sediments deposited within the Mediterranean basins. The sedimentary response of the

Interbedded Evaporites and Argillaceous Evaporites (Units 5 and 6, respectively; Gvirtzman et al., 2013; 2017; Manzi et al., 20018) in the Levant Dolphin and Leviathan-1 wells (from ~2270 m in the Dolphin well, Figs 5, 12) resembles similar observations reported from shallower deposits in the Levant. For example, the Afiq Formation overlies the anhydrite-siliciclastic stage 2-RLG equivalent Mavqiim Formation (Druckman et al., 1995; Lugli et al., 2013) and was penetrated by the Or-South 1 well. It consists of Eocene-aged lithoclasts made of limestone, dolomite, and chert- and quartz-rich sand, overlying a conglomerate unit with brackish ostracods indicating a plausible correlation to the Lago-Mare stage (Derin, 2000). A fluvial or sabkha environment is attributed to this interval with subaerial exposure, supporting the idea of a considerable desiccation phase and subaerial exposure near the end of the MSC (Cita et al., 1978; Lofi et al., 2011; Madof et al., 2019; Ryan, 1978). Similar lithologies, including clasts of Eocene and Cretaceous age, were described from the marginal Nir-1 well in the Levant Basin above an erosion surface and beneath earliest Pliocene marls (Frey-Martınez et al., 2007). Similar clastic-conglomeratic and sandy lithologies are also reported from the Messinian Qawasim and Rosetta formations offshore Egypt (Leila et al., 2016); the latter correlates with the Afiq Formation in the Levant (Derin, 2000). Unfortunately, no samples are available from above the base of the Interbedded Evaporites in the deep Levant Basin to further confirm the lithological correlation between these sections and the deep Levant Basin. Correlation to more proximal sections and well-log interpretations indicate that the overlying Argillaceous Evaporites mark a shift to more clastic and gypsum/anhydrite deposition (see also Gvirtzman et al., 2013; 2017; Manzi et al., 2018).

We argue that the main change in the halite unit, characterized by mixing of clastic material into the deep-basin deposits at the base of the Interbedded Evaporites correlates with the beginning of major sea-level drawdown and introduction of clastic material into the entire Mediterranean Basin, from stage 2 of the MSC (5.6 Ma) through the Upper Gypsum and Lago Mare stages in the marginal basins (5.55-5.33 Ma; Argillaceous Evaporites in Fig. 12). During stage 2, sea-level drawdown eroded and redeposited the PLG gypsum into the marginal and intermediate parts of the basin (e.g., Lofi et al., 2011). The deep-basin expression of this regression might be the fine-grained clastics, including older reworked fauna, reaching the Mediterranean depocenters. However, to further test this idea and try to distinguish between stage 2 and 3 sediments, we compare biomarker distribution across the basin, and identify sedimentary cycles within the MSC of the Levant Basin.

5.2.3 Basin-wide transport of organic matter

The *n*-alkane distribution and CPI values of the Levant samples (Figs 7 and 8; Table 1) are similar to some extent to those obtained from marginal and onshore MSC successions (Vasiliev et al., 2017), and provide further support for the introduction of reworked and mixed material into the Levant during the deposition of the Interbedded Evaporites. The *n*-alkane distribution of Mediterranean MSC samples covering the entire 640-kyr-long MSC interval shows distinct dissimilarities between several marginal to intermediate-depth sections (Vasiliev et al., 2017): The Monte Tondo (Primary Lower Gypsum; MSC stage 1), Realmonte salt mine (Halite and Re-sedimented Lower Gypsum; MSC stage 2), and Eraclea Minoa (Upper Gypsum/Lago Mare; MSC stage 3). The Delphine well *n*-alkane distribution shows a higher abundance of short-chain homologues in the Levant relative to marginal sections (Vasiliev et al., 2017), likely due to the lower relative input of terrestrial organic matter in more distal depositional settings. Several similarities exist between both data sets. Vasiliev et al. (2017) reported CPI values of 3.0-7.9 at Monte Tondo (stage 1), and 1.7-3.7 at Eraclea Minoa (stage 3; Fig. 10). While CPI values were not reported from the halite samples of the Realmonte salt mine, Vasiliev et al. (2017) show two different types of organic matter: 1) autochthonous sediment associated with gypsum or halite deposited in place, and 2) allochthonous material associated with clastic sediments and transport. Marked similarities in CPI values are therefore noted between the Levant and marginal locations described by Vasiliev et al. (2017), with CPI values of 4.0-12.3 in the Main Halite interval (indicating stage 1), and 1.9-2.9 in the Interbedded Evaporites interval (indicating stages 2-3) (Fig. 10).

Vasiliev et al. (2017) also suggest that dissimilarities in the biomarker and isotopic composition of stages 1 and 2, relative to stage 3 sediments, may be attributed to the outflow of Black Sea (i.e., Paratethys) waters and their mixing into the Mediterranean, which paved the way for Paratethyan 'Lago-Mare' type fauna. For instance, the distribution of *n*-alkanes and CPI values in stage 3 at Eraclea Minoa are more evenly distributed and lower relative to those of stage 1 (fig. 3 in Vasiliev et al., 2017). We report a similar distinction in the *n*-alkane distribution between the upper clastic samples and underlying sediments (Table 1, Fig. 9). A much stronger odd-over-even predominance (i.e., higher CPI values) is observed in the Argillaceous Diatomites, together with more elevated long-chain over short-chain *n*-alkanes values (LCA/SCA; Table 1) and maturity parameters (Fig. 11; Table 2). This indicates more immature source rocks with significantly different sources of the organic matter in the Main Halite relative to the Interbedded Evaporites sediments (Bray and Evans, 1961; Scalan and Smith, 1970).

The distribution of stereoisomers of algal steranes and bacterial hopanes (Fig. 11; Table 2) reflects the transformation, or stereoisomerization from biological epimers to a more stable geological molecular configuration as a consequence of thermal alteration (Peters, 1986; Peters et al., 2005, 1980). The evidence for enhanced thermal maturity in the Interbedded Evaporites relative to the underlying deposits (Fig. 11; Table 2) is counterintuitive, as thermal maturity should increase with depth (Peters et al., 2005, 1980). Furthermore, the Interbedded Evaporites exhibit mixed signals that include high values of the C_{31} αβ S/R ratio (indicative of thermally mature organic matter) in addition to C_{31} hopanes with the ββ biological configuration (indicative of immature organic matter) (Fig. 11; Table 2). This aspect further supports the occurrence of organic matter mixtures from differing ages and thermal histories, i.e., a higher proportion of allochthonous, thermally mature organic matter in the Interbedded Evaporites compared with the Main Halite and Pre-Evaporite samples. This interpretation is consistent with similar trends observed in early Paleogene (Sepúlveda et al., 2009) and Quaternary (Rashid and Grosjean, 2006) studies. Such trends may reflect an intensification of the hydrological cycle, and thus enhanced precipitation, continental runoff, and the transport of reworked, and pre-aged, continental or marginally-derived organic matter during the deposition of the Interbedded Evaporites. Another mechanism through which transport can occur is dense shelf-water cascading (DSWC) transport of sediment and associated organic matter from marginal settings to deep Mediterranean basins, as reported to occur in the Mediterranean today (Canals et al., 2009). The interpretation of transport in these intervals is consistent with the occurrence of clastic material, larger sub-rounded minerals, and re-worked Cretaceous and Eocene foraminifera within samples from the Interbedded Evaporites, which also supports the presence of reworked, older sediments. Both Cretaceous and Eocene organic-rich source rocks are known around the Mediterranean Basin (e.g., Almogi-Labin et al., 1993; Bayliss, 1973; Meilijson et al., 2014), and might represent sources of pre-aged weathered and transported organic matter, matching the apparent higher maturity measured from the organic-matter extract of the Interbedded Evaporites sediments.

In summary, the similarities between our data and of Vasiliev et al. (2017) suggest that organic geochemical analysis from the Dolphin well might be used as regional chemostratigraphic markers to distinguish between Pre-Evaporites and Argillaceous Diatomites sediments, and the overlying Interbedded and Argillaceous Evaporites. A correlation between MSC stage 3 and the upper part of theMSC in the Levant Basin has been previously proposed based on seismic interpretation and the sampling of shallower deposits (Druckman et al., 1995; Gvirtzman et al., 2017; Lugli et al., 2013). Here, we present evidence supporting the occurrence of stage 2 sea-level drawdown or stage 3 and 'Lago-Mare'-type deposits in the deep domains of the Eastern Mediterranean. This includes increased supply of clastic material into the basin, reworked fauna, and chemostratigraphic markers (Figs 3, 9 and 10).

5.3 From cycles to astronomical tuning

Cyclostratigraphy and astronomical tuning of sediment sections, geochemical signals, and well-log responses have been extensively used for stratigraphic interpretations of MSC deposits across the Mediterranean (Dela Pierre et al., 2014; Hilgen et al., 2007, 2000, 1995; Hilgen and Krijgsman, 1999; Hüsing et al., 2010, 2009, Krijgsman et al., 2001, 1999, 1997; Lugli et al., 2015; Manzi et al., 2015, 2013, 2012; Ochoa et al., 2015; Topper et al., 2014). The CIESM stratigraphic model of the MSC has halite deposited in stage 2 of the MSC, during four precession cycles (e.g., Roveri et al., 2014a, with reference to Laskar et al., 2004; Fig. 12). These are part of the 32 precession-controlled cycles (Laskar et al., 2004) identified across the Mediterranean, with a periodicity of about 20 kyr per cycle, amounting to the 640 kyr time frame of the MSC. Manzi et al. (2015) proposed to tune the high-reflectivity intervals in the seismic section of the Levant (interpreted as clastic units; Gvirtzman et al., 2013a) to summer insolation maxima, and the transparent intervals (interpreted as halite) to summer insolation minima, within these four insolation cycles. By contrast, the study of the Pre-Evaporites in the Dolphin well by Meilijson et al. (2018) and the results of this study suggest that salt formation began around 5.97 Ma, i.e., more or less synchronously with the marginal deposition of the PLG. According to this age model, the evaporitic sequence in the Levant Basin (Fig. 12) was deposited between 5.97 and 5.33 Ma, corresponding to a time span of ~640 kyr rather than 50 kyr, and encompassing 32 insolation cycles (Laskar et al., 2004). Our suggested scenario would imply an average cycle thickness of ~50 m, as the studied section is 1590 m thick.

Bandpass filtering of the Dolphin well logs resulted in the identification of 31 cycles, closely matching the 32 precession-controlled cycles (Laskar et al., 2004) in the interval between 5.97 and 5.33 Ma. However, this age model includes several assumptions: (1) the evaporite record at the studied site is complete with no hiatus, (2) it is largely undisturbed by salt tectonics, and (3) the sedimentation rate is approximately constant, with no significant changes between the halite-rich intervals and clastic-diatomitic intervals. The Dolphin record lacks chronostratigraphic tie points and contains intervals in which the log data are erratic (Figs 5, S2). Furthermore, the Dolphin well area appears deformed in the upper part of the section, and Unit 6 is missing (overlying the Interbedded Evaporites; Fig. 6). These sources of uncertainty suggest that the Dolphin well spectral analysis provides a first order approximation of the number of cycles, primarily across the lower part of the section. However, the large number of cycles observed in the Main Halite interval, if assumed to reflect precessional cycles, suggests a longer period of deposition than ~50 kyr. The Leviathan-1 well is much less deformed (Figs 5, 6) and has a thick interval of Unit 6 (Gvirtzman et al., 2013; 2017), similar to the sequence at the Aphrodite well (Manzi et al., 2018). It also presents a good fit between the seismic and the RE well-log response. The observed regularity produced a filtered cycles curve (Fig. 5), which reveals a good fit with the well log curve. We hypothesize that these cycles represent the 32 precession cycles identified in MSC sections across the Mediterranean. This would imply that the Main Halite interval in the lower part of the studied section is equivalent to stage 1 (PLG) in marginal sections, as also proposed by Meilijson et al. (2018).

However, lacking chronostratigraphic tie points in the evaporitic section, an alternative explanation for the cyclicity observed in the well logs of the halite and the seismic profiles should be considered to reconcile the age model suggested by Manzi et al. (2018) for the Levant Basin. In this model the FBI unit, which represents the uppermost part of the Pre-Evaporites in the Aphrodite well, corresponds to MSC stage 1 (the PLG; Manzi et al., 2018), while the uppermost part of the section corresponds to stage 3 (Unit 7; Gvirtzman et al., 2017). Following this model, the ~33 cycles identified within the Leviathan-1 MSC section (Figs 5, 7) correspond to the ~50 kyr estimated for the duration of stage 2 of the MSC (Roveri et al., 2014), and have therefore a cycle duration of ca. 1560 years. If we take into account the likely different sedimentation rates of the Argillaceous Diatomites facies, this period could correspond to the period inferred for the Dansgaard-Oescher events (1470 years), as observed during the second half of the last glacial (Schulz, 2002) (although see comments by Ditlevsen et al. (2007) and Lohmann and Ditlevsen (2018) on the validity and interpretation of these cycles). Alternatively, they could be explained by the Bond cycles, as observed for the North Atlantic during the Holocene (1500 years; Bond et al., 2001). Another alternative are the periods of ca. 1000 years corresponding to the so-called Eddy cycle observed in the ^{14}C record, which relate to variations in solar activity (Steinhilber et al., 2012). However, this last alternative is unlikely: if the regular alternations in the halite would correspond to Eddy cycles, it implies that stage 2 of the MSC lasted only ~32 kyr. This means that the climax stage of the MSC cannot encompass both glacial stages TG14 and 12 (Fig. 12), as is assumed in the CIESM model.

In the Realmonte salt mine in Sicily, 10-15 cm alternations in the salt have been interpreted as annual cycles (Manzi et al. 2012). Such sedimentation rates of ca. 10 cm/yr would imply that the 1,060 m thick Main Halite interval in the Levant could have been formed in a short time period of 10,600 years, although average sedimentation rate may be lower in the Argillaceous Diatomites. However, it is hard to reconcile such a short duration of deposition with the amounts of halite required to build up the thickness of the Levant Basin halite layer.

In the absence of a simple explanation for the cyclicity observed in the Dolphin well, we now consider its interpretation in relation to the different elements of the CIESM model for marginal MSC deposits. The CIESM (2008) consensus stratigraphic model for the MSC is strongly based on astronomical tuning of different MSC sections and includes the following division of the 32 orbital-related cycles identified during this time frame (Laskar et al., 2004): cycles 1-18 in stage 1 (PLG), 19-23 in stage 2 (RLG), 24-28 in stage 3.1 (lower part of Upper Gypsum), and 29-32 in stage 3.2 (the Lago Mare). The correlation between the Levant MSC well-log-based astrochronology, the orbital target curves, and the chronology of shallow to marginal sections (CIESM, 2008) of the MSC indicates the following: (1) the Main Halite interval (3759-2800 m in the Leviathan-1 well) is bound between the Levant filtered cycles 1 through 19 (Fig. 12). A comparison with the current MSC chronology (CIESM, 2008; Roveri et al., 2014a) shows a correlation with the number of cycles in the interval between 5.97 and 5.6 Ma from the base of the PLG (stage 1) to the base of the RLG (stage 2); (2) the Interbedded Evaporites interval (2800-2320 m) is bound between the Levant filtered cycles 19 through 28 (Fig. 12), which correlates to the number of cycles in in stage 2 (the RLG; 5.6-5.55 Ma; cycles 19-23), with its top known as the ‘top salt’ horizon, and the lower part of stage 3 (stage 3.1 the Upper Gypsum who’s base is at 5.42 Ma). Thus, the lower part of the Interbedded Evaporites is also equivalent to stage 2 halite deposits recognized in intermediate basins, such as the Realmonte salt mine in Sicily; (3) at the upper part of the Interbedded Evaporite and the Argillaceous Evaporites interval are equivalent to stage 3 of the MSC (2320-2090 m; Fig. 12), ending with the clastic Lago-Mare interval.

Following the suggestion of Meilijson et al. (2018) for an early onset of halite deposition in the deep Mediterranean basins, similar claims were made by García-Veigas et al. (2018) based on sulfur stable-isotopes analysis of marginal and intermediate basin gypsum deposits. They hypothesize that the deep-basin halite deposits are not equivalent to one phase of deposition during stage 2 of the MSC, but rather comprise two to three phases of halite deposition, beginning with halite deposition during stage 1 of the MSC. Our astronomical tuning agrees with this idea by positioning the boundary between stage 1 and 2 of the MSC (2762 m in the Dolphin well, 2800 m in Leviathan-1) at the top of the Main Halite interval. Consequently, we propose that the Main Halite is equivalent to stage 1 gypsum deposits of the PLG, as indicated independently by the diatomite facies. The increase in clastic and reworked faunal material into the basin fits well with our astrochronology, placing the Interbedded Evaporites within the time period of the Reworked Lower Gypsum (stage 2 of the MSC). Sea-level drawdown promoted the scraping of the shelf, reshaping of drainage and transport systems across the basin, and redepositing of vast amounts of eroded sediment into the intermediate basins. It also delivered vast amounts of fine-grained material to the deep basins, as observed in the Interbedded Evaporites in the Levant Basin. Lastly, the identification of the *Discoaster quinqueramus* in Unit

5 (the Interbedded Evaporites) by Manzi et al. (2018) supports this conclusion, as this species went extinct towards the end of stage 2.

5.4 Implications of a new MSC chronology in the Mediterranean

While not conclusive, the integration of our different stratigraphic proxies supports an early and long-lasting deposition of deep-basin halite. The direct implication of this age model is that halite was deposited in the deep Eastern Mediterranean when sea level was high and partial, episodic connection with the Atlantic still prevailed (Dela Pierre et al., 2014; Flecker and Ellam, 2006; Krijgsman et al., 2002; Roveri et al., 2014b), synchronously with gypsum deposition along the Mediterranean margins and intermediate basins (Ochoa et al., 2015). Our results do not exclude an evaporative drawdown (e.g., Lofi, et al., 2011; Rouchy and Caruso, 2006; Ryan, 2008) and lower sea level at the acme of the MSC during stage 2 (Ohneiser et al., 2015). The lack of sedimentological features within the monotonously clean halite, and our interpretation of long-lasting deep-water evaporite depositional settings, indicate that salt must have started to precipitate within a deep-basin deep-water environment, and not in shallow waters. We propose that sea-level drawdown prompted enhanced transport of clastic sediments into the deep basin resulting in the deposition of the Interbedded Evaporites unit, analog to the marginal deposition of the RLG. Studies of strontium isotopes from the Lower Evaporites (PLG, MSC stage 1) consistently report isotopic values close to those characteristic of the global ocean (Flecker and Ellam, 2006; Roveri et al., 2014b), and do not support an early desiccation model (Cita, 1976; Hsü, 1973). While advocating a different chronological model, our study is consistent with these interpretations and shows that halite deposition started during a time when Atlantic inflow was still evident.

A coeval initiation of basinal halite and marginal gypsum precipitation calls for a reevaluation of previous models for MSC development, as well as its effect on global ocean salinity and climate. We refer to the timing and persistence of halite deposition (which may have been an order of magnitude larger than previously thought), and also to the substantially lower rates of deposition of the deep-basin salt unit, from a previous assumption of 3,000 cm/kyr (according to CIESM chronology) to 250 cm/kyr as deduced from our new age model. Although this assumes continuous precipitation and no dissolution, which we consider unlikely if the water is being relatively refreshed with additional seawater throughout deposition. The Levant chronostratigraphic model suggests that steady state of halite deposition was achieved and maintained earlier in the MSC than previously thought. Both halite and gypsum could have been precipitated synchronously, with their partitioning possibly governed by their different solubility product constants (K_{sp}) and ion availability. Furthermore, if we allow for an order of magnitude change in the time scale of halite precipitation, then the required sedimentation flux that removes sodium and chlorine from seawater is reduced. This exercise substantially reduces the total sea-level drawdown (Ryan, 2008) required to explain the deposition of a ~2 km-thick salt deposit. A further possible mechanism to explain the synchronous deposition of gypsum and halite in marginal and deeper parts of the basin, respectively, includes density stratification and down-shelf cascading of brines (Roveri et al., 2014c; Sirota et al., 2017). While salt-saturated shallow waters seem to have reached gypsum saturation values, brine formation might have continuously flowed down-shelf, in a similar manner as dense shelf-water cascading (DSWC) is observed today around the Mediterranean Basin (Canals et al., 2009, 2006). DSWC is associated with mass-transport complexes and submarine channels, and has a significant impact on the sediment and organic-matter supply from continental and shallow-marine settings to deep-sea ecosystems.

Mass-balance calculations suggest that the input of dissolved organic carbon and suspended particulate organic carbon from ocean margins to the open ocean interior may be more than an order of magnitude greater than direct inputs of organic carbon produced near the ocean surface today (Bauer and Druffel, 1998). Similarly, highly saturated waters produced in an evaporitic Mediterranean may have produced vast quantities of brine accumulating in the deep depocenters. Brine formation may have been at least partly controlled by precession-induced increases in river runoff (Marzocchi et al., 2015), and potentially by surface inflow from the Paratethys (Karakitsios et al., 2017; Krijgsman et al., 2010). Salinity stratification is supported by geochemical evidence for the occurrence of low-salinity surface waters overlying deep brines at gypsum and halite saturation (Christeleit et al., 2015), as well as by the presence of brackish-water faunas of Paratethyan origin in the Lago-Mare phase (Stoica et al., 2016). Our data, including high concentrations of long-chain *n*-alkanes (Table 1) and high LCA/SCA values (Table 1), also support the occurrence of increased river runoff into the basin during the deposition of the Interbedded Evaporites.

Our interpretation of a deep-basin deep-water model and early onset of halite, rejuvenates an idea that has been a focus of debate in the past (e.g., Garcia-Castellanos and Villaseñor, 2011; Lofi et al., 2011; Ryan, 2008; Schmalz, 1969). Simon and Meijer (2017) used a box-model setup to model the MSC events forced by Atlantic exchange and evaporative loss. This model demonstrated that a significantly stratified Mediterranean water column could have been established early in the crisis, while the duration of halite deposition must have taken longer than currently considered in the MSC stratigraphic consensus model. The synchronous formation of gypsum and halite in proximal and distal basins, respectively, could have occurred at different levels within the basin, with lower rates of halite sedimentation than previously thought. Our data support the model by Simon and Meijer (2017) and calls to reevaluate Mediterranean MSC sections, while considering a possible early deposition of halite.

Sea-level drop during stage 2 of the MSC may have added more proximal basins to the regional deep-sea deposition of halite, which might explain why those intermediate-basin halite deposits correlate to the stage 2 RLG. Such a mechanism can explain the existence of marginal or intermediate-depth basins with relatively thin halite deposits, which only correlate with the Interbedded Evaporites interval in the Levant (Fig. 12), in which halite is still the dominant lithology. For example, the marginal Realmonte salt mine has a ~600 m thick halite sequence (Lugli et al., 1999; Roveri et al., 2014a) compared with the thick (>2 km) halite deposits in deep Mediterranean basins. In a similar manner, recent studies from the Dead Sea demonstrate downslope-flowing brines, in which the deep basinal areas accumulate the most brine and the marginal areas are influenced by fresher waters and hence subject to more dissolution (Sirota et al., 2016).

Being one of the largest and youngest salt giant formation episodes in Earth's history, the MSC is repeatedly used as a cornerstone for explaining evaporite deposition. Our new model, which includes the synchronous deposition of sulfates in the margins of the basin and halite at its center, calls for a re-evaluation of the mechanisms governing evaporite deposition in other salt-giant deposits in the geologic record. For example, in the Permian Zechstein, similar to the Mediterranean, sulfates appear to have been limited to the margins while halite was deposited in the deeper parts of the basin (Richter-Bernburg, 1985). This is also the case for the Permian Delaware Basin in Texas and New Mexico, where clear inter-fingering between sulfates and halite are observed as brine concentrations oscillate (Anderson and Dean, 1995).

The alternating clastic and evaporitic sediments of the Interbedded Evaporites (Unit 5; Gvirtzman et al., 2013; 2017) include cycles 19-28, matching in its lower part the time frame of MSC stage 2, the RLG. Isolation from the Atlantic and significant sea-level drawdown are proposed as the formation mechanism for both the onshore deep subaerial canyons and offshore erosion surfaces across the Mediterranean (Lofi et al., 2011; Ryan, 1976; Ryan and Cita, 1978). Different models were proposed to explain the mechanisms behind erosion, transport, and re-deposition, such as early subaqueous large-scale mass-wasting processes occurring at the beginning of the MSC drawdown, subaerial rivers down-cutting by retrogressive action to adjust for their new base level, or marine abrasion as possible agent for late erosion (Lofi et al., 2011 and references therein). Regardless of the mechanism, clastic geometries are clear in MSC seismic sections and are partly controlled by local factors such as the dimension of the drainage basin, resulting in major differences between the Messinian sedimentary successions in the different areas of the Mediterranean. The whereabouts of the massive products of these basin-wide erosional processes has been one of the MSC's enigmas (Ryan, 1976; Ryan and Cita, 1978; Lofi et al., 2011). The seismic facies defined as the Complex Unit (CU; Lofi et al., 2011) in the Western Mediterranean is either chaotic or roughly bedded, and is believed to account for some of the waste products. CU deposits are absent on the margin shelves, rarely observed on the upper slopes, and mainly observed along the base of the slopes, either as fan-shaped deposits at the Messinian river mouths or as poorly organized bodies elsewhere. This unit marks the transition between the eroded slopes and deep-basin deposits (Lofi et al., 2011). The CU is positioned above or parallel to the Mobile Unit (the halite).

In summary, stage 2 of the MSC is characterized by massive sediment displacement, for which only a portion is accounted for. We propose that the Interbedded Evaporites (Unit 5;

Gvirtzman et al., 2017) are part of this high-energy system and that the interbedding of clastics represents the deep-basin depocenters for the fine grained material at the distal part of the drainage system. These precession-controlled clastic incursions reached into an evaporitic system, which in the deep basins has been depositing halite for ~360 kyr during stage 1 of the MSC. We argue that this idea could not be examined before due to lack of a sedimentary record from the deep basin and the difficulty of correlating marginal and deep-basin units based on seismostratigraphy. The call for caution regarding the interpretation of MSC-related offshore data was recently presented by Roveri et al. (2019). They pointed out that MSC units with different age, nature and depositional setting, may show similar seismic facies and geometries. On the other hand, the same unit may appear as belonging to different seismic facies, either with parallel and high-amplitude reflections or even transparent or chaotic reflectivity due to seismic interference patterns related to the dominant frequency. We therefore argue against lumping the different facies of the Interbedded Evaporites into a unified deep-basin halite deposit, disregarding its clastic nature, as done in past interpretations of the Levant Basin MSC section (e.g., Manzi et al., 2018). Here we offer new sedimentological analysis of the non-evaporitic facies, interpreted in the past as clastic deposits through seismic and well-log interpretation (e.g., Feng et al., 2016). We argue that two different 'non-halite' deposits exist in the Levant deep MSC deposits: 1) the mostly biogenic remains of diatoms (the Argillaceous Diatomites) within the stage 1 Main Halite interval, and 2) the clastic and reworked deposits of the Interbedded Evaporites/Argillaceous Evaporites belonging to stage 2 and 3 of the MSC.

Stage 3 of the MSC is generally characterized by reworking of shelf sediments and their occasional influx into the basin during renewed gypsum deposition. We position the base of stage 3 within the Interbedded Evaporites at cycle 23 (Figs 5, 6, 12), pointing to a much thicker stage 3 section in the Levant than in the model of Gvirtzman et al. (2017), Manzi et al. (2018), or Madof et al. (2019). Relying on the CIESM (2008) stratigraphic model, these separate studies position the halite into stage 2, and continue stage 2 until almost the top of the Levant MSC section. They position stage 3 at the topmost part of the section, represented only by Unit 7 - a thin anhydrite and shale unit (interpreted by well-log data in the deep basin as no study has recovered samples from this interval thus far). These studies mainly differ in their interpretation of the stage 3 depositional environment, namely subaerial (Madof et al., 2019) or subaqueous (Gvirtzman ey al., 2017) dissolution and truncation. According to our depositional model (Fig. 12), Unit 6 belongs to stage 3 of the MSC (the Upper Gypsum and Lago Mare; CIESM, 2008), and the IMTS (Gvirtzman et al., 2017) or IES (Madof et al., 2019) unconformities in the Levant represent the transition between stage 3.1 (Upper Gypsum) and 3.2 (Lago Mare) of the MSC. The latter stage (3.2) was attributed to Unit 7 and perhaps also to parts of the overlying brackish Afiq Formation (Druckman et al., 1995) by Gvirtzman et al. (2017). The introduction of Paratethyan waters and sediment, termed Lago Mare deposits along the Paratethyan side of the Mediterranean, is also likely to have reached the deep basins. However, while those might have reached the Levant Basin, different local drainage systems are most likely the sources for the MSC stage 3 transported sediments in the Levant area. A local source for transported sediments is the Nile drainage and fan systems, identified as reaching further northwest, beyond the Dolphin and Leviathan wells, towards the Eratosthenes Seamount offshore Cyprus (Hawie et al., 2013a, 2013b). In addition, local drainage systems that may have supplied the transported sediments include the Afiq and Ashdod canyons (Bertoni and Cartwright, 2007; Druckman et al., 1995), and the southern Turkey and western Syria drainage systems proposed by Madof et al. (2019).

6. Conclusions

Over the past 50 years, models explaining the formation of offshore MSC deposits have remained hypothetical in the absence of a complete sedimentary record of the deep Mediterranean Basin. The current study presents results from the offshore Dolphin and Leviathan-1 wells, which penetrated MSC evaporites from 2025 to 3616 m, and from 2090 to 3759 m, respectively. Our results challenge some of the current models for the MSC regarding the synchronicity or diachronism of evaporite deposits across the Mediterranean Basin, their composition, and controlling factors. A longer duration for halite deposition than previously assumed impacts our understanding of the biochemical and spatial constraints of this time period. While similar ideas have been previously raised (e.g., Van Couvering et al., 1976; Govers, 2009; Hardie and Lowenstein, 2004; Meilijson et al., 2018; Ryan, 2011; Simon and Meijer, 2017), we provide the first report on sedimentological data from the deep basin MSC halite deposits supporting the scenario of long-lasting salt deposition. We call for a re-evaluation of models based on a ~50 kyr-long deposition of halite in the deep basins. However, samples from the upper part of the deep MSC deposits in the Eastern Mediterranean are not yet available, while the existing sedimentary record drilled by the industry consists of well cuttings and not a continues core. The complexity revealed by this study makes a strong case for future scientific drilling efforts that can retrieve cores from different parts of the deep-basin halite deposits of the Mediterranean.

This study aimed at addressing the composition and key stratigraphic questions regarding the timing and correlation of MSC events in the deep Mediterranean. Our main findings can be summarized as follows:

1. The formation of thick halite deposits in the Levant Basin occurred in a deep-basin deep-water environment that began earlier than previously thought, during the PLG phase of gypsum precipitation in the marginal basins. This implies that a shallow desiccated scenario is not necessarily required to generate halite precipitation during the MSC. The presence of well-preserved marine planktonic diatoms within the massive halite deposits strongly supports a periodic connectivity between the Atlantic and the Eastern Mediterranean during halite deposition.
2. The exact timing for the end of deep-basin halite precipitation is still unclear. Well-log interpretation, cyclostratigraphy, and the astronomical tuning model presented here suggest that halite deposition continued at least until 5.45 Ma, and interbedded clastic material and evaporites (probably mainly gypsum/anhydrite) persisted until ca. 5.33 Ma.
3. The transition into the Interbedded Evaporites interval at 2560 m at Dolphin and 2800 m at Leviathan-1 marks a major shift in the mode of deposition. An increase in basin-ward transport of sediments is indicated by the high abundance of larger sub-rounded clastic grains such as quartz and plagioclase, clay, micrite, and reworked Cretaceous to Eocene benthic and planktic foraminifera. Variable thermal maturity indices also point to mixed sources of organic matter. In general, biomarker indices in the Interbedded Evaporites resemble those measured elsewhere in the Mediterranean Basin from strata with transported material and mixed sources. The transition from the Main Halite to the Interbedded Evaporites at 2560 m most likely represents the transition between stage 1 and 2 of the MSC. The large amounts of clastic sediments in the Interbedded Evaporites are possibly an answer to one of the MSC enigmas regarding the location of the

transported material related to the sea-level drawdown of stage 2 and the interruption of the connection with of the Atlantic Ocean.

4. During the MSC, high sea level and partial connectivity with the global ocean promoted the deposition of deep-basin deep-water halite, while see-level drawdown promoted deposition of reworked and transported material from the margins into deep Mediterranean basins.

Acknowledgments

The authors would like to thank Ratio Oil Exploration, Noble Energy, and Delek Energy for kindly providing data and permission to publish. This work was supported by the State of Israel Ministry of Energy, the Maurice Hatter Foundation, and by the Marie Curie Career Integration Grants (CIG) FP7-PEOPLE-2011-CIG under the GASTIME project framework. The work was also supported by the COST Action "Uncovering the Mediterranean salt giant" (MEDSALT) supported by COST (European Cooperation in Science and Technology). We are grateful to Emerson-Paradigm for software sponsorship. We would also like to thank Tanja Kouwenhoven for her contribution with foraminiferal analysis, Revital Bookman and Beverly Goodman for the use of laboratory equipment, Nimer Taha and Alexander Surdyaev for laboratory assistance with the XRD/XRF analysis and seismic interpretation, respectively. Nadia Dildar, Alexander Weber, and Ian Bishop are thanked for laboratory assistance for biomarker analysis and diatom taxonomy. We thank William B.F. Ryan, Andre Strasser, and an anonymous reviewer for suggestions which significantly improved the manuscript.

References

Alinat, J., Cousteau, J., 1962. Accidents de terrain en mer de Ligurie. Océanographie géologique et géophysique de la Mediterranee occidentale, 121. Centre national de la recherche scientifique, Paris.

Almogi-Labin, A., Bein, A., Sass, E., 1993. Late Cretaceous upwelling system along the Southern Tethys Margin (Israel): Interrelationship between productivity, bottom water environments, and organic matter preservation. Paleoceanography 8, 671–690. doi:10.1029/93PA02197

Anderson, R.Y., Dean, W.E., 1995. Filling the Delaware Basin: Hydrologic and Climatic Controls on the Upper Permian Castile Formation Varved Evaporite, in: Scholle, P.A., Peryt, T.M., Ulmer-Scholle, D.S. (Eds.), The Permian of Northern Pangea: Volume 2: Sedimentary Basins and Economic Resources. Springer Berlin Heidelberg, Berlin, Heidelberg, pp. 61–78. doi:10.1007/978-3-642-78590-0_4

Arnon, A., Selker, J.S., Lensky, N.G., 2016. Thermohaline stratification and double diffusion diapycnal fluxes in the hypersaline Dead Sea. Limnol. Oceanogr. 61, 1214–1231. doi:10.1002/lno.10285

Bauer, J.E., Druffel, E.R.M., 1998. Ocean margins as a significant source of organic matter to the deep open ocean. Nature 392, 20–23. doi:10.1038/33122

Bayliss, D.D., 1973. Micropalaeontology of sections Cenomanian to Middle Eocene West Bank of Jordan. London.

Bellaiche, G., Gennesseaux, M., Mauffret, A., Rehault, J.P., 1974. Prélèvements systématiqus et caractérisation des réflecteurs acoustiques: nouvelle étape dans la compréhension de la géologie de la Méditerranée occidentale. Marine Geology 16, M47–M56.

Berggren, W.A., Kennett, J.P., Srinivasan, M.S., 2006. Neogene Planktonic Foraminifera: A Phylogenetic Atlas. Micropaleontology. doi:10.2307/1485586

Bertoni, C., Cartwright, J.A., 2007. Major erosion at the end of the Messinian Salinity Crisis: Evidence from the Levant Basin, Eastern Mediterranean. Basin Res. 19, 1–18. doi:10.1111/j.1365-2117.2006.00309.x.

Bertoni, C., Cartwright, J.A., 2006. Controls on the basinwide architecture of late Miocene (Messinian) evaporites on the Levant margin (Eastern Mediterranean). Sediment. Geol. 188–189, 93–114. doi:10.1016/j.sedgeo.2006.03.019.

Biehl, B.C., Reuning, L., Strozyk, F., Kukla, P.A., 2014. Origin and deformation of intra-salt sulphate layers: An example from the Dutch Zechstein (Late Permian). Int. J. Earth Sci. 103, 697–712. doi:10.1007/s00531-014-0999-4

Blanc, P., 2000. Of sills and straits : a quantitative assessment of the Messinian Salinity Crisis. Deep. Res. I 47, 1429–1460.

Bond, G., Kromer, B., Beer, J., Muscheler, R., Evans, M.N., Showers, W., Hoffmann, S., Lotti-Bond, R., Hajdas, I., Bonani, G., 2001. Persistent Solar Influence on North Atlantic Climate During the Holocene. Science (80-.). 294, 2130–2136.

Borsetti,, A. M., Curzi, P. V., Landuzzi, V., Mutti, M., Ricci Lucchi, F., Sartori, R., Tomadin, L., Zuffa, G.G., 1990. Messinian and pre-Messinian sediments from ODP leg 107 Sites 652 and 654 in the Tyrrhenian Sea: sedimentological and petrographic study and possible comparisons with Italian sequences, in: Kastens, K. A., Mascle, J., et al. (Ed.), Proc. Ocean Drill. Program, 107 Sci. Results 107, 169–186. doi:10.2973/odp.proc.sr.107.161.1990.

Bourcart, J., Boillot, G., Cousteau, J.Y., Gennesseaux, M., Klimek, C., 1958. Les sediments profonds au large de la cote nicoise. Comptes Rendus de 1'Academie des Sciences Paris 147, 116.

Bray, E.E., Evans, E.D., 1961. Distribution of n-paraffins as a clue to recognition of source beds. Geochim. Cosmochim. Acta 22, 2–15. doi:10.1016/0016-7037(61)90069-2

Buchbinder, B., Zilberman, E., 1997. Sequence stratigraphy of Miocene-Pliocene carbonate-siliciclastic shelf deposits in the eastern Mediterranean margin (Israel): effects of eustasy and tectonics. Sediment. Geol. 112, 7–32.

Camerlenghi, A., Aoisi, V., Lofi, J., Hübscher, C, deLange, G., Flecker, R., Garcia-Castellanos, D., Gorini, C., Krijgsman, W., Lugli, S., Makovsky, Y., Manzi, V., McGenity, T., Pan, N., 2014. Uncovering a Salt Giant. Deep-Sea Record of Mediterranean Messinian Events (DREAM) multi-phase drilling project, in: EGU. Vienna, p. 1.

Canals, M., Danovaro, R., Heussner, S., Lykousis, V., Puig, P., Trincardi, F., Calafat, A., Durrieu de Madron, X., Palanques, A., 2009. Cascades in Mediterranean Submarine Grand Canyons. Oceanography 22, 26–43. doi:10.5670/oceanog.2009.03

Canals, M., Puig, P., de Madron, X.D., Heussner, S., Palanques, A., Fabres, J., 2006. Flushing submarine canyons. Nature 444, 354–357. doi:10.1038/nature05271

Christeleit, E.C., Brandon, M.T., Zhuang, G., 2015. Evidence for deep-water deposition of abyssal Mediterranean evaporites during the Messinian salinity crisis. Earth Planet. Sci. Lett. 427, 226–235. doi:10.1016/j.epsl.2015.06.060

CIESM, 2008. The Messinian Salinity Crisis from mega-deposits to microbiology - A consensus report. N° 33. CIESM Work. Monogr. 7–10.

Cita, M.B., 1976. Biodynamic effects of the messinian salinity crisis on the evolution of planktonic foraminifera in the mediterranean. Palaeogeogr. Palaeoclimatol. Palaeoecol. 20, 23–42. doi:10.1016/0031-0182(76)90023-7

Cita, M.B., Ryan, W.B.F., Kidd, R.B., 1978. Sedimentation rates in neogene deep-sea sediments from the mediterranean and geodynamic implications of their changes, in: Initial Reports of the Deep Sea Drilling Project. pp. 991–1002.

Cita, M.B., Santambrogio, S., Melillo, B., Rogate, F., 2006. Messinian Paleoenvironments: New Evidence from the Tyrrhenian Sea (ODP Leg 107). Proc. Ocean Drill. Program, 107 Sci. Results 107, 211–227. doi:10.2973/odp.proc.sr.107.161.1990.

Clauzon G., Suc, J.P., Gautier, F., Berger, A., Loutre, M.F., 1996. Alternate interpretation of the Messinian salinity crisis, controversy resolved? Geology, 24, 363-366. Doi: 10.1130/0091-7613

Cornet, C., 1968. Le graben médian (zone A) de laMéditerranée occidentale pourrait etre pontien. Sommaire Societé Géologique de France 149.

Couto, D. Do, Popescu, S., Suc, J., Melinte-dobrinescu, M.C., Barhoun, N., Gorini, C., Jolivet, L., Poort, J., Jouannic, G., Auxietre, J., 2014. Lago Mare and the Messinian Salinity Crisis : Evidence from the Alboran Sea Lago Mare and the Messinian Salinity Crisis : Evidence from the Alboran Sea (S . Spain). Mar. Pet. Geol. 52, 57–76. doi:10.1016/j.marpetgeo.2014.01.018

Van Couvering, J.A., Berggren, W.A., Drake, R.E., Aguirre, E., Curtis, G.H., 1976. The terminal Miocene event. Mar. Micropaleontol. 1, 263–286.

Debenedetti, A., 1982. The problem of the origin of the salt deposits in the mediterranean and of their relations to the other salt occurrences in the neogene formations of the contiguous regions. Mar. Geol. 49, 91–114.

Dela Pierre, F., Clari, P., Natalicchio, M., Ferrando, S., Giustetto, R., Lozar, F., Lugli, S., Manzi, V., Roveri, M., Violanti, D., 2014. Flocculent layers and bacterial mats in the mudstone interbeds of the Primary Lower Gypsum unit (Tertiary Piedmont basin, NW Italy): Archives of palaeoenvironmental changes during the Messinian salinity crisis. Mar. Geol. 355, 71–87. doi:10.1016/j.margeo.2014.05.010

Derin, B., 2000. Stratigraphic and environments of deposition of Or South 1075–2090 m. Ramat Gan, Derin Consulting & Micropaleontological Services LTD, Internal Isramco Consultant Report 2/00.

Ditlevsen, P.D., Andersen, K.K., Svensson, A., 2007. The DO-climate events are probably noise induced: Statistical investigation of the claimed 1470 years cycle. Clim. Past 3, 129–134. doi:10.5194/cp-3-129-2007

Driussi, O., Maillard, A., Ochoa, D., Lofi, J., Chanier, F., Gaullier, V., Briais, A., Sage, F., Sierro, F., Garcia, M., 2015. Messinian Salinity Crisis deposits widespread over the Balearic Promontory: Insights from new high-resolution seismic data. Mar. Pet. Geol. 66, 41–54. doi:10.1016/j.marpetgeo.2014.09.008

Druckman, Y., Buchbinder, B., Martinotti, G.M., Tov, R.S., Aharon, P., 1995. The buried Afiq Canyon (eastern Mediterranean, Israel): a case study of a Tertiary submarine canyon exposed in Late Messinian times. Mar. Geol. 123, 167–185. doi:10.1016/0025-3227(94)00127-7

Ensminger, A., Joly, G., Albrecht, P., 1978. Rearranged steranes in sediments and crude oils. Tetrahedron Letters. 1575–1578. doi:https://doi.org/10.1016/S0040-4039(01)94608-8

Feng, Y.E., Yankelzon, A., Steinberg, J., Reshef, M., 2016. Lithology and characteristics of the Messinian evaporite sequence of the deep Levant Basin, Eastern Mediterranean. Mar. Geol. 376, 118–131. doi:10.1016/j.margeo.2016.04.004

Flecker, R., Ellam, R.M., 2006. Identifying Late Miocene episodes of connection and isolation in the Mediterranean-Paratethyan realm using Sr isotopes. Sediment. Geol. 188–189, 189–203. doi:10.1016/j.sedgeo.2006.03.005

Flecker, R., et al., 2015. Evolution of the Late Miocene Mediterranean-Atlantic gateways and their impact on regional and global environmental change. *Earth-Science Reviews,* 150**,** 365–392.

Frey-Martınez, J., Hall, B., Cartwright, J., Huuse, M., 2007. Clastic Intrusion at the Base of Deep-water Sands: A Trap-forming Mechanism in the Eastern Mediterranean. Sand Inject. Implic. Hydrocarb. Explor. Prod. AAPG Mem. 87 49–63. doi:10.1306/1209849M873255

Garcia-Castellanos, D., Villaseñor, A., 2011. Messinian salinity crisis regulated by competing tectonics and erosion at the Gibraltar arc. Nature 480, 359–363. doi:10.1038/nature10651

García-Veigas, J., Cendón, D.I., Gibert, L., Lowenstein, T.K., Artiaga, D., 2018. Geochemical indicators in Western Mediterranean Messinian evaporites: Implications for the salinity crisis. Mar. Geol. 403, 197–214. doi:10.1016/j.margeo.2018.06.005

Gardosh, M., Druckman, Y., Buchbinder, B., Rybakov, M., 2008. The Levant Basin Offshore Israel: Stratigraphy, Structure, Tectonic Evolution and Implications for Hydrocarbon Exploration - revised edition. Geological Survey of Israel report GSI/4/2008.

Garrison, R.E., Schreiber, B.C., Bernoulli, D., Fabricius, F.H., Kidd, R.B.., Mélières, F., 1978. Sedimentary Petrology and Structures of Messinian Evaporitic Sediments in the Mediterranean Sea, Leg 42A, Deep Sea Drilling Project, in: Initial Reports of the Deep Sea Drilling Project 42, No. 1. pp. 571–612.

Geletti, R., Zgur, F., Del Ben, A., Buriola, F., Fais, S., Fedi, M., Forte, E., Mocnik, A., Paoletti, V., Pipan, M., Ramella, R., Romeo, R., Romi, A., 2014. The Messinian Salinity Crisis: New seismic evidence in the West-Sardinian Margin and Eastern Sardo-Provencal basin (West Mediterranean Sea). Mar. Geol. 351, 76–90. doi:10.1016/j.margeo.2014.03.019

Gennari, R., Manzi, V., Angeletti, L., Bertini, A., Ceregato, A., Faranda, C., Gliozzi, E., Menichetti, E., Rosso, A., Roveri, M., Taviani, M., 2013. A shallow water record of the onset of the Messinian salinity crisis in the Adriatic foredeep (Legnagnone section, Northern Apennines).NU SC. Palaeogeogr. Palaeoclimatol. Palaeoecol. doi:10.1016/j.palaeo.2013.05.015

Govers, R., 2009. Choking the Mediterranean to dehydration: The Messinian salinity crisis. Geology 37, 167–170. doi:10.1130/G25141A.1

Gvirtzman, Z., Manzi, V., Calvo, R., Gavrieli, I., Gennari, R., Lugli, S., Reghizzi, M., Roveri, M., 2017. Intra-Messinian truncation surface in the Levant Basin explained by subaqueous dissolution. Geology 45, 4–7. doi:10.1130/G39113.1

Gvirtzman, Z., Reshef, M., Buch-leviatan, O., Ben-avraham, Z., 2013a. Intense salt deformation in the Levant Basin in the middle of the Messinian Salinity Crisis. Earth Planet. Sci. Lett. 379, 108–119. doi:10.1016/j.epsl.2013.07.018

Gvirtzman, Z., Reshef, M., Buch-Leviatan, O., Ben-Avraham, Z., 2013b. Intense salt deformation in the Levant Basin in the middle of the Messinian Salinity Crisis. Earth Planet. Sci. Lett. 379, 108–119. doi:10.1016/j.epsl.2013.07.018

Hall, J.K., Udintsev, G.B., Odinikov, Y.Y., 1994. The bottom relief of the Levantine Sea, in Geologic Structure of the Northeastern Mediterranean. Krasheninnikov, V. A., Hall, J.K., pp. 5–32, Historical Productions-Hall Ltd., Jerusalem.

Hall, J.K., Lippman, S., Gardosh, M., Tibor, G., Sade, A.R., Sade, H., 2015. A New Bathymetric Map for the Israeli EEZ: Preliminary Results. State of Israel, Ministry of National

Infrastructure Energy and Water, Jerusalem.

Hardie, L.A., Lowenstein, T.K., 2004. Did the Mediterranean Sea Dry Out During the Miocene? a Reassessment of the Evaporite Evidence From Dsdp Legs 13 and 42a Cores. J. Sediment. Res. 74, 453–461. doi:10.1306/112003740453

Hawie, N., Deschamps, R., Nader, F.H., Gorini, C., 2013a. Sedimentological and stratigraphic evolution of northern Lebanon since the Late Cretaceous: implications for the Levant margin and basin. doi:10.1007/s12517-013-0914-5

Hawie, N., Gorini, C., Deschamps, R., Nader, F.H., Montadert, L., Granjeon, D., Baudin, F., 2013b. Tectono-stratigraphic evolution of the northern Levant Basin (offshore Lebanon). Mar. Pet. Geol. 48, 392–410. doi:10.1016/j.marpetgeo.2013.08.004

Hernández-Molina F.J, et al., 2014. Onset of Mediterranean outflow into the North Atlantic. Science 344, 1244–1250. doi: 10.1126/science.1251306

Hilgen, F., Kuiper, K., Krijgsman, W., Snel, E., Laan, E. Van Der, van der Laan, E., 2007. Astronomical tuning as the basis for high resolution chronostratigraphy: The intricate history of the Messinian Salinity Crisis. Stratigraphy 4, 231–238.

Hilgen, F.J., Bissoli, L., Iaccarino, S., Krijgsman, W., Meijer, R., Negri, A., Villa, G., 2000. Integrated stratigraphy and astrochronology of the Messinian GSSP at Oued Akrech (Atlantic Morocco). Earth Planet. Sci. Lett. 182, 237–251. doi:10.1016/S0012-821X(00)00247-8

Hilgen, F.J., Krijgsman, W., 1999. Cyclostratigraphy and astrochronology of the Tripoli diatomite formation (pre-evaporite Messinian, Sicily, Italy). Terra Nov. 11, 16–22. doi:10.1046/j.1365-3121.1999.00221.x

Hilgen, F.J., Krijgsman, W., Langereis, C.G., Lourens, L.J., Santarelli, A., Zachariasse, W.J.,

1995. Extending the astronomical (polarity) time scale into the Miocene. Earth Planet. Sci. Lett. 136, 495–510. doi:10.1016/0012-821X(95)00207-S

Hsü, K.J., 1973. The desiccated deep-basin model for the Messinian events, in: Drooger, C.W. (Ed.), Messinian Events in the Mediterranean. North-Holland Publ. Co., Amsterdam, pp. 60–67.

Hsü, K .J., Ryan, W.B.F., Schreiber, B.C., 1973. Petrography of a halite sample from hole 134 - balearic abyssal plain, in: Initial Reports of the Deep Sea Drilling Project 13, No. Part 2. pp. 708–711.

Hsü, K.J., Montadert, L., Bernoulli, D., Bizon, G., Cita, M., Erickson, A., Fabricius, F., Garrison, R.E., Kidd, R.B., Mélières, F., Müller, C., Wright, R.C., 1978a. Site 374: Messina Abyssal Plain, in: Initial Reports of the Deep Sea Drilling Project: DSDP Volume XLII Part 1. p. 43. doi:10.2973/dsdp.proc.42-1.105.1978

Hsü, K.J., Montadert, L., Bernoulli, D., Bizon, G., Cita, M., Erickson, A., Fabricius, F., Garrison, R.E., Kidd, R.B., Mélières, F., Müller, C., Wright, R.C., 1978b. Sites 375 and 376: Florence Rise, in: Initial Reports of the Deep Sea Drilling Project: DSDP Volume XLII Part 1. p. 86.

Hüsing, S.K., Cascella, A., Hilgen, F.J., Krijgsman, W., Kuiper, K.F., Turco, E., Wilson, D., 2010. Astrochronology of the Mediterranean Langhian between 15 . 29 and 14 . 17 Ma. Earth Planet. Sci. Lett. 290, 254–269. doi:10.1016/j.epsl.2009.12.002

Hüsing, S.K., Kuiper, K.F., Link, W., Hilgen, F.J., Krijgsman, W., 2009. The upper Tortonian-lower Messinian at Monte dei Corvi (Northern Apennines, Italy): Completing a Mediterranean reference section for the Tortonian Stage. Earth Planet. Sci. Lett. 282, 140–157. doi:10.1016/j.epsl.2009.03.010

Karakitsios, V., Cornée, J.J., Tsourou, T., Moissette, P., Kontakiotis, G., Agiadi, K., Manoutsoglou, E., Triantaphyllou, M., Koskeridou, E., Drinia, H., Roussos, D., 2017. Messinian salinity crisis record under strong freshwater input in marginal, intermediate, and deep environments: The case of the North Aegean. Palaeogeogr. Palaeoclimatol. Palaeoecol. 485, 316–335. doi:10.1016/j.palaeo.2017.06.023

Keogh, S.M., Butler, R.W.H., 1999. The Mediterranean water body in the late Messinian: interpreting the record from marginal basins on Sicily. J. Geol. Soc. London. 156, 837–846. doi:10.1144/gsjgs.156.4.0837

Krijgsman, W., Blanc-Valleron, M.M., Flecker, R., Hilgen, F.J., Kouwenhoven, T.J., Merle, D., Orszag-Sperber, F., Rouchy, J.M., 2002. The onset of the Messinian salinity crisis in the Eastern Mediterranean (Pissouri Basin, Cyprus). Earth Planet. Sci. Lett. 194, 299–310. doi:10.1016/S0012-821X(01)00574-X

Krijgsman, W., Fortuin, A.R., Hilgen, F.J., Sierro, F.J., 2001. Astrochronology for the Messinian Sorbas basin (SE Spain) and orbital (precessional) forcing for evaporite cyclicity. Sediment. Geol. 140, 43–60. doi:10.1016/S0037-0738(00)00171-8

Krijgsman, W., Garces, M., Agusti, J., Raffi, I., Taberner, C., Zachariasse, W.J., 2000. The “Tortonian salinity crisis” of the eastern Betics (Spain). Earth Planet. Sci. Lett. 181, 497–511. doi:10.1016/S0012-821X(00)00224-7

Krijgsman, W., Hilgen, F.J., Negri, A., Wijbrans, J.R., Zachariasse, W.J., 1997. The Monte del Casino section (Northern Apennines, Italy): A potential Tortonian/Messinian boundary stratotype? Palaeogeogr. Palaeoclimatol. Palaeoecol. 133, 27–47. doi:10.1016/S0031-0182(97)00039-4

Krijgsman, W., Hilgen, F.J., Raffi, I., Sierro, F.J., Wilson, D.S., 1999. Chronology, causes and progression of the Messinian salinity crisis. Nature 400, 652–655. doi:10.1038/23231.

Krijgsman, W., Meijer, P.T., 2008. Depositional environments of the Mediterranean “Lower Evaporites” of the Messinian salinity crisis: Constraints from quantitative analyses. Mar. Geol. doi:10.1016/j.margeo.2008.04.010

Krijgsman, W., Stoica, M., Vasiliev, I., Popov, V. V., 2010. Rise and fall of the Paratethys Sea during the Messinian Salinity Crisis. Earth Planet. Sci. Lett. 290, 183–191. doi:10.1016/j.epsl.2009.12.020.

Lange, G.J. De, Krijgsman, W., 2010. Messinian salinity crisis: A novel unifying shallow gypsum / deep dolomite formation mechanism. Mar. Geol. 275, 273–277. doi:10.1016/j.margeo.2010.05.003

Laskar, J., Robutel, P., Joutel, F., Gastineau, M., Correia, A.C.M., Levrard, B., 2004. A long-term numerical solution for the insolation quantities of the Earth. Astron. As-trophys. Astron. Astrophys. 428, 261–285. doi:10.1051/0004-6361:20041335

Leila, M., Kora, M.A., Ahmed, M.A., Ghanem, A., 2016. Sedimentology and reservoir characterization of the Upper Miocene Qawasim Formation, El-Tamad Oil Field onshore Nile Delta, Egypt. Arab. J. Geosci. 9, 1–13. doi:10.1007/s12517-015-2088-9

Lofi, J., Camerlenghi, A., 2014. Messinian Salinity Crisis - DREAM (Deep-sea Record of Mediterranean Messinian events) drilling projects Messinian Salinity Crisis - DREAM (Deep-sea Record of Mediterranean Messinian events) drilling projects, in: EGU. Vienna, p. 1.

Lofi, J., Sage, F., Deverchere, J., Loncke, L., Maillard, A., Gaullier, V., Thinon, I., Gillet, H., Guennoc, P., Gorini, C., 2011. Refining our knowledge of the Messinian salinity crisis records in the offshore domain through multi-site seismic analysis. Bull. la Soc. Geol. Fr. 182, 163–180. doi:10.2113/gssgfbull.182.2.163

Lohmann, J., Ditlevsen, P.D., 2018. Random and externally controlled occurrences of Dansgaard-Oeschger events. Clim. Past 14, 609–617. doi:10.5194/cp-14-609-2018

Lugli, S., Gennari, R., Gvirtzman, Z., Manzi, V., Roveri, M., Schreiber, B.C., 2013. Evidence of clastic evaporites in the canyons of the Levant Basin (Israel): implications for the Messinian Salinity Crisis. J. Sediment. Res. 83, 942–954. doi:10.2110/jsr.2013.72

Lugli, S., Manzi, V., Roveri, M., Schreiber, B.C., 2015. The deep record of the Messinian salinity crisis: Evidence of a non-desiccated Mediterranean Sea. Palaeogeogr. Palaeoclimatol. Palaeoecol. 433, 201–218. doi:10.1016/j.palaeo.2015.05.017

Lugli, S., Schreiber, B.C., Triberti, B., 1999. Giant polygons in the Realmonte Mine (Agrigento, Sicily); evidence for the desiccation of a Messinian halite basin. J. Sediment. Res. 69, 764–771. doi:10.2110/jsr.69.764

McArthur, J. M., Howarth, R. J., Shield, G. A., 2012. Chapter 7: Strontium Isotope Stratigraphy. In The Geologic Time Scale, eds. F. M. Gredstein, J. G. Ogg, M. D. Schmotz & G. M. Ogg, 1144 Elsevier.

Madof, A.S., Bertoni, C., Lofi, J., 2019. Discovery of vast fluvial deposits provides evidence for drawdown during the late Miocene Messinian salinity crisis. Geology 47, 171–174. doi:10.1130/G45873.1

Manzi, V., Gennari, R., Hilgen, F., Krijgsman, W., Lugli, S., 2013. Age refinement of the Messinian salinity crisis onset in the Mediterranean. doi:10.1111/ter.12038

Manzi, V., Gennari, R., Lugli, S., Persico, D., Reghizzi, M., Roveri, M., Schreiber, B.C., Calvo, R., Gavrieli, I., Gvirtzman, Z., 2018. The onset of the Messinian salinity crisis in the deep Eastern Mediterranean basin. Terra Nov. 38, 42–49. doi:10.1111/ter.12325

Manzi, V., Gennari, R., Lugli, S., Roveri, M., Scafetta, N., Charlotte, B., 2012. High-frequency cyclicity in the Mediterranean Messinian evaporites: evidence for solar-lunar climate forcing. J. Sediment. Res. 82, 991–1005. doi:10.2110/jsr.2012.81

Manzi, V., Lugli, S., Roveri, M., Dela Pierre, F., Gennari, R., Lozar, F., Natalicchio, M., Schreiber, B.C., Taviani, M., Turco, E., 2015. The Messinian salinity crisis in Cyprus: A further step towards a new stratigraphic framework for Eastern Mediterranean. Basin Res. 28, 207–236. doi:10.1111/bre.12107

Manzi, V., Lugli, S., Roveri, M., Schreiber, B.C., 2009. A new facies model for the Upper Gypsum of Sicily (Italy): Chronological and palaeoenvironmental constraints for the Messinian salinity crisis in the Mediterranean. Sedimentology 56, 1937–1960. doi:10.1111/j.1365-3091.2009.01063.x

Manzi, V., Lugli, S., Roveri, M., Schreiber, B.C., Gennari, R., 2011. The Messinian "Calcare di Base" (Sicily, Italy) revisited. Bull. Geol. Soc. Am. 123, 347–370. doi:10.1130/B30262.1

Marzocchi, A., Lunt, D.J., Flecker, R., Bradshaw, C.D., Farnsworth, A., Hilgen, F.J., 2015. Orbital control on late Miocene climate and the North African monsoon: Insight from an ensemble of sub-precessional simulations. Clim. Past 11, 1271–1295. doi:10.5194/cp-11-1271-2015

Meilijson, A., Ashckenazi-Polivoda, S., Ron-Yankovich, L., Illner, P., Alsenz, H., Speijer, R.P., Almogi-Labin, A., Feinstein, S., Berner, Z., Püttmann, W., Abramovich, S., 2014. Chronostratigraphy of the Upper Cretaceous high productivity sequence of the southern Tethys, Israel. Cretac. Res. 50. doi:10.1016/j.cretres.2014.04.006

Meilijson, A., Steinberg, J., Hilgen, F., Bialik, O.M., Waldmann, N.D., Makovsky, Y., 2018. Deep-basin evidence resolves a 50-year-old debate and demonstrates synchronous onset of Messinian evaporite deposition in a non-desiccated Mediterranean. Geology 46, 4–7.

Müller, D.W., Mueller, P.A., 1991. Origin and age of the Mediterranean Messinian evaporites: implications from Sr isotopes. Earth Planet. Sci. Lett. doi:10.1016/0012-821X(91)90039-K

Nam, M., Görür, N., Flecker, R., Sak, M., Tüno, C., Ellam, R., Krijgsman, W., Vincent, S., Dikba, A., 2006. Paratethyan–Mediterranean connectivity in the Sea of Marmara region (NW Turkey) during the Messinian. Sediment. geo 188–189, 171–187. doi:10.1016/j.sedgeo.2006.03.004

Netzeband, G.L., Hübscher, C.P., Gajewski, D., 2006. The structural evolution of the Messinian evaporites in the Levantine Basin. Mar. Geol. 230, 249–273. doi:10.1016/j.margeo.2006.05.004

Ochoa, D., Sierro, F.J., Lofi, J., Maillard, A., Flores, J.A., Suarez, M., 2015. Synchronous onset of the Messinian evaporite precipitation: First Mediterranean offshore evidence. Earth Planet. Sci. Lett. 427, 112–124. doi:10.1016/j.epsl.2015.06.059

Ogniben, L., 1957. Petrografia della Serie Solfifera Siciliana e considerazioni geologiche relative. Memorie Descriptive della Carta Geologica d'Italia 33, 1–275.

Ohneiser, C., Florindo, F., Stocchi, P., Roberts, A.P., DeConto, R.M., Pollard, D., 2015. Antarctic glacio-eustatic contributions to late Miocene Mediterranean desiccation and reflooding. Nat. Commun. 6, 8765. doi:10.1038/ncomms9765

Peters, K.E., A.E. Kontorovich, J.M.M., 1993. Geochemistry of selected oils and rocks from the central portion of the west Siberian Basin, Russia. Am. Assoc. Pet. Geol. Bull. 77, 87–863.

Peters, K.E., 1986. Guidelines for Evaluating Petroleum Source Rock Using Programmed Pyrolysis. Am. Assoc. Pet. Geol. Bull. 70, 318–329. doi:10.1306/94885688-1704-11D7-8645000102C1865D

Peters, K.E., Rohrback, B.G., Kaplan, I.R., 1980. Laboratory-simulated thermal maturation of

Recent sediments. Phys. Chem. Earth 12, 547–557. doi:10.1016/0079-1946(79)90136-8

Peters, K.E., Walters Clifford C, Moldowan, J.M., 2005. The Biomarker Guide, Biomarkers and Isotopes in Petroleum Exploration and Earth Histroy, Volume 2. Cambridge. doi:10.1017/s0016756806212056

Rashid, H., Grosjean, E., 2006. Detecting the source of Heinrich layers: An organic geochemical study. Paleoceanography 21. doi:10.1029/2005PA001240

Reiche, S., Hübscher, C., Beitz, M., 2014. Fault-controlled evaporite deformation in the Levant Basin, Eastern Mediterranean. Mar. Geol. 354, 53–68. doi:10.1016/j.margeo.2014.05.002

Richter-Bernburg, G., 1996. Zechstein-Anhydrite: Fazies und Genese, Geologisches Jahrbuch. Reihe A, Allgemeine und regionale Geologie Bundesrepublik Deutschland und Nachbargebiete, Tektonik, Stratigraphie, Paläontologie. Bundesanstalt für Geowissenschaften und Rohstoffe.

Roberts, G., Peace, D., 2007. Hydrocarbon plays and prospectivity of the Levantine basin, offshore Lebanon and Syria from modern seismic data. GeoArabia 12, 99–124.

Rouchy, J.M., Caruso, A., 2006. The Messinian salinity crisis in the Mediterranean basin : A reassessment of the data and an integrated scenario. Sediment. Geol. 188–189, 35–67. doi:10.1016/j.sedgeo.2006.02.005

Roveri, M., Flecker, R., Krijgsman, W., Lofi, J., Lugli, S., Manzi, V., Sierro, F.J., Bertini, A., Camerlenghi, A., De Lange, G., Govers, R., Hilgen, F.J., Hübscher, C., Meijer, P.T., Stoica, M., 2014a. The Messinian Salinity Crisis: Past and future of a great challenge for marine sciences. Mar. Geol. 352, 25–58. doi:10.1016/j.margeo.2014.02.002

Roveri, M., Gennari, R., Ligi, M., Lugli, S., Manzi, V., Reghizzi, M., 2019. The synthetic seismic expression of the Messinian salinity crisis from onshore records: implications for shallow- to deep-water correlations. Basin Res.. doi:10.1111/bre.12361

Roveri, M., Lugli, S., Manzi, V., Gennari, R., Schreiber, B.C., 2014b. High-resolution strontium isotope stratigraphy of the messinian deep Mediterranean basins: Implications for marginal to central basins correlation. Mar. Geol. 349, 113–125. doi:10.1016/j.margeo.2014.01.002

Roveri, M., Manzi, V., Bergamasco, A., Falcieri, F.M., Gennari, R., Lugli, S., Schreiber, B.C., 2014c. Dense shelf water cascading and messinian canyons: A new scenario for the mediterranean salinity crisis. Am. J. Sci. 314, 751–784. doi:10.2475/05.2014.03

Rullkötter, J., R.M., 1988. Natural and artificial maturation of biological markers in a Toarcian shale from northern Germany, in: Novelli, L.M. and L. (Ed.), Advances in Organic Geochemistry 1987. Oxford Pergamon Press, pp. 639–645.

Ryan, W.B.F., 2011. Geodynamic responses to a two-step model of the Messinian salinity crisis. Bull. la Soc. Geol. Fr. 182, 73–78. doi:10.2113/gssgfbull.182.2.73

Ryan, W.B.F., 2008. Modeling the magnitude and timing of evaporative drawdown during the Messinian salinity crisis. Stratigraphy 5, 227–243.

Ryan, W.B.F., 1978. Messinian badlands on the southeastern margin of the Mediterranean Sea. Mar. Geol. 27, 349–363. doi:10.1016/0025-3227(78)90039-7

Ryan, W.B.F., 1976. Quantitative evaluation of the depth of the western Mediterranean before, during and after the late Miocene salinity crisis. Sedimentology 23, 791–813.

Ryan, W.B.F., 1973. Geodynamic implications of the Messinian crisis of salinity, in: Drooger, D.W. (Ed.), Messinian Events in the Mediterranean. Elsevier, Amsterdam, pp. 26–38.

Ryan, W.B.F., Cita, M.B., 1978. The nature and distribution of Messinian erosional surfaces - Indicators of a several-kilometer-deep Mediterranean in the Miocene. Mar. Geol. doi:10.1016/0025-3227(78)90032-4

Ryan, W.B.F., Hsü, K.J., Cita, M.B., Dumitrica, P., Lort, J., Maync, W., Nesteroff, W.D., Pautot, G., Stradner, H., 2007. DSDP Volume XIII: 6. Balearic Rise - Site 124. The Shipboard Scientific Party. doi:10.2973/dsdp.proc.13.1973

Ryan, W.B.F., Stanley, D.J., Hersey, J.B., Fahlquist, D.A., Allan, T.D., 1971. The tectonics and geology of the Mediterranean Sea. In: Maxwell, A.E. (Ed.), The Sea. Wiley- Interscience, New York, pp. 387–492.

Scafetta, N., Milani, F., Bianchini, A., Ortolani, S., 2016. On the astronomical origin of the Hallstatt oscillation found in radiocarbon and climate records throughout the Holocene. Earth-Science Rev. 162, 24–43. doi:10.1016/j.earscirev.2016.09.004

Scalan, E.S., Smith, J.E., 1970. An improved measure of the odd-even predominance in the normal alkanes of sediment extracts and petroleum. Geochim. Cosmochim. Acta 34, 611–620. doi:10.1016/0016-7037(70)90019-0

Schmalz, R.F., 1969. Deep-Water Evaporite Deposition: A Genetic Model. Am. Assoc. Pet. Geol. Bull. 53, 798–823. doi:10.1306/5D25C7FD-16C1-11D7-8645000102C1865D

Schulz, M., 2002. On the 1470-year pacing of Dansgaard-Oeschger warm events. Paleoceanography 17, 4-1-4–9. doi:10.1029/2000PA000571

Schulz, M., Mudelsee, M., 2002. REDFIT: Estimating red-noise spectra directly from unevenly spaced paleoclimatic time series. Comput. Geosci. 28, 421–426. doi:10.1016/S0098-3004(01)00044-9

Selli, R., 1954. Il Bacino del Metauro. Giornale di Geologia 24, 1–294.

Sepúlveda, J., Wendler, J.E., Summons, R.E., Hinrichs, K.U., 2009. Rapid Resurgence of Marine Productivity After the Cretaceous-Paleogene Mass Extinction. Science (80-.). 326, 129–132.

Sierro, F.J., Hilgen, F.J., Krijgsman, W., Flores, J.A., 2001. The Abad composite (SE Spain): A Messinian reference section for the Mediterranean and the APTS. Palaeogeogr. Palaeoclimatol. Palaeoecol. 168, 141–169. doi:10.1016/S0031-0182(00)00253-4

Simon, D., Marzocchi, A., Flecker, R., Lunt, D.J., Hilgen, F.J., Meijer, P.T., 2017. Quantifying the Mediterranean freshwater budget throughout the late Miocene: New implications for sapropel formation and the Messinian Salinity Crisis. Earth Planet. Sci. Lett. 472, 25–37. doi:10.1016/j.epsl.2017.05.013

Simon, D., Meijer, P.T., 2017. Salinity stratification of the Mediterranean Sea during the Messinian crisis: A first model analysis. Earth Planet. Sci. Lett. 479, 366–376. doi:10.1016/j.epsl.2017.09.045

Sirota, I., Ali, A., Lensky, N.G., 2016. Seasonal variations of halite saturation in the Dead Sea. Water Resour. Res. 52. doi:10.1002/2014WR016618

Sirota, I., Enzel, Y., Lensky, N.G., 2017. Temperature seasonality control on modern halite layers in the Dead Sea: In situ observations. Bull. Geol. Soc. Am. 129, 1181–1194. doi:10.1130/B31661.1

Sonnenfeld, P., Finetti, I., 2011. Messinian Evaporites in the Mediterranean: A Model of Continuous Inflow and Outflow, in: Geological Evolution of the Mediterranean Basin. doi:10.1007/978-1-4613-8572-1-17

Sonnenfeld, P., Hudec, P.P., 1983. Clay laminations in Halite: Their Cause and Effect, in: Sixth International Syposyum on Salt. pp. 51–56.

Steinberg, J., Gvirtzman, Z., Folkman, Y., 2010. New age constraints on the evolution of the Mt Carmel structure and its implications on a Late Miocene extensional phase of the Levant continental margin. J. Geol. Soc. London. 167, 203–216. doi:10.1144/0016-76492009-089

Steinberg, J., Gvirtzman, Z., Folkman, Y., Garfunkel, Z., 2011. Origin and nature of the rapid late Tertiary filling of the Levant Basin. Geology 39, 355–358. doi:10.1130/G31615.1

Steinhilber, F., Abreu, J.A., Beer, J., Brunner, I., Christl, M., Fischer, H., Heikkila, U., Kubik, P.W., Mann, M., McCracken, K.G., Miller, H., Miyahara, H., Oerter, H., Wilhelms, F., 2012. 9,400 Years of Cosmic Radiation and Solar Activity From Ice Cores and Tree Rings. Proc. Natl. Acad. Sci. 109, 5967–5971. doi:10.1073/pnas.1118965109

Steinhorn, I., 1983. In situ salt precipitation at the Dead Sea. Limnol. Oceanogr. 28, 580–583. doi:10.4319/lo.1983.28.3.0580

Stiller, M., Gat, J.R., Kaushansky, P., 1997. Halite Precipitation and Sediment Deposition As Measured in Sediment Traps Deployed in the Dead Sea: 1981-1983. Dead Sea lake its settings 161–170.

Stoica, M., Krijgsman, W., Fortuin, A., Gliozzi, E., 2016. Paratethyan ostracods in the Spanish Lago-Mare: More evidence for interbasinal exchange at high Mediterranean sea level. Palaeogeogr. Palaeoclimatol. Palaeoecol. 441, 854–870. doi:10.1016/j.palaeo.2015.10.034

ten Haven, H.L., de Leeuw, J.W., Schenck, P.A., 1985. Organic geochemical studies of a Messinian evaporitic basin, northern Apennines (Italy) I: Hydrocarbon biological markers for a hypersaline environment. Geochim. Cosmochim. Acta 49, 2181–2191.

Tomas, C.R., 1996. Identifying Marine Phytoplankton, Academic Press Inc. San Diego. doi:10.1016/S0025-3227(97)81154-1

Topper, R. P. M., Flecker, R., Meijer, P., Wortel, M. J. R., 2011. A box model of the Late Miocene Mediterranean Sea: implications from combined 87Sr/86Sr and salinity data. Paleoceanography, 26.

Topper, R.P.M., Lugli, S., Manzi, V., Roveri, M., Meijer, P.T., 2014. Precessional control of Sr ratios in marginal basins during the Messinian Salinity Crisis? Geochemistry, Geophys. Geosystems 15, 1926–1944. doi:10.1002/2013GC005192

van den Berg, B.C.J., Sierro, F.J., Hilgen, F.J., Flecker, R., Larrasoaña, J.C., Krijgsman, W., Flores, J.A., Mata, M.P., Bellido Martín, E., Civis, J., González-Delgado, J.A., 2015. Astronomical tuning for the upper Messinian Spanish Atlantic margin: Disentangling basin evolution, climate cyclicity and MOW. Glob. Planet. Change 135, 89–103. doi:10.1016/j.gloplacha.2015.10.009

Vasiliev, I., Mezger, E.M., Lugli, S., Reichart, G., Manzi, V., Roveri, M., 2017. How dry was the Mediterranean during the Messinian salinity crisis ? Palaeogeogr. Palaeoclimatol. Palaeoecol. 471, 120–133. doi:10.1016/j.palaeo.2017.01.032

Supplementary Figures

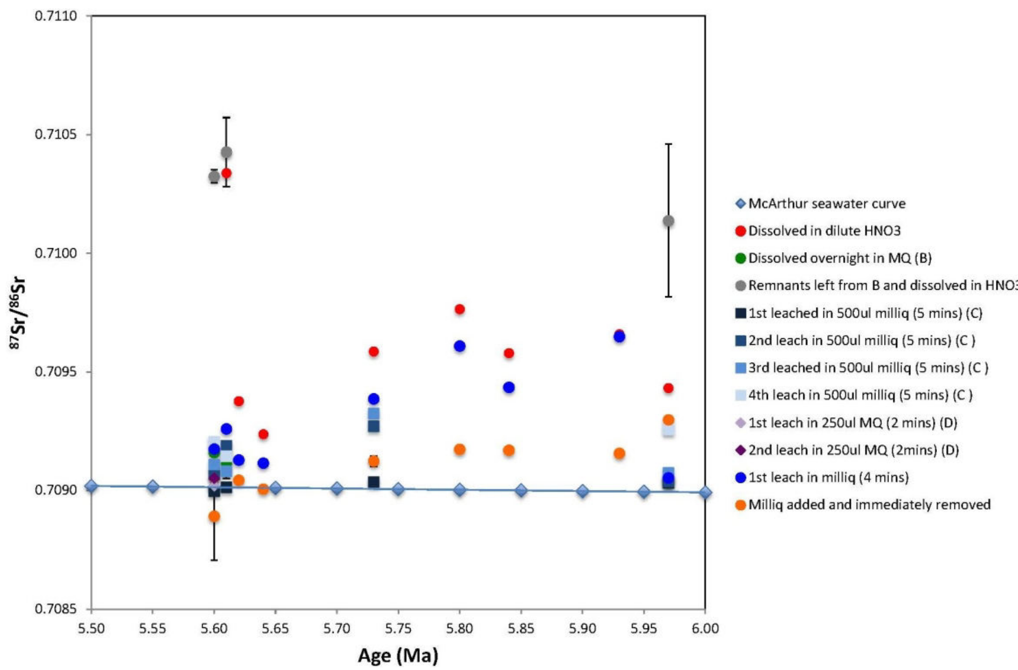

Figure S1. Strontium stable isotope analysis

Results obtained by the different protocols used for strontium stable isotope analysis with respect to the McArthur et al. (2012) seawater curve. Note the large discrepancies between the results obtained by the different methods used, indicating a highly probable contamination from the drilling mud used during the retrieval of the halite cuttings samples.

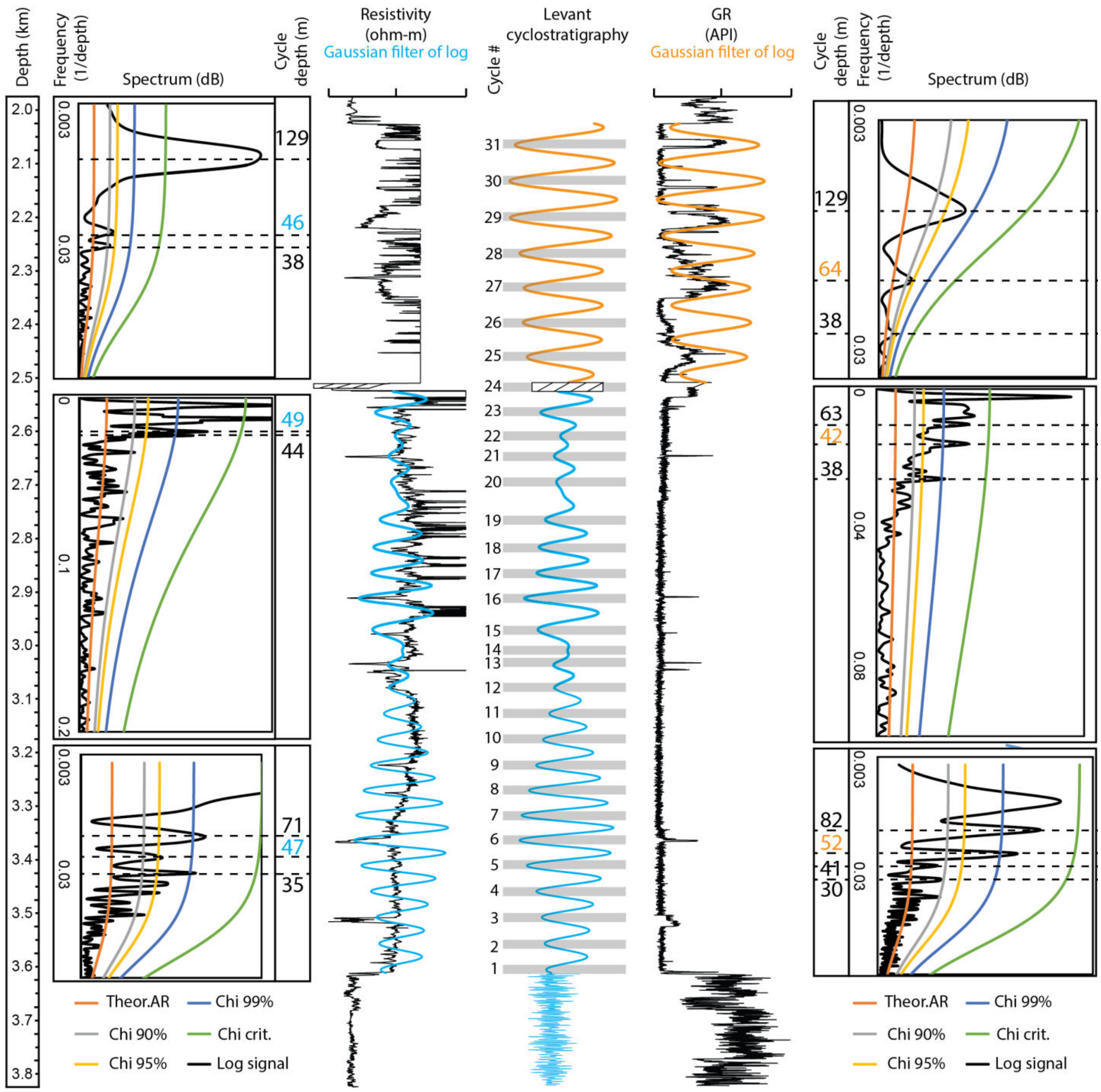

Figure S2. Spectral analysis of the Dolphin well-log curves.

Data shown are the spectral analysis of the resistivity (blue, left) and gamma ray (orange, right) well log curves using REDFIT spectral analysis procedure in Matlab, PAST and Analyseries software. Each log is bounded by respective REDFIT (left of resistivity and right of gamma ray logs) and the combined optimal cyclostratigraphy (center). The REDFIT procedure fits the time series to a red noise model null hypothesis (Theor. AR), produces 'false-alarm' parametric approximations (chi^2 of 90%, 95%, and 99%) and a 'critical false-alarm' level (chi crit.). REDFIT analyses were run by intervals, defined according to the logs expression as follows: from the base to 3175 m, from 3175 to 2560 m, and from 2560 m to the top of the evaporitic bed.

Sample depth (m)	Depositional units, Dolphin-1, Levant Basin	*n*-alkane distribution					
		ng SCA/g rock	ng LCA/g rock	LCA/SCA	ACL	CPI	Pr/Ph
2655	Interbedded Evaporites	5.3	8.3	1.6	25	2.9	0.6
2709		9.9	17.0	1.7	25	1.9	0.1
3402	Argillaceous Diatomites	15.9	32.3	2.1	25	4.1	0.9
3474		29.2	52.2	1.8	25	12.3	1.1
3675	Pre-Evaporites	16.4	26.9	1.6	25	5.8	1.0
3810		7.5	5.5	0.7	23	7.4	1.1

Table 1. Indices and distribution of *n*-alkanes as measured from the aliphatic hydrocarbons, Levant Basin MSC lipid extract. Depositional units are described in the text and presented in Figs. 2 and 3. SCA – short chain alkanes (C_{15-21}), LCA – long chain alkanes (C_{27-35}), ACL – average chain length, CPI – carbon preference index (Bray and Evans, 1961), expressed as the following relation (*sensu* Vasiliev et al., 2017): $CPI = (((N_{25} + N_{27} + N_{29} + N_{31} + N_{33}) / (N_{24} + N_{26} + N_{28} + N_{30} + N_{32})) + ((N_{25} + N_{27} + N_{29} + N_{31} + N_{33}) / (N_{26} + N_{28} + N_{30} + N_{32} + N_{34}))) * 0.5$, where N represents the relative abundance for individual *n*-alkanes. Pr/Ph is the ratio between the pristane and phytane measured from the extracts.

Sample depth (m)	Depositional units, Dolphin-1, Levant Basin	Steranes				Hopanes		
		C_{27}		C_{28}		C_{30}	C_{31}	
		$C_{27}\alpha\alpha\alpha20S/C_{27}\alpha\alpha\alpha20R$	Amount of rearranged steranes	$C_{28}\alpha\beta\beta20S/C_{28}\alpha\beta\beta20R$	$C_{28}\alpha\alpha\alpha 20S/C_{28}\alpha\alpha\alpha 20R$	$C_{30}\beta\alpha/C_{30}\alpha\beta$	$C_{31}\alpha\beta S/C_{31}\alpha\beta R$	$C_{31}\beta\alpha/C_{31}\beta\beta$
2655	Interbedded Evaporites	0.74	High	1.37	0.43	0.02	1.19	0.64
2709		0.82	High	1.39	0.50	0.07	1.15	0.39
3402	Argillaceous Diatomites	0.26	Low	0.01	0.04	1.16	0.07	0.16
3474		0.29	Low	0.03	0.08	1.40	0.03	0.10
3675	Pre-Evaporites	1.66	Moderate	0.06	0.28	0.32	0.79	0.16
3810		0.72	Moderate	1.14	0.43	0.22	0.73	0.02

Table 2. Indices and distribution of steranes and hopanes measured by selective reaction monitoring (SRM) of the aliphatic hydrocarbons, Levant Basin MSC lipid extract. Depositional units as in Table 1. Selected samples and thermal maturity-dependent ratios from SRM analysis include C_{27} steranes (Ensminger et al., 1978; Peters et al., 2005, 1980), and C_{30} and C_{31} hopanes (Peters and Moldowan, 1993; Rullkötter and Marzi,1988). Note the higher maturity values in the Interbedded Evaporites relative to the over- and underlying intervals.

Sample depth (m)	Depositional units, Dolphin-1, Levant Basin	*n*-alkane distribution					
		ng SCA/g rock	ng LCA/g rock	LCA/SCA	ACL	CPI	Pr/Ph
2655	Interbedded Evaporites	5.3	8.3	1.6	25	2.9	0.6
2709		9.9	17.0	1.7	25	1.9	0.1
3402	Argillaceous Diatomites	15.9	32.3	2.1	25	4.1	0.9
3474		29.2	52.2	1.8	25	12.3	1.1
3675	Pre-Evaporites	16.4	26.9	1.6	25	5.8	1.0
3810		7.5	5.5	0.7	23	7.4	1.1

Table 1. Indices and distribution of *n*-alkanes as measured from the aliphatic hydrocarbons, Levant Basin MSC lipid extract. Depositional units are described in the text and presented in Figs 2 and 3. SCA – short chain alkanes (C_{15-21}), LCA – long chain alkanes (C_{27-35}), ACL – average chain length, CPI – carbon preference index (Bray and Evans, 1961), expressed as the following relation (*sensu* Vasiliev et al., 2017): $CPI = (((N_{25} + N_{27} + N_{29} + N_{31} + N_{33}) / (N_{24} + N_{26} + N_{28} + N_{30} + N_{32})) + ((N_{25} + N_{27} + N_{29} + N_{31} + N_{33}) / (N_{26} + N_{28} + N_{30} + N_{32} + N_{34}))) * 0.5$, where N represents the relative abundance for individual *n*-alkanes. Pr/Ph is the ratio between the pristane and phytane measured from the extracts.

Sample depth (m)	Depositional units, Dolphin-1, Levant Basin	Steranes				Hopanes		
		C_{27}		C_{28}		C_{30}	C_{31}	
		$C_{27}\alpha\alpha\alpha20S/C_{27}\alpha\alpha\alpha20R$	Amount of rearranged steranes	$C_{28}\alpha\beta\beta20S/C_{28}\alpha\beta\beta20R$	$C_{28}\alpha\alpha\alpha\ 20S/C_{28}\alpha\alpha\alpha\ 20R$	$C_{30}\beta\alpha/C_{30}\alpha\beta$	$C_{31}\alpha\beta S/C_{31}\alpha\beta R$	$C_{31}\beta\alpha/C_{31}\beta\beta$
2655	Interbedded Evaporites	0.74	High	1.37	0.43	0.02	1.19	0.64
2709		0.82	High	1.39	0.50	0.07	1.15	0.39
3402	Argillaceous Diatomites	0.26	Low	0.01	0.04	1.16	0.07	0.16
3474		0.29	Low	0.03	0.08	1.40	0.03	0.10
3675	Pre-Evaporites	1.66	Moderate	0.06	0.28	0.32	0.79	0.16
3810		0.72	Moderate	1.14	0.43	0.22	0.73	0.02

Table 2. Indices and distribution of steranes and hopanes measured by selective reaction monitoring (SRM) of the aliphatic hydrocarbons, Levant Basin MSC lipid extract. Depositional units as in Table 1. Selected samples and thermal maturity-dependent ratios from SRM analysis include C_{27} steranes (Ensminger et al., 1978; Peters et al., 2005, 1980), and C_{30} and C_{31} hopanes (Peters and Moldowan, 1993; Rullkötter and Marzi,1988). Note the higher maturity values in the Interbedded Evaporites relative to the over- and underlying intervals.